QUALITY OF SERVICE AWARE CONTENTION AND DEPLOYMENT QUALITY ANALYSIS IN MULTIMEDIA WIRELESS SENSOR NETWORKS

by

Mehmet Yunus Dönmez

B.S., Mathematics, Boğaziçi University, 1999

M.S., Computer Engineering, Boğaziçi University, 2003

Submitted to the Institute for Graduate Studies in
Science and Engineering in partial fulfillment of
the requirements for the degree of
Doctor of Philosophy

Graduate Program in Computer Engineering

Boğaziçi University

2011

QUALITY OF SERVICE AWARE CONTENTION AND DEPLOYMENT QUALITY ANALYSIS IN MULTIMEDIA WIRELESS SENSOR NETWORKS

APPROVED BY:

Prof. Cem Ersoy (Thesis Supervisor)	.....
Assist. Prof. Sanem Kabadayı	.....
Prof. Sema Oktuğ	.....
Assoc. Prof. Can Özturan	.....
Assoc. Prof. Tuna Tuğcu	.....

DATE OF APPROVAL: 28.09.2011

ACKNOWLEDGEMENTS

In the course of pursuing my PhD degree, I feel myself extremely fortunate to study with Prof. Cem Ersoy, who always have been more than an advisor for me and showed his confidence in me. I would like to give my grateful and sincere thanks to him for his guidance, patience, and support during my graduate studies. I am inspired by not only his research capability but also his humanity and friendship, as he has never withheld his morale support even when I felt myself extremely depressed and demotivated. Regarding him as my academic father, I never ignored his valuable comments not only on my academic studies but also on my life, which structured my academic and personal character.

I thank all of my thesis jury members, Assist. Prof. Sanem Kabadayı, Prof. Sema Oktuğ, Assoc. Prof. Can Özturan and Assoc. Prof. Tuna Tuğcu for their time and valuable comments. Their remarks have improved the quality of this thesis significantly.

I would like to express my special thanks to my dear fried Sinan Işık, whom I see as a brother, for his supportive comments and discussions on any subject throughout our academic journey started in 1999.

I would like to express all of the faculty members in the Mathematics Department, especially Prof. Alp Eden for all they have taught me in my B.S. study which constituted the basis of this thesis, and for the opportunity they provided to me to work as a research assistant since 1999.

In the course of my academic life, I had the chance to meet with the friends and colleagues to exchange knowledge on the research topics: İlker Demirkol, Can Komar, Rabun Koşar, Itır Karaç, Birkan Yılmaz, Atay Özgovde, Hande Alemdar and Yunus Durmuş.

I would like to express my respect and love to my mother Şaduman Dönmez, my father Turgut Dönmez for all their efforts to raise me and for all the confidence they have shown in me. I would like to thank my sisters Binnur Dönmez Yılmaz and Zehra Türköz having been my parents rather than my sisters since my childhood.

I finally would like to thank the dearest of all, my wife, Tülin Bayram Dönmez for all the respect and confidence she has shown in me. I could not have finalized this study if I had not met her. I cannot deny the power and concentration that she provided to me with her presence.

This work is supported by The Scientific and Technological Council of Turkey (TUBITAK) under the Grant Number 108E207 (COST ACTION IC0906-WINEMO), by Bogazici University Research Fund (BAP) under the Grant Number 5146 and 5344, and by the European Community's Seventh Framework Programme (FP7-ENV-2009-1) under the grant agreement FP7-ENV-244088 FIRESENSE.

ABSTRACT

QUALITY OF SERVICE AWARE CONTENTION AND DEPLOYMENT QUALITY ANALYSIS IN MULTIMEDIA WIRELESS SENSOR NETWORKS

Emerging multimedia applications for wireless sensor networks (WSN) require the co-existence of different types of traffic with different quality of service (QoS) provisions in terms of latency and throughput. Prioritization based service differentiation mechanisms are applied in all layers of communication to satisfy the QoS requirements of each traffic class. The prioritization in contention is one of the differentiation methods applied in the medium access layer. In this thesis, we propose an analytical model for the contention latencies and energy expenditures of different classes in a prioritized contention structure consisting of contention partitions allocated to priority classes. In the analysis, we explore the optimum sizes of these partitions in terms of contention latency and the total energy expenditure in the neighborhood for each priority class. This analytical model is also useful for the evaluation of various recent contention prioritization schemes in WSNs. We adapt this generic analysis to SMAC protocol which introduces the low-duty-cycle operation for energy efficiency. We explore the effects of the duty cycle, the contention window size and the data size on the performance of networks with single and multiple types of traffic. Apart from the communication based QoS, the sensing quality of the network brings about another perspective to the QoS in WSNs regarding the quality of the deployment. We provide a theoretical analysis which derives a quality measure for the deployment in terms of network parameters accounting the loss of sensors or loss of communication due to jamming.

ÖZET

ÇOKLU ORTAM KABLOSUZ ALGILAYICI AĞLARINDA SERVİS KALİTESİ BİLİNÇLİ ÇEKİŞME VE YERLEŞTİRME KALİTESİ ANALİZİ

Kablosuz algılayıcı ağlar (KAA) için geliştirilen yeni çoklu ortam uygulamaları gecikme ve net veri iletim hızı cinsinden farklı hizmet kalitesi koşulları olan farklı trafik tiplerinin bir arada bulunmasını gerektirir. Önceliklendirmeye dayalı hizmet ayrım mekanizmaları, her trafik sınıfının hizmet kalitesi ihtiyaçlarını karşılayabilmek için bütün iletişim katmanlarında uygulanmaktadır. Çekişme önceliklendirmesi, ortam erişim katmanında uygulanan ayrım metodlarından biridir. Bu tezde, öncelik sınıflarının kullanımına tahsis edilen çekişme bölmelerinden oluşan öncelikli çekişme yapısında, farklı sınıfların çekişme gecikmelerini ve güç tüketimlerini bulabilmek için analitik bir model öneriyoruz. Analizde, her bir öncelik sınıfı için çekişme gecikmesi ve komşuluktaki toplam güç tüketimi bakımından en uygun bölme boyutlarını araştırıyoruz. Bu analitik model aynı zamanda KAA'lar için geliştirilmiş çesitli güncel çekişme önceliklendirme şemalarının değerlendirilmesi için kullanılabilir. Bu genel analiz, enerji verimliliği için düşük görev döngülü işleyişi tanıtan SMAC protokolüne uyarlanmıştır. Görev döngüsü, çekişme penceresi boyutu ve veri boyutunun tek ve çok trafik tipi taşıyan ağların başarımına etkisi araştırılmıştır. İletişime dayalı hizmet kalitesinden ayrı olarak, ağın algılama kalitesi KAA'larda yerleştirme kalitesini göz önüne alan başka bir hizmet kalitesi bakış açısını beraberinde getirir. Yerleştirme için algılayıcı düğümlerinin veya sinyal bozucular yüzünden iletişimin kaybını hesaba katan ağ parametreleri cinsinden bir kalite ölçüsü sağlayan teorik bir analiz sağlanmıştır.

TABLE OF CONTENTS

ACKNOWLEDGEMENTS iii
ABSTRACT v
ÖZET vi
LIST OF FIGURES x
LIST OF TABLES xv
LIST OF SYMBOLS xvi
LIST OF ACRONYMS/ABBREVIATIONS xxii
1. INTRODUCTION 1
1.1. Addressed Problems 2
1.2. Contributions and Structure of Thesis 6
2. LITERATURE REVIEW 10
2.1. Prioritized Contention in WSNs 10
2.2. Analysis of SMAC and Duty Cycle Optimization in WSNs 12
2.3. Deployment Quality in WSNs 13
2.3.1. Analytical Target Detection Studies 13
2.3.2. Jammer and Network Attack Detection and Defense Studies . . 15
3. EFFECT OF PRIORITIZED CONTENTION SCHEMES ON NETWORK STATISTICS 16
3.1. Motivation 16
3.2. Evaluated Prioritization Schemes 18
3.2.1. Queue Prioritization 18
3.2.2. Contention Prioritization 18
3.3. Evaluation of the Prioritization Approaches 20
3.3.1. Simulation Scenarios 21
3.3.2. Prioritization Schemes Used in Simulations 22
3.3.3. Evaluation of Scenario 1 23
3.3.4. Evaluation of Scenario 2 27
3.3.5. Evaluation of Scenario 3 29
3.3.6. Interpretation of Results 33

4. ANALYSIS OF PRIORITIZED CONTENTION IN WIRELESS SENSOR NETWORKS 35
4.1. Prioritized Contention Model 35
4.2. Analysis of Priority Class Contention Latencies 36
4.2.1. Analysis of Average Carrier Sense Durations 37
4.2.2. Analysis of Average Unsuccessful Medium Access Times 40
4.3. Analysis of the Expected Energy Expenditures for Priority Classes . . . 45
4.4. Effect of the Contention Window Partitioning Strategy 48
4.4.1. Effect of the Partitioning Strategy on the Probability of Success and Collision 48
4.4.2. Effect of the Non-Existence of the Opponent Class on the Contention Latency 52
4.4.3. Effect of the Partitioning Strategy on the Contention Latency . 53
4.4.4. Effect of the Partitioning Strategy on the Energy Expenditure . 59
5. ADAPTATION OF PRIORITIZED CONTENTION ANALYSIS FOR DUTY CYCLED SENSOR NETWORKS 61
5.1. SMAC Model 61
5.2. Throughput and Energy Expenditure Analysis of SMAC 63
5.2.1. Expected Time to Finalize a Transmission 64
5.2.2. Expected Energy Expenditure to Finalize a Transmission 67
5.2.3. Derivation of Energy Expenditure in the Synchronization Period 70
5.3. Effect of Contention Window Size and Duty Cycle on SMAC Operation 73
5.4. SMAC Protocol with Multiple Priority Classes 81
6. DEPLOYMENT QUALITY ANALYSIS IN WIRELESS SENSOR NETWORKS 86
6.1. Model Assumptions 86
6.2. Problem Definition 88
6.3. Deployment Quality of a Border Surveillance WSN 91
6.4. Analytical Results 100
6.4.1. The Combined Effect of Sensor Count and Sensing Range on DQM Values 104

6.4.2. The Combined Effect of Area Size and Sensor Count on DQM Values 105
6.4.3. The Combined Effect of Jamming Area Radius and Jamming Area Count on DQM Values 106
6.4.4. Comparison of the Intruder Detection Probabilities for the Linear and Meandering Paths 108
7. CONCLUSIONS 110
REFERENCES 114

LIST OF FIGURES

Figure 1.1. A sample border surveillance wireless sensor scheme. 6

Figure 3.1. A queue containing packets sorted with respect to their priorities. 18

Figure 3.2. Contention prioritization schemes. 19

Figure 3.3. Average latency and percentage of received packets for each priority class using different prioritization schemes in Scenario 1 for video frame rate: 12 fps, duty cycle: 0.5. 24

Figure 3.4. Average latency and percentage of received packets for each priority class using different prioritization schemes in Scenario 1 for video frame rate: 12 fps, duty cycle: 0.95. 25

Figure 3.5. Average latency and percentage of received packets for each priority class using different prioritization schemes in Scenario 1 for video frame rate: 5 fps, duty cycle: 0.5. 26

Figure 3.6. Average latency and percentage of received packets for each priority class using different prioritization schemes in Scenario 1 for video frame rate: 5 fps, duty cycle: 0.95. 26

Figure 3.7. Average latency and percentage of received packets for each priority class using different prioritization schemes in Scenario 2 for video frame rate: 12 fps, duty cycle: 0.5. 27

Figure 3.8. Average latency and percentage of received packets for each priority class using different prioritization schemes in Scenario 2 for video frame rate: 12 fps, duty cycle: 0.95. 28

Figure 3.9. Average latency and percentage of received packets for each priority class using different prioritization schemes in Scenario 2 for video frame rate: 5 fps, duty cycle: 0.5. 29

Figure 3.10. Average latency and percentage of received packets for each priority class using different prioritization schemes in Scenario 2 for video frame rate: 5 fps, duty cycle: 0.95. 30

Figure 3.11. Average latency and percentage of received packets for each priority class using different prioritization schemes in Scenario 3 for video frame rate: 12 fps, duty cycle: 0.5. 31

Figure 3.12. Average latency and percentage of received packets for each priority class using different prioritization schemes in Scenario 3 for video frame rate: 12 fps, duty cycle: 0.95. 31

Figure 3.13. Average latency and percentage of received packets for each priority class using different prioritization schemes in Scenario 3 for video frame rate: 5 fps, duty cycle: 0.5. 32

Figure 3.14. Average latency and percentage of received packets for each priority class using different prioritization schemes in Scenario 3 for video frame rate: 5 fps, duty cycle: 0.95. 33

Figure 4.1. The contention window with two priority classes. 35

Figure 4.2. A contention-based medium access with two priorities. 37

Figure 4.3. Probability of success for varying x_1: (a) for high priority class. (b) for low priority class. 49

Figure 4.4. Probability of success for varying x_2: (a) for high priority class. (b) for low priority class when $N_1 = 5$. (c) for low priority class when $N_1 = 10$. (d) for low priority class when $N_1 = 15$. 50

Figure 4.5. Probability of collision: (a) with respect to x_1. (b) with respect to x_2. 51

Figure 4.6. Average latency in the non-existence of the opponent priority class: (a) for high priority class. (b) for low priority class. 53

Figure 4.7. Average latency for varying x_1: (a) for high priority class. (b) for low priority class when $N_1 = 5$. (c) for low priority class when $N_1 = 10$. (d) for low priority class when $N_1 = 15$. 54

Figure 4.8. Average latency for varying x_2: (a) for high priority class. (b) for low priority class when $N_1 = 5$. (c) for low priority class when $N_1 = 10$. (d) for low priority class when $N_1 = 15$. 55

Figure 4.9. Average latency where $x_2 - x_1 = 32$: (a) for high priority class. (b) for low priority class when $N_1 = 5$. (c) for low priority class when $N_1 = 10$. (d) for low priority class when $N_1 = 15$. 57

Figure 4.10. Average latency for varying x_1 and x_2 where $x_2 \geq x_1$: (a) for high priority class. (b) for low priority class. 58

Figure 4.11. Average energy consumption for varying x_1 and x_2 where $x_2 \geq x_1$: (a) for high priority class. (b) for low priority class. 59

Figure 5.1. Frame structure of SMAC. 62

Figure 5.2. The effect of contention window size on Ω' for N=5,10,15. 75

Figure 5.3. The expected number of SMAC frames for Λ, Γ' and Ω' for N=15. 75

Figure 5.4. The effect of contention window size on E_{tot} for N=5,10,15. 77

Figure 5.5. The effect of contention window size on message throughput ($1/\Omega'$) for message sizes of 1, 5 and 10 packets for N=15. 78

Figure 5.6. The effect of duty cycle on message throughput ($1/\Omega'$) for message sizes of 1, 5 and 10 packets for N=15. 79

Figure 5.7. The effect of duty cycle on energy expenditure for message sizes of 1, 5 and 10 packets for N=15. 80

Figure 6.1. Graphical representation of the border surveillance intruder detection avoiding jammers problem. 89

Figure 6.2. Graphical representation of the line-set intersection problem. . . . 91

Figure 6.3. Effect of high sensor count and sensing range on the analytical and simulated DQM values. (a) Circular deployment region scenario. (b) Rectangular deployment region scenario. 103

Figure 6.4. Effect of low sensor count and sensing range on the analytical and simulated DQM values. (a) Circular deployment region scenario. (b) Rectangular deployment region scenario. 104

Figure 6.5. Effect of area size and high sensor count on the analytical and simulated DQM values. (a) Circular deployment region scenario. (b) Rectangular deployment region scenario. 105

Figure 6.6. Effect of area size and low sensor count on the analytical and simulated DQM values. a) Circular deployment region scenario. (b) Rectangular deployment region scenario. 106

Figure 6.7. Effect of jamming area radius and jamming area count on the analytical and simulated DQM values. (a) Circular deployment region scenario (b) Rectangular deployment region scenario. 107

Figure 6.8. Comparison of DQM values for the shortest vs. meandering paths. 108

LIST OF TABLES

Table 3.1. Simulation parameters for the evaluation of the presented schemes. 21

Table 3.2. Scenarios used in the simulations. 22

Table 4.1. Simulation parameters for the proposed contention model. 49

Table 5.1. Simulation parameters for the presented SMAC model. 74

Table 6.1. Tested parameters for circular deployment region scenario. 102

Table 6.2. Tested parameters for rectangular deployment region scenario. . . 102

LIST OF SYMBOLS

A	Deployment area
c	Radio channel bitrate
c	The event representing the collision in slot selection
C	Random variable for the number of colliding nodes
C	A bounded set
E_{ci}	Total idle energy consumed during the synchronization periods with transmissions
E_i	Total idle energy consumed during the synchronization periods without transmissions
E_i'	Total energy consumed in a cluster till the end of a transmission of class i
E_{idle}	Energy consumed in the idle state by a node per second
E_r	Total energy consumed for the reception of SYNC messages
E_{rx}	Energy consumed for reception by a node per second
E_{sync}	Average energy consumed by a node in the synchronization period
E_t	Total energy consumed for the transmissions of SYNC messages
E_{tot}	Cluster energy consumption for a successful transmission including collisions
E_{tx}	Energy consumed for transmission by a node per second
G	Intruder path line
h_j	Index of a jammer
H_j	Jamming coverage area of a jammer h_j
L	Perimeter of deployment area
L_i	Perimeter of sensing coverage area of a sensor s_i
m	Number of colliding nodes
M	Number idle nodes in the neighborhood
$\mathbf{M}$	The fundamental matrix of $\mathbf{P}$

n	Number of data packets in a message
N	Number of contending nodes in the data period
N_h	Number of jammers
N_i	Number of contenders in the neighborhood of class i
N_s	Number of deployed sensors
N_{sync}	Initial number of nodes in the synchronization period
p	Distance of the intruder line to the origin
$\mathbf{P}$	The state transition matrix of the absorbing DTMC model of SYNC message transmissions
P_a	Probability that a sensor resides outside all of the jamming areas
P_D	Probability that the network detects an intruder
$P_D(k)$	Probability that intruder is detected by at least one sensor
$P_{\overline{D}}$	Probability that the network misses an intruder
P_{H_j}	Probability that a sensor resides in jamming area H_j
$P_{\overline{H}_j}$	Probability that a sensor resides outside of the jamming area H_j
P_i	Probability that intruder is detected by a single sensor s_i
P_{s_i}	Probability that a sensor s_i detects an intruder
$P_{\overline{s}_i}$	Probability that a sensor s_i misses an intruder
$P_{\mathbf{z_{k,v}}}$	Probability that at least one of the members of sensor set $\mathbf{z_{k,v}}$ detect the intruder
$P_{\overline{\mathbf{z}}_{\mathbf{k,v}}}$	Probability that none of the members of sensor set $\mathbf{z_{k,v}}$ detect the intruder
$P_{Z_{k,v}}$	Probability that at least one of the alive members of sensor set $\mathbf{z_{k,v}}$ detect the intruder
R	Radius of circular deployment area
r_{dc}	Duty cycle
R_h	Radius of jamming area, where all jammers have identical effective area
R_s	Radius of sensing coverage of a sensor, where all sensors have

	identical coverage
S	Convex deployment area
s_i	Index of a sensor
s_i	The event of success of class i in slot selection
S_i	Sensing coverage area of a sensor s_i
$\mathbf{t}$	The transition count matrix to reach absorbing state from any state of $\mathbf{P}$
t_c	The duration required to detect a collision till the beginning of a new slot selection
t_s	The duration of a contention slot
t_{ack}	Transmission duration of an ACK message
t_{ACK}	Duration of an ACK packet
T_{active}	Duration of the awake period
t_{cts}	Transmission duration of a CTS message
t_{CTS}	Duration of a CTS packet
t_{DATA}	Duration of a DATA packet
T_{frame}	Duration of an SMAC frame
T_{listen}	Duration of the listen period
t_{rts}	Transmission duration of an RTS message
t_{RTS}	Duration of an RTS packet
T_{sleep}	Duration of the sleep period
t_{slot}	Duration of a single contention slot
t_{SYNC}	Duration of a SYNC packet
T_{sync}	Duration of the synchronization period
t_{tout}	Timeout duration in case of a collision
t_{tr}	The duration required for a successful transmission
T_{tr}	Duration of message transmission
W	Contention window size for the data period
W_s	Contention window size for the synchronization period
X	Intruder
x_1	Last slot of α

x_2	Last slot of β
x_3	Last slot of γ
$X_{\mathbf{z_{k,v}}}$	Probability that intruder passes through the sensing area of any of the members of sensor set $\mathbf{z_{k,v}}$
$Y_{\mathbf{z_{k,v}}}$	Probability that only the members of sensor set $\mathbf{z_{k,v}}$ is alive
$\mathbf{z_{k,v}}$	Vector containing ordered and distinct list of k sensors
$\mathbf{z'_{k,v}}$	Complement of $\mathbf{z_{k,v}}$ with respect to the vector $[1, \ldots, N_s]$
$Z_{N_s,k}$	Set of all $\mathbf{z_{k,v}}$ vectors
α	Contention window partition assigned to class 1 (high)
α_ψ	Expected number of SMAC frames required to finalize a data transmission
γ	Contention window partition assigned to class 2 (low)
β	Contention window partition assigned to class 1 and 2
β	Expected number of collisions before a successful contention
Γ	Expected carrier sense time elapsed until ψ
Γ'	Expected time for a successful transmission after collisions
Γ_i	Expected carrier sense time elapsed until ψ of class i
δ_i	Expected energy consumed during a transmission of opponent of class i
ζ	Probability of collision in the contention
$\zeta_{(\psi,m,n,c)}$	Probability that ψ is the first occupied slot m class 1 and n class 2 selects ψ and there is a collision
$\zeta_{(\psi\|c)}$	Probability that ψ is the first occupied slot in a collision
$\zeta_{(\psi,c)}$	Probability that ψ is the first occupied slot and the slot selection ends with a collision
θ	Expected energy consumption in a collision
θ	Expected energy consumption in a frame with collision
$\dot{\theta}(\psi, k)$	Energy consumption until ψ where k nodes collide
Θ	Expected energy consumption during frames with collision
Θ_i	Expected energy consumption during collisions and transmis-

	sions of opponent of class i
λ	Expected time elapsed in one collision
Λ	Expected time for collisions before a successful transmission
Λ_i	Expected time for collisions and opponent class transmissions before the transmission of class i
μ_i	Expected time elapsed in one transmission of the opponent of class i
ξ	Probability of success in the contention
ξ_i	Probability of success in the contention for class i
$\xi_{(\psi)}$	Probability that ψ is the first occupied slot and it is selected by only one node
$\xi_{(\psi\|i)}$	Probability that ψ is the first occupied slot in a successful slot selection for class i
$\xi_{(\psi,i)}$	Probability that ψ is the first occupied slot and it is selected by only one node of class i
τ_{sync}	The period of SYNC message generation
$\tau(\psi, m)$	Probability that ψ is the first occupied slot and m nodes select ψ
$\tau(\psi, m, n)$	Probability that ψ is the first occupied slot and m class 1 and n class 2 nodes selects ψ
Υ	Random variable indicating the status of the slot selection
ϕ	Angle of line perpendicular to intruder line with respect to x axis
Φ	Expected energy consumption during successful transmission
$\chi_i()$	Characteristic function of class i based on selected slot
ψ	First occupied contention slot number
ψ^*	Expected first occupied slot in a successful contention
Ψ	Random variable representing the first occupied slot
Ω	Expected time for a successful transmission including collisions
Ω'	Expected total SMAC frame time required for a successful

	transmission to finalize including collisions
Ω_i	Expected time for a successful transmissions including collisions for class i
Ω'_i	Expected total SMAC frame time required for a successful transmission to finalize including collisions for class i

LIST OF ACRONYMS/ABBREVIATIONS

ACK	Acknowledgment
CTS	Clear-to-Send
DQM	Deployment Quality Metric
DTMC	Discrete Time Markov Chain
FOV	Field of View
KAA	Kablosuz Algılayıcı Ağ
MAC	Medium Access
NSC	Non-Starving Contention
QoS	Quality of Service
RTS	Request-to-Send
SC	Starving Contention
SMAC	Sensor-MAC
SWSN	Surveillance Wireless Sensor Network
SYNC	Synchronization
VSN	Video Sensor Network
WSN	Wireless Sensor Network

1. INTRODUCTION

Wireless sensor networks (WSNs) attract the attention of the researchers in the wireless community, considering both the economical and technological constraints and the vast majority of the application scenarios based on their capabilities [1]. The evolution of the sensors to bear devices such as low-cost camera hardware has led WSNs to be a potential candidate for the solutions of inherently difficult multimedia tasks such as border surveillance, target tracking, fire, environmental/habitat monitoring applications and health applications [2].

A typical sensor network can be considered as a collection of tens to thousands of sensor nodes which are distributed in the area, where some desired phenomenon to be traced is likely to be observed. One or more nodes among them act as the data collection points named sink(s) that are capable of communicating with the user either directly or through the existing wired networks. The communication between the nodes and the sink is established in a multihop manner to consume less power than the traditional single hop communication.

WSNs frequently suffer from the common problems of wireless networks that affect the throughput, latency and energy expenditure performances such as network traffic density which brings out the problem of the high probability of packet collision, the contention latency which may be triggered by the contention based protocols proposed to address the collision problem, the saturation and overflow of the buffers in the sensor nodes triggered by the throughput of a node, failure of components of sensor node or depletion of battery energy.

One of the most important constraints on sensor nodes is the low power consumption requirement. Sensor nodes carry limited, generally irreplaceable, power sources. Therefore, while traditional networks aim to achieve high quality of service (QoS) provisions, sensor network protocols focus primarily on power conservation. The traffic types generated in emerging WSN applications such as fire monitoring, border surveil-

lance and target tracking applications can be event-triggered or periodic, which have application specific QoS requirements. These applications require the time-critical phenomena to be forwarded to the sink(s) within a given latency bound to preserve their validity since a late report is considered as a lost report. In a fire surveillance system, sensors collect and send periodic samples from the environment such as heat and humidity levels. In addition, in case of any critical event such as a sudden increase in the temperature, detecting sensors may transmit critical packets or trigger its video device to capture real-time video frames from the environment to inform about the condition in the vicinity [3, 4]. The co-existence of multiple types of traffic in a single system with different QoS requirements necessitates prioritization schemes in each communication layer for the realization of the QoS provisions [5, 6]. Hence, it is necessary to provide necessary power-efficient mechanisms for such environments where critical and non-critical data coexist in the environment.

The event-triggered traffic is generally urgent for the success of the application and hence, should be quickly delivered to the sink to preserve their validity. For the time-critical applications, latency is the primary QoS metric. The latency of a packet traveling towards the sink in a multi-hop sensor network is commonly affected by several factors. The main factors are the network topology, the network traffic density, the medium access model and the signal quality. We concentrate on the medium access model, since the routing and queuing latencies induced on a packet is directly affected by the medium access performance.

1.1. Addressed Problems

Majority of the WSN MAC protocols are contention-based since they do not require precise time synchronization, extra circuitry or extra computational ability as their TDMA [7–9], FDMA [10] and CDMA [11] based counterparts require respectively. In a contention-based medium access, all sensors selects a random slot in the contention window and idle listening is performed till the first occupied slot. If multiple sensors select the first occupied slot, the selection results with a collision, and after a predefined timeout duration a new slot selection starts.

In the first part of the thesis, we concentrate on the effect of the prioritized contention mechanisms on the latency and energy consumption. The main latency component induced by a contention-based MAC layer protocol is the contention latency, which may be defined as the time required to resolve the mentioned series of slot selections that finalizes when the first slot is selected by only one sensor. We call the total time elapsed for these repetitions and the following successful slot selection, "the retrial duration" and "the carrier sense duration" respectively. The contention window size inherently induces a tradeoff between these duration components, since a smaller contention window size causes an increase in the number of collisions, whereas a larger contention window size causes an increase in the carrier sense time. The energy consumption during contention depends on the transmissions and idle listening durations, which should be optimized in a good MAC layer protocol. A tradeoff similar to the latency case is observed in the energy consumption between the carrier sense and retrial energy consumptions. Hence, a proper setting of the contention window size is crucial for low latency and energy-efficient operation.

Since the contention latency is one of the factors that determine the packet latency, a delay critical packet shall be favored in the contention. For this purpose, the packets in the system are classified into priority classes where the most critical data is given the highest priority. One of the prioritization methods proposed for the MAC layer is the differentiation of the contention window sizes for each priority class. The differentiation can be established by resizing the contention window for each priority class [12, 13] or partitioning the contention window into several parts which are assigned to one or more priority classes [14, 15], depending on the proposed MAC layer. The most common example is to assign each partition to a distinct priority class where the partitions containing smaller slots is assigned to higher priority classes [16, 17]. Another typical example is that the contention window of a priority class is included in the contention window of another priority class [12, 15]. To realize a QoS requirement for lower priority packets, a contention window assignment that overlaps with contention windows of higher priority class may also be possible. We need a mechanism to evaluate and compare these partitioning approaches. In our study, we provide an analytical approach that enables network engineers to make a comparison among

possible partitioning strategies. As far as we know, there is no study in the literature that evaluates the quality of the partitioning strategies including the adjustment of the contention window sizes for different priority classes considering their energy expenditures and packet latencies based on the collision and success probabilities of the contention resolution mechanism.

In the second part of the thesis, we concentrate on the energy consumption of the uniform contention mechanism. In wireless sensor networks, energy efficiency is the primary concern in all protocol designs regarding the communication of the data generated by the sensors which have limited energy budgets. SMAC [18] is the ancestor of many MAC protocols [19–22], which aims to reduce the energy consumption in wireless sensor networks by periodically putting sensors into sleep state to enable low-duty-cycle operation in a multi-hop network. Besides energy efficiency, the data delivery performances in terms of latency and throughput are also important for the functionality of some applications, such as border surveillance, target tracking and fire detection. Moreover, multimedia sensor networks [2] introduce the constraint of larger data sizes. In order to improve the performance of the sensor network, the operational parameters affecting the MAC layer performance should also be optimized regarding the requirements of the application. The node density is an important factor affecting the success of the contention resolution mechanism in SMAC protocol. The data size is also an important factor since improper duty cycle configurations may lead to significant performance degradations in terms of latency and throughput.

In SMAC protocol, sensors exchange their sleep schedules via the periodically broadcasted SYNC packets to their immediate neighbors. Consequently, virtual clusters are formed by the sensors following the same sleep schedule. The performance of the network is tightly bound to the performance of virtual clusters, which is determined by the node density, the contention window size, the duty cycle and the data size. Certain subsets of these parameters jointly determine the time components that constitute the throughput performance of a virtual cluster. The contention window size and duty cycle determines the SMAC frame duration. On the other hand, the node density and the contention window size determine the fail probability in a contention period of

an SMAC frame, and hence the expected number of frames to elapse till a successful contention. In addition, the data size, jointly with the contention window size and duty cycle, determine the number of frames required for a successful transmission to finalize.

The QoS requirements in the communication layers in a WSN are directly related with the sensing coverage of the sensing sensor network deployment. A minimal level of sensing coverage shall be satisfied in the network for target detection and MAC layer forwarding. Hence, apart from the communication based QoS, the sensing quality of the network brings about another perspective to the QoS in WSNs regarding the quality of the deployment.

In the third part of the thesis, we concentrate on the quality of the network deployment regarding the effect of node losses due to jamming and destruction to provide a lower bound for current sensing quality which is an important network parameter for the operability of critical-event applications. WSNs are suitable for tasks such as target tracking and surveillance applications due to their distributed and redundant deployment, requirement of little maintenance during operation and ability to operate in difficult deployment sites. A surveillance sensor network is illustrated in Figure 1.1. In this example, the sink is located at the secure side of the network, and the sensors report an intruder to the sink in a multi-hop manner. The intruder is assumed to trespass the deployment area from the insecure to the secure side.

The aforementioned applications rely on the overall sensing capability of the network, which may be defined as the ability to detect any target passing through the deployment site. The instantaneous sensing capability of the sensor network is altered by various factors, such as unpredictable changes in the network topology caused by the error-prone nature of the wireless channel, hardware fault and destruction of sensors, and jammer attacks [1]. However, especially in border surveillance systems, the sensing capability of the network, indicated by the total coverage of the sensors, is required to be above a certain threshold for the reliable detection of the intruders trespassing the deployment site at any time. The sensing capability is measured in terms of the

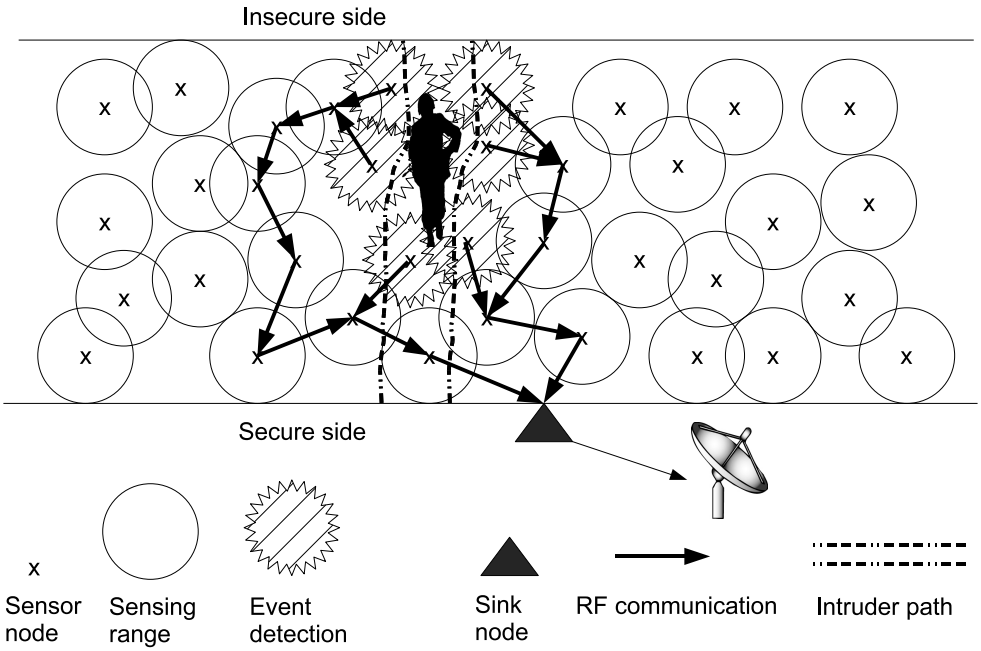

Figure 1.1. A sample border surveillance wireless sensor scheme.

deployment quality metric (DQM) [23] because it is directly related to the deployment characteristics of the network.

Node losses can occur due to different factors, such as intentional destruction of nodes by means of explosives, jamming and avalanche effects induced by fast battery depletion of critical nodes or underlying terrain obstructions. The area of the coverage holes caused by sensor losses may be heterogeneous, and the resulting active sensor distribution may not be uniform in these circumstances. Analytical approaches must take such factors into account to provide reliable deployment quality values for realistic scenarios.

1.2. Contributions and Structure of Thesis

A brief overview of the prioritized contention schemes, QoS based improvements on various contention models, and the analytical studies on the duty cycled MAC protocols, target detection and jammer attacks are presented in Chapter 2.

In Chapter 3, we combine several network scenarios carrying heterogenous traffic and various contention prioritization schemes in our simulations to demonstrate the effect of these prioritization schemes and various duty cycle settings of SMAC protocol on the packet latency and reliability.

In Chapter 4, we provide an analytical approach that evaluates the quality of the partitioning strategies including the adjustment of the contention window sizes for different priority classes considering their energy expenditures and packet latencies based on the collision and success probabilities of the contention resolution mechanism.

We assume a prioritized contention model of a sensor network which contains high and low priority classes. Our analysis focuses on the performance of the contention model in a local neighborhood, since the performance of the network is tightly bounded to the performance of a local neighborhood. The analysis is based on the number of nodes in a neighborhood, the number of contending nodes, the contention window size and the data size. Using the analysis, we derive the expected time and expected energy expenditure for a successful transmission to finalize including retrials caused by collisions.

The contention model analyzed in this study uses a uniform slot selection mechanism, where the selection of any slot is equally likely. In this model, the contention window is divided into three partitions, where the first, the second and the third parts are assigned to high, high/low and low priority classes respectively for slot selection. We analyze the effect of the sizes of these partitions on the local delay and the local energy consumption performances for both priority classes.

In Chapter 5, we introduce an analytical model for the expected throughput and the expected energy expenditure of an SMAC virtual cluster containing a single priority class to explore the effect of duty cycle, contention window size and data packet size on the network performance. Our analysis assumes that the virtual cluster is heavily loaded, the number of contenders is constant, and the nodes in the cluster are immediate neighbors of each other. These assumptions are valid especially for

applications with large data size such as multimedia sensor networks. The analysis is based on the number of nodes in a cluster, the number of contending nodes, the contention window size, the duty cycle and the data size, and it derives the expected time and expected energy expenditure for a successful transmission to finalize including retrials caused by collisions. Using the expected time, we introduce the throughput metric for a virtual cluster. Furthermore we extend the prioritized contention analysis provided in the first part of the thesis for the SMAC protocol by integrating the effect of the duty cycle in the analysis.

In Chapter 6, we aim to find an analytical solution to derive the DQM proposed in this thesis for a given sensor network with realistic node loss assumptions. For this purpose, we map the physical problem definition of the sensor network to the geometric domain and determine the probability of detection of a target following a linear trajectory by a single sensor. We generalize this solution to derive the deployment quality metric proposed in this thesis, which is the overall probability of intrusion detection in the network. Based on the shortest path strategy, such a solution provides a conservative estimation for the intruder detection performance. The probability of node losses is integrated into the analysis to increase the accuracy of the metric. The mathematical solution is further simplified to provide a closed-form DQM formulation. Providing a closed-form DQM with loss assumptions provides assistance to the WSN designers and supervisors in the following situations:

- A fast and precise calculation of the sensing quality is required for the robust operation of an initially deployed surveillance wireless sensor network (SWSN) [24].
- At any point in the lifetime of a network, critical decisions should be made on sensor redeployment, relocation, and sleep/wake commands [25].
- Online monitoring of the sensing quality, which affects the reliable detection of intruders, is required to estimate the current network performance [26].
- The network parameters should be determined carefully to obtain an adequate level of sensing capability in the network [27].

These major factors that guide the SWSN engineers in designing and maintaining

the network are the main motivations for proposing a deployment quality metric with sensor loss provisions. The network engineers can utilize the given metric to find a solution to these situations in the following ways:

- SWSNs bear mission- and time- critical tasks that require minimum levels of deployment quality. The DQM monitoring approaches based on simulations require unacceptably long periods, whereas our analytical approach will provide instantaneous results.
- The critical decisions about the network operation depend mostly on the sensing quality metrics for SWSNs. Simulation based decisions demand long processing times, extending the total operation latencies. Our analytical method provides a low-cost calculation of the DQM value in terms of the processing time.
- The detection reliability of the network can be estimated by an online calculation of the DQM value using our analysis.
- Our analysis can be used as a tool to calculate network parameters, such as the required sensor node count and node sensing range, to monitor a region when certain parameters are provided as inputs by the network engineers.

Chapter 7 concludes the thesis and hints some future work.

2. LITERATURE REVIEW

In this chapter, we provide brief overviews of the literature on the subjects that constitutes the basis of the thesis. Initially, we will provide a literature survey on the studies proposing prioritized access schemes. Secondly, a list of analytical approaches on SMAC and optimization of the duty cycle are provided. Finally, the analytical approaches on the deployment quality and studies on sensor losses including jammers and network attacks are discussed.

2.1. Prioritized Contention in WSNs

The inter-node differentiation of packets in the MAC layer is established by assigning medium access priorities for each packet type. This prioritization in a contention-based MAC protocol is established by the adjustment of the duration and the starting time of the contention windows. The contention-based protocols are classified into two groups, namely uniform and exponential backoff which has the disadvantage of exponential increase in the contention window in case of collisions [28].

The prioritized uniform backoff schemes generally partition the fixed sized contention window and assign these partitions to one or more priority classes. In [16] and [17], an inter-node arbitration scheme is proposed where the contention window is partitioned among different priority classes in the order of their precedence and the probability of selection in each segment increases geometrically as in [28]. The work in [4] introduces contention-free slots for packet delivery, which contains four sub slots assigned to distinct priority groups to be used in emergency mode contention. Traffic is categorized into three priority classes in [29] and the higher priority class is assigned a shorter contention window which is a subset of the contention windows of lower priority classes with uniform selection probability. A combination of contention-free and contention based transmission is proposed for ad-hoc networks in [30], where each segment is assigned to a priority class by their precedence order, wherein these segments may overlap in the contention based phase with uniform selection probability. A MAC layer

with frame ownership priority is proposed in [14], which gives precedence to nodes in their preassigned transmission frames, if they have data to transmit, by splitting the contention window into two disjoint segments and reserving them to the owner node (first segment) and other nodes (second segment). Kim *et al.* [15] extends [14] and proposes a four level prioritization scheme along with the frame ownership precedence. In this protocol, a lower priority level is assigned a shorter contention segment at the end of the contention window contained in higher priority contention segments. In addition, each segment is further split into two segments to apply the ownership prioritization scheme. In [31], three schemes are proposed to provide a prioritized medium access. The first scheme applies a variable size contention window for each event type which is similar to the approach in [29]. The second scheme applies different inter-frame spacing for each event type as seen in [15]. In the third scheme, an additional burst period is added to the inter-frame spacing to further discriminate and eliminate the lower priority levels.

A dynamic contention window size approach is proposed in [12] which adapts the window sizes for different priority classes. It monitors the dynamics of the sensor nodes and the medium by collecting relevant network statistics to determine the scaling factors for the sizes of the contention windows, where the highest priority level is given the shortest contention window size as in [29]. A similar model is proposed in [13].

The prioritized binary exponential backoff schemes used by IEEE 802.11, 802.11e and 802.15.4 standards generally apply similar approaches as in the prioritized uniform backoff schemes. In [32] and [33], a differentiated contention window approach is proposed for IEEE 802.11 with a contention window structure similar to [29]. The RAP protocol [34] introduces another IEEE 802.11 based differentiation scheme which combines a similar contention window structure with differentiated inter-frame spacing. A non-contiguous contention window approach in which segments of contention window are alternatingly assigned to priority classes is proposed in [35]. IEEE 802.11e introduces the enhanced distributed coordination function which defines different window size settings for different traffic classes to achieve QoS requirements. The sliding contention window method [36] is proposed to adjust the backoff ranges of the traffic classes

according to the QoS requirements and dynamic network behavior. Another method proposed in [37] takes the congestion level of the network into account by considering the previous window size values to reset the window size. For IEEE 802.15.4, a memorized backoff scheme is proposed in [38] to dynamically adjust the window size based on the traffic load. Smaller contention window sizes and the binary exponent factors are assigned to higher priority levels for saturated and non-saturated conditions in [39] and [40] respectively. Several analytical studies for IEEE 802.15.4 standard based on Markov Chain model have been proposed in the literature [41–43]. Among these models, the work in [41] proposes an analytical approximation for the optimization of the window size as a function of the probability of collision in the contentions.

In [44], an analytical approach that is not based on a Markov model is introduced for non-prioritized contention schemes. This study aims to derive energy and delay optimized contention window sizes for non-sleeping contention based sensor network MAC protocols. Our study incorporates the contention analysis approach of [44] to analyze the contention window partitioning strategies in a prioritized uniform backoff scheme.

2.2. Analysis of SMAC and Duty Cycle Optimization in WSNs

SMAC introduces the low-duty-cycle operation for energy conservation in sensor networks using periodic listen/sleep schedules. An analysis based on Markov models for wireless sensor networks that contains nodes with sleeping behavior is proposed in [45]. However, the proposed sensor model is not suitable for the analysis of SMAC since this common model ignores some protocol details such as fixed duty cycle, overhearing avoidance and message passing. An analytical model for the energy consumption of sensors using SMAC for different traffic conditions and network topologies is proposed in [46]. In addition to the energy consumption, in order to evaluate the service latency and throughput of SMAC protocol for unsaturated conditions, [47] provides an M/G/1 queuing model using the classical Bianchi model [48] for IEEE 802.11 protocol. A similar study based on Markov model for unsaturated conditions is proposed in [49]. In [50], the analysis in [47] is extended to model the multihop network performance of

SMAC. The behavior of SMAC with a finite queue capacity is evaluated in [51] using a model based on [48]. These models explore the effects of different parameters such as the number of nodes, queue capacities, contention window sizes, and data arrival rates on the service latency, throughput and energy consumption. However, they do not consider the interdependency between duty cycle, contention window size and data size which significantly affects the throughput and energy expenditure of SMAC. In addition, these studies ignore the time and the energy spent in the synchronization period, which actually affects the contention window size and the duty cycle configurations for the optimal throughput and the energy expenditures of the SMAC protocol.

The duty cycle optimization for SMAC is studied in [52]. This work considers a Gaussian traffic distribution and proposes an optimization approach for the listening time in SMAC based on energy and latency models. In [53], the average packet delivery latency of RMAC [21], a successor of SMAC, is numerically analyzed in a probabilistic manner to obtain the optimal duty cycle that minimizes the power consumption while meeting a given latency constraint. In addition, a duty cycle optimization approach is presented in [54] for the unslotted IEEE 802.15.4 based wireless sensor networks, where the objective function is the total energy consumption subject to the constraints of latency and reliability of the packet delivery.

2.3. Deployment Quality in WSNs

2.3.1. Analytical Target Detection Studies

Lazos *et al.* [55] provide analytical results for target detection in a convex deployment site. They assume that the sensors have convex coverage areas and are uniformly placed in the deployment site. They use the presented results to compare random and heuristic-based sensor placement methods. They also assume that the sensors may have heterogeneous sensing capabilities. Wang *et al.* [56] propose a scheme for an analytical coverage calculation of a heterogeneous wireless sensor network. However, the heterogeneity of the network is due to the type of sensor nodes which have different sensing capabilities. In our work, the deployment and the holes inside the network

cause the heterogeneity.

Dousse *et al.* [57] present a model for calculating the latency for an intruder to be detected by a sensor that is connected to the network. They assume a fixed sensing range of sensors. Cao *et al.* [58] present closed form results for target detection under given network parameters and assume a uniform distribution of sensors with a fixed sensing range. Wang *et al.* [59] present an analytical model to measure the event detection latency using a probabilistic approach. The model incorporates detection models involving detection using one or more sensors. The model is used to evaluate the coverage performance of a WSN. Ren *et al.* [60] try to calculate the detection probability of a network based on the operation schedule of the sensors.

Clouqueur *et al.* [61] present algorithms for collaborative target detection. In this work, the faulty detecting sensors are meant to be excluded from the detection probability using a decision fusion. The overall sensing performance of the WSN is analyzed in [62]. The authors present a fusion based detection model for wireless sensor networks. Their distributed approach tries to calculate the detection probability locally using hypothesis testing on the number of detections in the vicinity, and the system level detection performance is approximated analytically using the central limit theorem. However, this approach requires a dense network to sustain a sufficient number of detections to perform the hypothesis test.

All of the works presented have the implicit assumption that the area of interest is homogeneously covered. On the contrary, our approach in this thesis assumes that there are holes within the sensing field caused by the destruction of sensors, energy depletion or jammers that render some sensors unusable. As a result, the overall sensor distribution is no longer homogeneous.

In a different approach, Saipulla *et al.* [63] concentrate on the deployment of sensors as a line and barrier coverage for surveillance. The aim is to analyze the deployment performance of a tripwire-like sensor network. In our approach, barrier coverage is not analyzed; instead, the coverage of the total intrusion area is assumed.

2.3.2. Jammer and Network Attack Detection and Defense Studies

The subject of jammers is studied in [64] which presents algorithms to detect the existence of radio interference jamming inside the network. Ngai *et al.* [65] consider sinkhole attacks where an attacker tries to alter the data obtained by the sink by attacking the surrounding nodes. They present an intrusion detection algorithm that tries to overcome such attacks using statistical and geographical information-based operations. The malicious nodes can be excluded from the network using this algorithm. Li *et al.* [66] present a model for controllable jamming attacks and possible solutions to such attacks. Cagalj *et al.* [67] propose probabilistic communication wormholes out of the jammed region inside the network. Their approach attempts to decrease the event reporting latency caused by jammers. Jamming and other possible attacks on WSNs are modeled in [68]. They also present a routing model to stand against attacks on the network. In [69], Li and Hunter present a distributed algorithm to detect and recover holes in the network.

3. EFFECT OF PRIORITIZED CONTENTION SCHEMES ON NETWORK STATISTICS

In this chapter, we will provide a demonstrative network design carrying three types of traffic to express the effect of various prioritization schemes applied to the contention window on the latency and the reliability of each priority class, where the underlying MAC protocol is SMAC [18] and the routing protocol is GPSR [70].

3.1. Motivation

The reports on critical phenomena are considered to be much more valuable and informative than regular periodic data packets [71]. Consequently, time-sensitive applications such as critical condition monitoring and security surveillance have little tolerance for long latencies. In the cases, where the latency exceeds the tolerable latency margins of the application, the application may require the packet to be:

- forwarded to the sinks anytime as a regular data for the cases where reception of the packet is necessary to inform the system about the existence of the phenomenon.
- simply discarded since a late packet is a lost packet.

Real-time streaming data triggered by the detection of a target in video or audio applications may be referred as loss-tolerant latency-critical data, where the stream is reconstructed at the sink with acceptable or no comprehensible errors. However, the loss rate of packets is required to be below a certain percentage and the latency jitter should be below a threshold value which is specific to the sensor network application [72]. The emergence of real-time applications in sensor networks reveals the problem of providing a packet latency within application specific latency margins to be one of the topics on WSN.

A forest activity monitoring system is one of our main targets which may be summarized as follows: This network is deployed in a forest and sensors periodically collect and report samples such as heat, humidity. In addition, in case of any critical event sensed by the nodes such as the temperature exceeding a predefined threshold value, the node is triggered into the alert mode and sends a high priority alert message to the sink, indicating that there is a probability of a forest fire in the region. If the temperature does not decrease below the threshold value for a given period, the system will be triggered into the alarm mode, sending a high priority alert message and the video sensors in the region will be activated to provide real-time data about the suspicious situation.

Our second group of interest are the applications, namely terrain, battlefield monitoring and border surveillance systems. Here, the sensors are deployed in a battlefield area, a critical border zone or on a reinforcement transportation route. There are three types of sensors in these applications; scalar sensors (transmitting one packet), sensors with an audio or video capture device (transmitting a stream, having QoS requirements) and sensors periodically reporting a phenomenon in the area such as humidity and illumination. The sensors equipped with a capture device stream the captured target data to the sinks, such as movement of troops or passage of reinforcement convoy. The scalar sensors are required to report the geographical location estimation of the target within the coverage area of the sensor.

The solutions proposed for the network layers for satisfying the latency constraints of the data to be transferred focus on the protocols regulating the transmissions in the wireless medium. The latency of the packets in the system depends on the number of data sources and number of packets forwarded to the sink. The latency-sensitive data suffer extra latency due to the number of lower priority packets, timed-out data and more frequently observed latency-tolerant periodic data. These packets cause extra processing load, an increase in the number of contenders decreasing the throughput per node and an increase in traffic load, causing collisions in the MAC layer.

3.2. Evaluated Prioritization Schemes

All contention based MAC protocols have two common components: the contention window and the link layer queue. Each proposed protocol comes along with its own mechanisms for these components. Being common to all protocols, initially these components shall be adjusted in order to achieve timeliness for the packets.

The contention and queuing mechanisms introduced here are mainly based on service differentiation of different packet types. This differentiation is established by applying a prioritization mechanism which requires each packet to have a specific priority level, depending on the latency sensitivity and timeliness of a packet, sensor buffer level and aging of a packet. The transmission schedules and contention windows utilized in the transmission of these packets are organized accordingly.

3.2.1. Queue Prioritization

The queue prioritization scheme applied in the MAC layer uses a single droptail queue where higher priority packets are placed nearer to the queue head [73, 74]. The packets with the same priority are placed in the queue according to their arrival times in a first come first served manner. If the queue is full then the packets with lower priority are dropped to provide the required buffer for the high priority packet. An illustration of the queue prioritization is given in Figure 3.1.

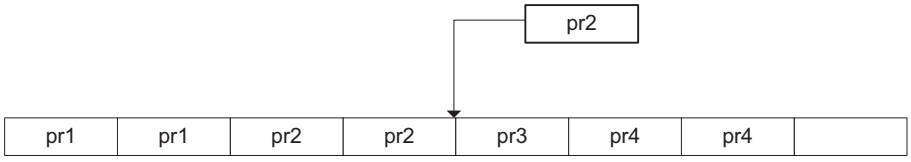

Figure 3.1. A queue containing packets sorted with respect to their priorities.

3.2.2. Contention Prioritization

Contention prioritization acts like a reservation protocol where a node with a higher priority packet gets the chance to access the medium earlier. Two prioritization

schemes are proposed. Both schemes are applied on the fixed sized contention window and uniform random contention scheme, where each node is likely to select any backoff timer value from the contention window.

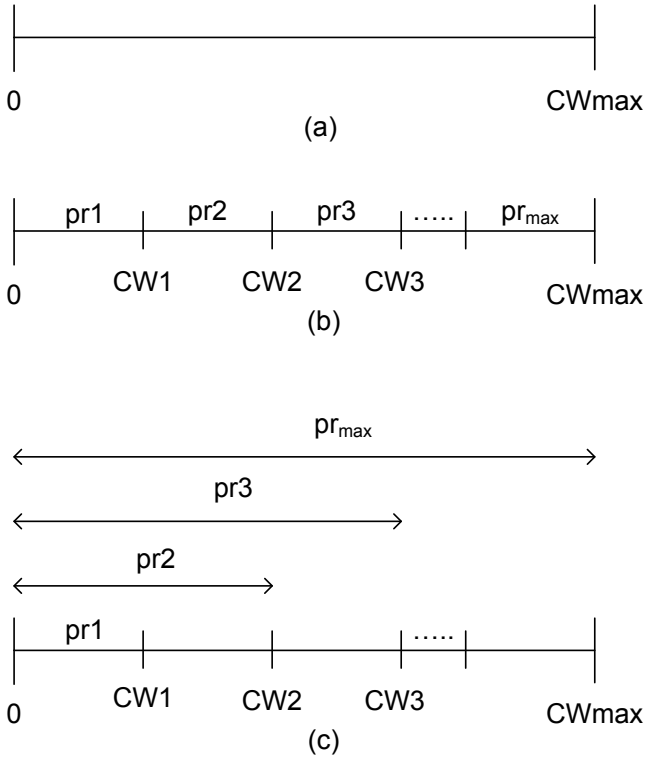

Figure 3.2. Contention prioritization schemes.

In the first scheme, no segmentation is applied on the contention window and each priority class is allowed to contend in the whole contention window (Figure 3.2a). The second scheme is the previously proposed method where the contention window is divided into distinct segments and assigning each segment to a priority class. This approach restricts the nodes with similar priority to have a similar contention pattern, i.e. similar priorities will contend among themselves, as lower priorities wait for the transmission of higher priorities. An illustration of this approach is given in Figure 3.2b.

The third scheme is the overlapping segments method where lower priority classes are assigned a larger contention window starting from slot 0 to slot CW_i which are the supersets of the contention windows of higher priority classes where i corresponds to a priority class (the highest priority class is denoted as *class 1*). This approach helps the contention to be uniform and the prioritization is provided by increasing the average

backoff timer value for lower priority classes. An illustration of this approach is given in Figure 3.2c.

3.3. Evaluation of the Prioritization Approaches

We designed simulations on OPNET Modeler [75] simulation tool to observe the effects of prioritization on packet latencies in a target tracking video application scenario. Our prioritization mechanism is integrated into the SMAC [18] protocol. We used the GPSR protocol [70] as the routing protocol in our simulations. In each simulation, 100 video sensors are uniformly deployed in a square shaped environment of each side 400 m. There are five targets moving in the environment according to the random waypoint mobility model where the target speeds are 10 m/s and the pause times are 0 seconds. In each scenario, the sink node is placed in the center of the deployment area.

In the simulation, we assumed that the video sensors are capable of taking images and compressing them with the cameras integrated on their hardware [76,77]. Since the size of the data transmitted is directly related to the size of the image, SQCIF (128 x 96) format is assumed. The image module employs intra-frame encoding which results in compressed images of size 10 Kbits. Predictive encoding alternatives such as ISO MPEG and H.26x cannot practically be used in video sensor networks (VSN) due to the high complexity involved [2]. Distributed source coding techniques are promising alternatives for encoding video in VSNs as they exploit the inter-frame redundancy with affordable complexity in the sensor nodes [78]. However, due to the lack of practical implementations yet available, we resort to the JPEG compression available on the image module. Generally, higher video quality is required for better VSN application performance. Video quality can be adjusted in the system by varying the image resolution and the camera frame rate. In our case, we fix the image resolution since a lower resolution may not be tolerated by the identification application, whereas a higher resolution results in frame sizes that cannot effectively be carried in the network. Therefore, in the simulations the frame rate of the cameras on the sensors is varied to alter the video quality throughout the network. Event triggered data generation

is simulated where the triggering event is the visual detection of a target. Since the cameras equipped support background subtraction feature, they only produce an image when the scenery changes significantly. Hence triggering occurs when the target is within the camera detection range of 30 m and is within the Field of View (FOV) of 52 degrees. The simulation parameters are listed in Table 3.1.

Table 3.1. Simulation parameters for the evaluation of the presented schemes.

Parameter	**Value**
Surveillance Area	400×400 m^2
#Sensors in the Network	100 sensors
Duty Cycle	5%, 95%
#Data Packets per Frame Message	10 packets
#Data Packets per Scalar Message	1 packet
#Data Packets per Periodic Message	1 packet
Data Packet Size	1000 bits
RTS/CTS/ACK/SYNC Size	200 bits
Buffer Size	20 Kbits
Slot Size	20 bits
DATA Contention Window Size	63 slots
SYNC Contention Window Size	32 slots
Channel Bitrate	250 Kbps
Frame Rate	5 fps, 12 fps
Periodic Data Period	10 sec
Sensing Range	30 m
Communication Range	80 m
Camera Field of View	52°
Sink Position	center
Mobility Model	Random Waypoint
Simulation Time	1 hour

3.3.1. Simulation Scenarios

Three simulation instances are designed to evaluate the network performance (Table 3.2):

- *Scenario 1:* The nodes are deployed in the field where three types of packets are transmitted. The video streams, scalar data and periodic data are assigned the high, medium and low priority classes respectively. All nodes send periodic data to the sink. In addition, 1/3 of the nodes transmit video and 1/3 of the nodes transmit scalar data. Video and scalar transmissions are triggered by the detection of a target.
- *Scenario 2:* The nodes are deployed in the field where three types of packets are transmitted. This time, scalar data have the highest priority, where video streams and periodic data are assigned the medium and low priority classes respectively. All nodes send periodic data to the sink. In addition, 1/3 of the nodes transmit video and 1/3 of the nodes transmit scalar data. Video and scalar transmissions are triggered by the detection of a target.
- *Scenario 3:* The nodes are deployed in the field where only single type of packets are transmitted. All nodes transmit video streams upon detection of a target. 1/3 of the nodes transmit high priority video, 1/3 of them transmit medium priority and the remaining 1/3 of them transmit low priority video.

Table 3.2. Scenarios used in the simulations.

Parameter	**Scenario 1**	**Scenario 2**	**Scenario 3**
Nodes (Video Stream)	1/3	1/3	All
Nodes (Scalar Data)	1/3	1/3	None
Nodes (Periodic Data)	All	All	None
Priority (Video Stream)	High	Medium	1/3 High, 1/3 Medium, 1/3 Low
Priority (Scalar Data)	Medium	High	-
Priority (Periodic Data)	Low	Low	-

3.3.2. Prioritization Schemes Used in Simulations

For each scenario, we tested three different prioritization schemes. The first one is the utilization of only the queue prioritization, referred as Q in the simulation results.

The second scheme is the joint utilization of the queue prioritization and the

contention prioritization scheme illustrated in Figure 3.2b. This scheme causes the lower priority packets to suffer in existence of higher priority packets, so we refer this approach as "Starving Contention" (SC) in the simulation results. The contention window is divided into three equal sized segments here.

The third scheme is the joint utilization of the queue prioritization and the contention prioritization scheme illustrated in Figure 3.2c. This scheme enables the lower priority packets to select smaller backoff timer values since each contention window starts from slot 0. Hence, we refer this approach as "Non-Starving Contention" (NSC) in the simulation results. The contention window is again divided into three equal sized segments here.

3.3.3. Evaluation of Scenario 1

In this video target detection scenario, the highest priority is assigned to the video streams. The scalar sensors are given the medium priority. Results of four simulation cases are presented in this section by assigning 5 fps and 12 fps for video frame rate and 0.5 and 0.95 for duty cycle parameters.

When the duty cycle is set to 0.5, the effective usage of the bandwidth reduces to one half, since the sensor is in active state half of the time. In addition, the frame rate is 12 fps which produces 120 packets per second. If a target moves half the sensing range away from the sensor on the average, we can calculate the average residence time in coverage as 1.5 seconds which corresponds to 18 frames per target. The percentage of packets received by the sink, presented in Figure 3.3b, shows that 66% of the video packets are dropped. The packet loss is caused by the insufficient effective bit rate to transmit 18 back to back frames. The packets are dropped at sources due to buffer overflow.

The average latency for each priority class is presented in Figure 3.3a. Here the video packets are shown to incur a larger latency than other priority classes. This behavior again reflects the fact that the video packets accumulate in the buffers of the

sensors. The packets of the same priority class have to wait for the packets in front of the queue, which cause the latency to increase for the packets at the tail of the queue.

The proposed prioritization schemes are shown to improve the delivery ratio of the packets, while decreasing the average latency for the video traffic. When we consider all three priority classes, we can observe that the non-starving contention priority scheme provides a better improvement. We observe improvement in latency and reception ratio of video packets, whereas lower priorities suffer a minor performance degradation. However, if the objective is the transmission of high priority class with the least possible latency, the starving contention scheme outperforms the non-starving case (42% improvement with respect to no prioritization case and 19% improvement with respect to non-starving case), where the average latency incurred by scalar data and periodic data are increased to 0.65 seconds and 0.96 seconds respectively. These values are acceptable, since periodic data is latency tolerant and scalar data can be considered to be generated as a supplement to the video packets.

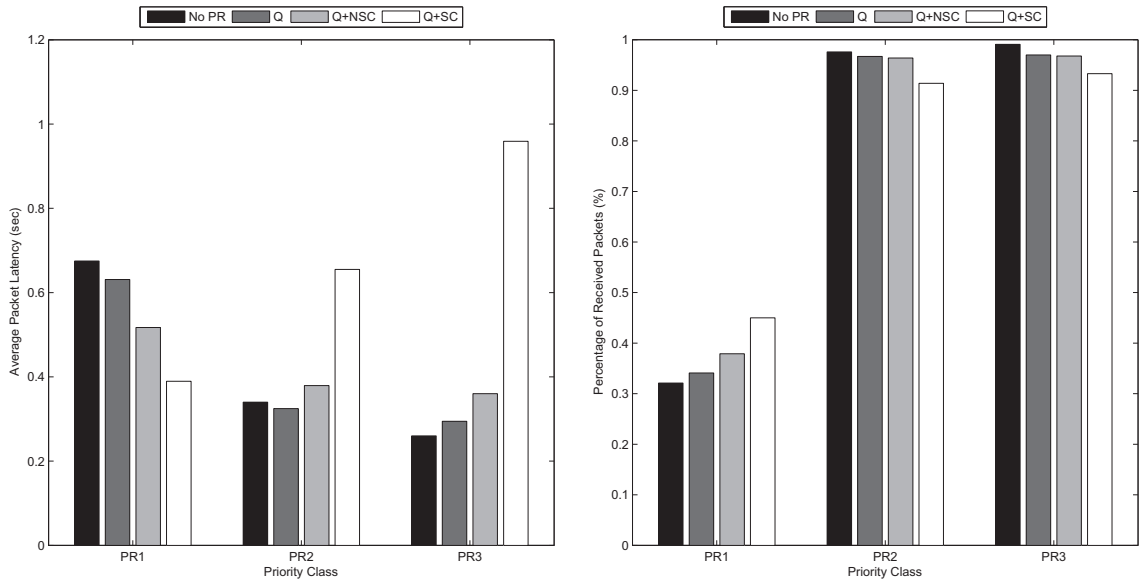

(a) (b)

Figure 3.3. Average latency and percentage of received packets for each priority class using different prioritization schemes in Scenario 1 for video frame rate: 12 fps, duty cycle: 0.5.

The improvement of average latencies is alleviated by the improvement of the packet reception rate, which is the joint effect of the queue and contention prioritization. The improvement of latency is an indication of the regulation of transmission for that priority class. Since the packets suffer lower latency in the buffers, the risk of buffer overflows decreases, which provides an increase in the packet reception rate.

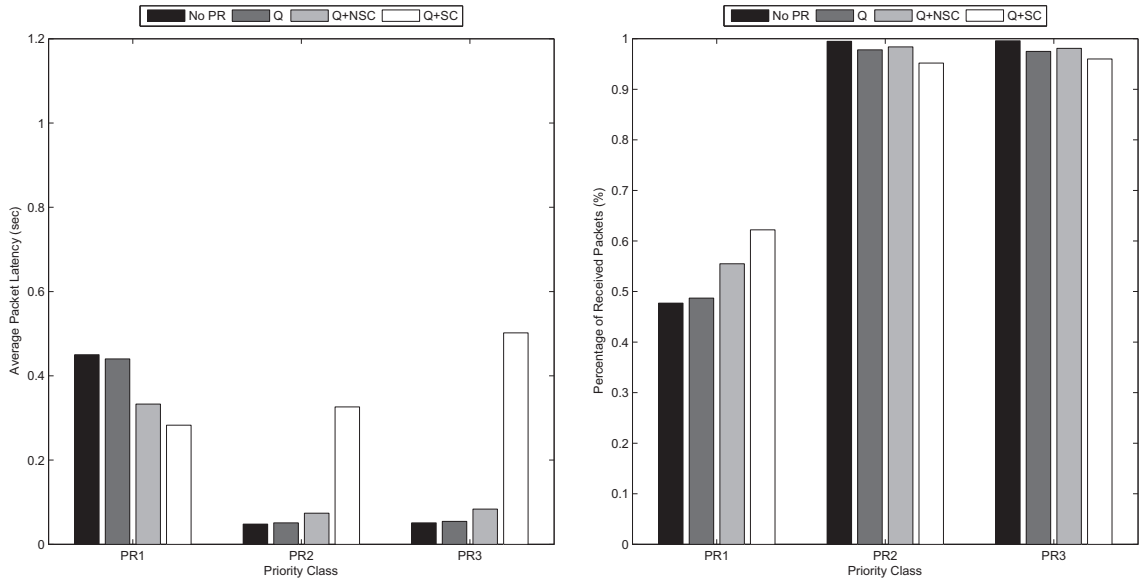

(a) (b)

Figure 3.4. Average latency and percentage of received packets for each priority class using different prioritization schemes in Scenario 1 for video frame rate: 12 fps, duty cycle: 0.95.

Figure 3.4 illustrates the results for the case where 12 fps video is transmitted with a duty cycle of 0.95. In this case, the sensors are nearly always in the active state. The system behaves similar to the case with the duty cycle of 0.5 in Figure 3.3. Due to the increase in the duration of the active period, the suffered latencies in all priority cases are shown to be lower than those in Figure 3.3a and the percentage of received packets are shown to be higher than those in Figure 3.3b.

In the scenarios with 5 fps frame rate, the decrease of the frame rate results in an increase in the percentage of reception rates and a decrease in the average latency of all priority classes because the negative effect of dominance of video packets in the buffers is decreased. An approximation for the average number of frames per target is 7.5

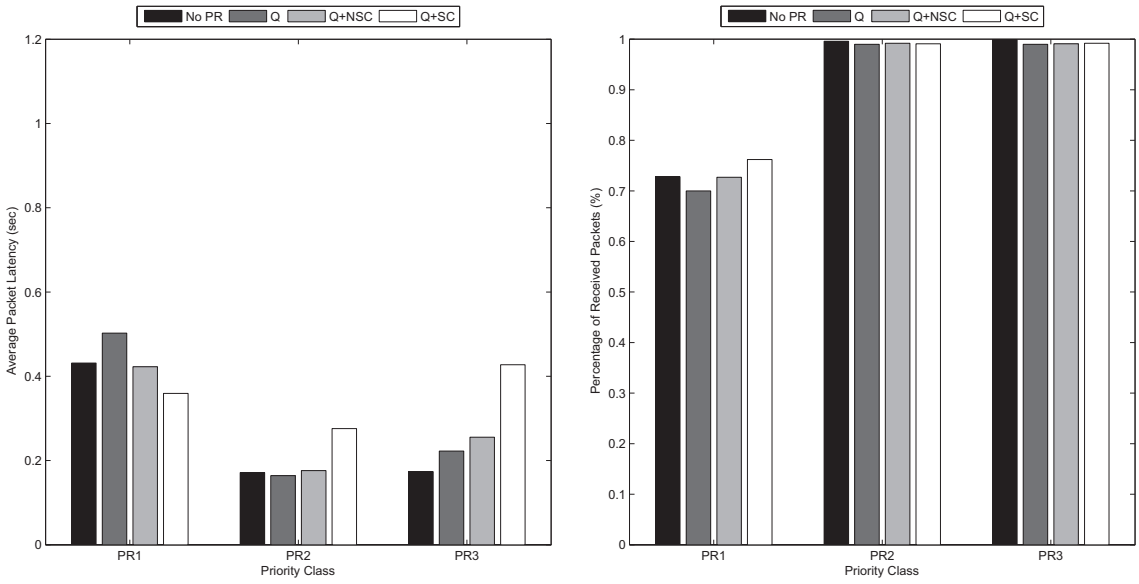

(a) (b)

Figure 3.5. Average latency and percentage of received packets for each priority class using different prioritization schemes in Scenario 1 for video frame rate: 5 fps, duty cycle: 0.5.

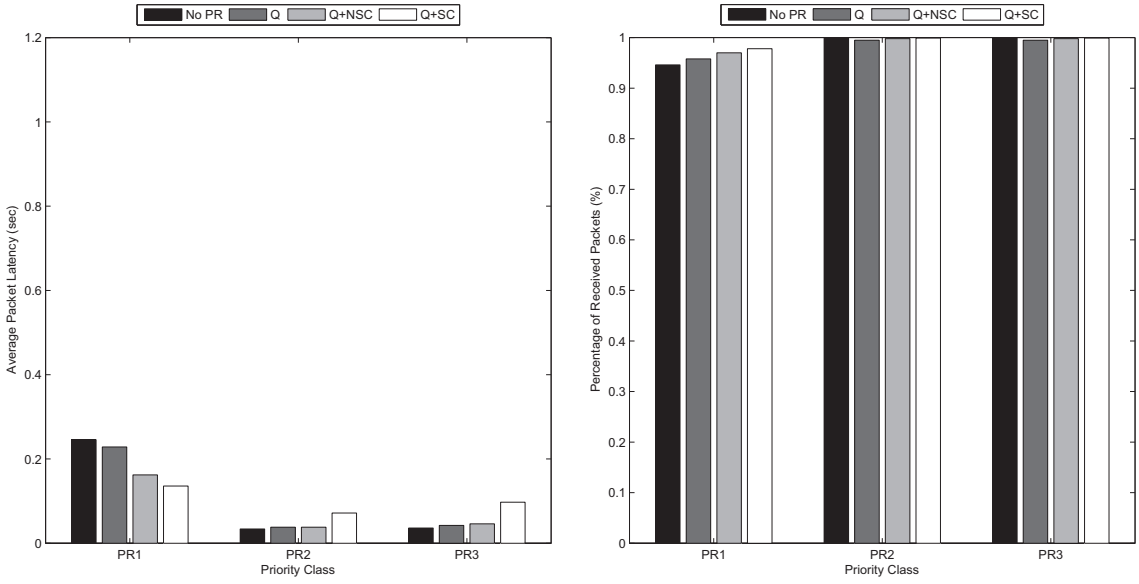

(a) (b)

Figure 3.6. Average latency and percentage of received packets for each priority class using different prioritization schemes in Scenario 1 for video frame rate: 5 fps, duty cycle: 0.95.

frames in 1.5 seconds. The received data percentages in Figure 3.5b and Figure 3.6b show that the system capacity is sufficient to transmit such packet bursts. Since the number of video packets is significantly reduced, the average latencies for lower priority classes are also reduced with respect to 12 fps video case, as shown in Figure 3.5a and Figure 3.6a. In addition, we observe that as the latency decreases for video traffic, the latency for lower priorities does not show a significant increase except for the case of starving contention prioritization scheme.

3.3.4. Evaluation of Scenario 2

In this scalar target detection scenario, the highest priority is assigned to the scalar data, which provides the geographical location of the target. The video sensors are assigned the medium priority, reporting the movement of the target, whose existence and position is reported via scalar sensors. Results of four simulation cases are presented in this section by assigning 5 fps and 12 fps for video frame rate and 0.5 and 0.95 for duty cycle parameters.

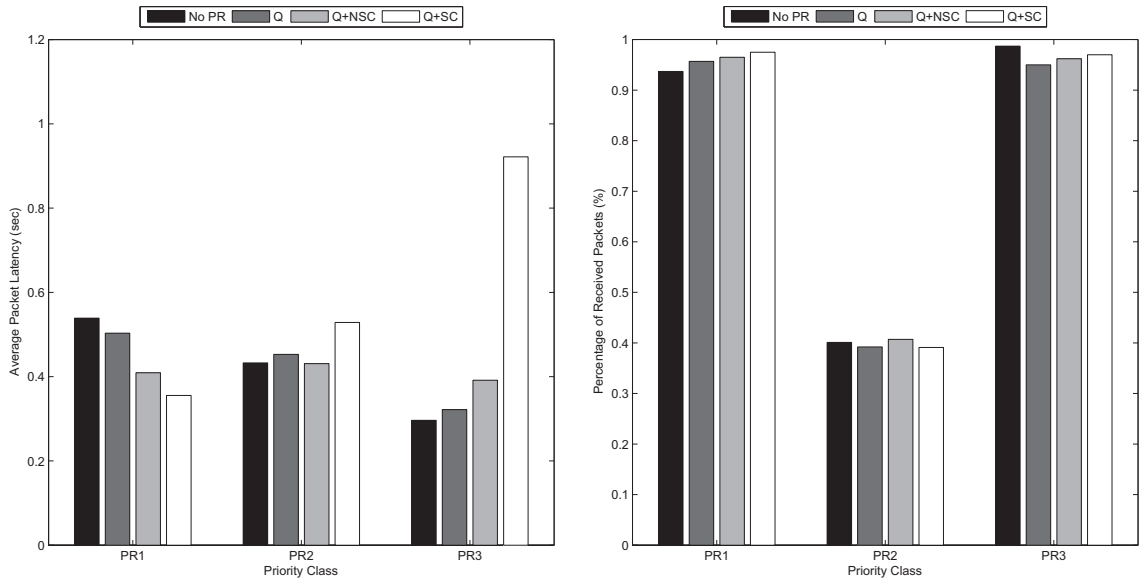

(a) (b)

Figure 3.7. Average latency and percentage of received packets for each priority class using different prioritization schemes in Scenario 2 for video frame rate: 12 fps, duty cycle: 0.5.

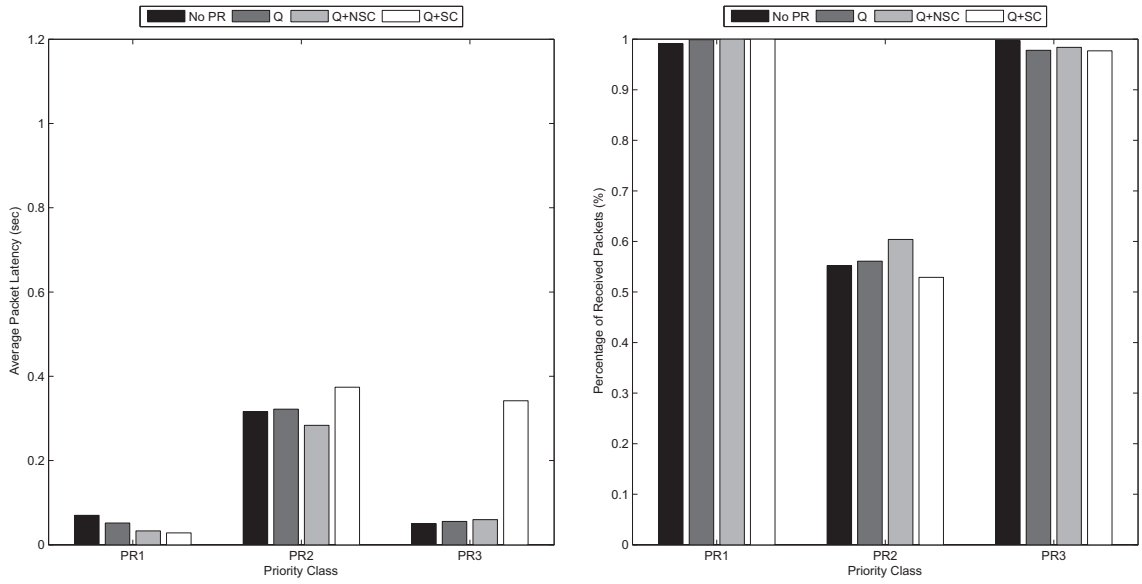

(a) (b)

Figure 3.8. Average latency and percentage of received packets for each priority class using different prioritization schemes in Scenario 2 for video frame rate: 12 fps, duty cycle: 0.95.

In Figure 3.7, the results of the simulations for the 12 fps video and 0.5 duty cycle case is presented. The results are similar to those of Scenario 1, however, the average latency of the scalar data packets are shown to improve significantly, while the increase in average latency for the starving contention case is less than the case in Scenario 1 for medium and low priority data. The packets of scalar sensors benefit from the priority schemes since the bursty video traffic is eliminated and a higher priority is assigned to the traffic with the lower packet rate.

Figure 3.8 demonstrates the case when the sensors are nearly always in the active state. As in Scenario 1, this case also shows that much of the video packets are lost. The latency improvements are visible in this figure; however, the priority classes with fewer number of packets are shown to be delivered with lower latency, and latency improvements for scalar data is insignificant. Here, the bit rate allows the scalar packets to be forwarded to sink without suffering a significant buffer latency. The video traffic accumulates in the queues and this causes the average latency to increase. Since the video traffic is dominant, most of the periodic packets that suffer excessive

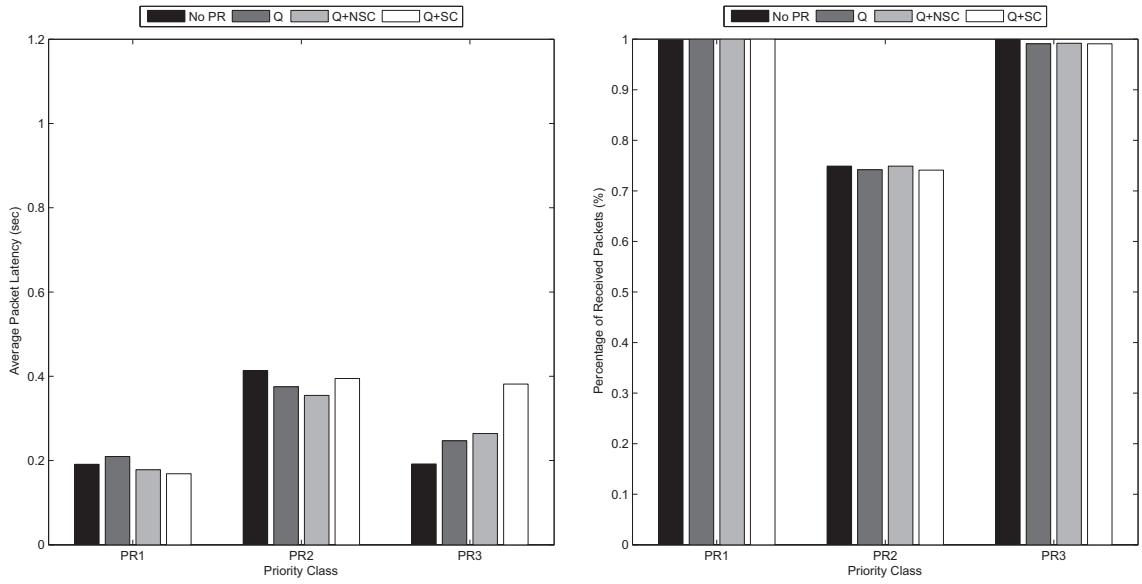

(a) (b)

Figure 3.9. Average latency and percentage of received packets for each priority class using different prioritization schemes in Scenario 2 for video frame rate: 5 fps, duty cycle: 0.5.

latencies in the queues are usually dropped due to buffer overflows. In the starving-contention case, these packets are forced to wait for the transmission of video packets, so the latency of periodic packets significantly increases.

Figure 3.9 and Figure 3.10 presents the 5 fps video case, for which the drop rate of the video packets in the source decreases significantly, due to the decrease in the arrival rate of packets. However, the improvements on the latencies are not significant for the scalar data. The packets are already transmitted with minimal latency since the system is not congested in these cases.

3.3.5. Evaluation of Scenario 3

In this pure video target detection scenario, each sensor transmits a video stream upon detection of a target until the target is out of range. One of the three priority classes is assigned to each sensor, which reflects the importance of the video packets received from a region. Results of four simulation cases are presented in this section

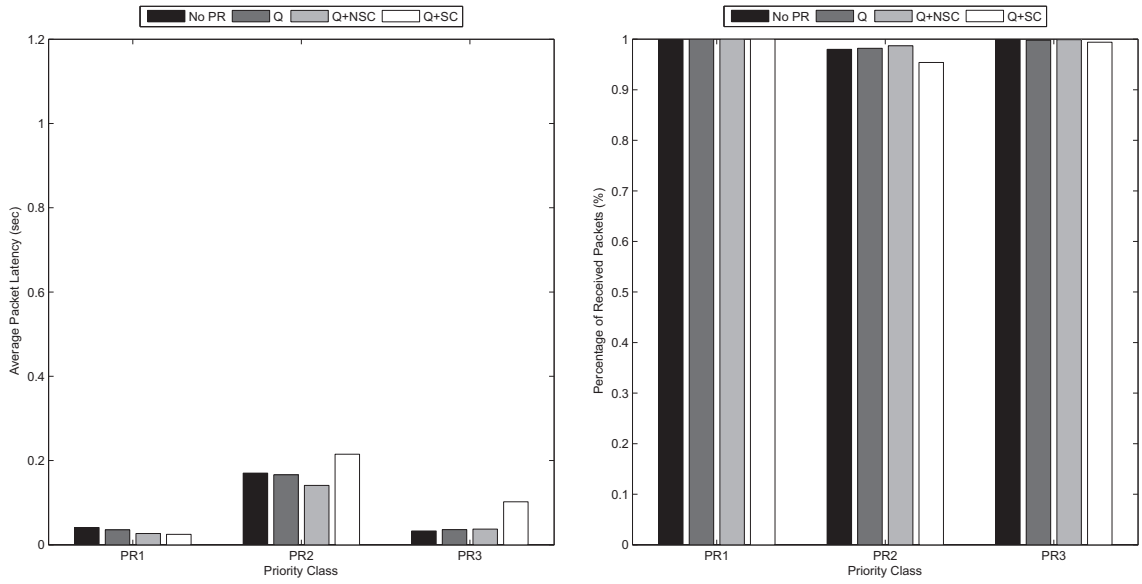

(a) (b)

Figure 3.10. Average latency and percentage of received packets for each priority class using different prioritization schemes in Scenario 2 for video frame rate: 5 fps, duty cycle: 0.95.

by assigning 5 fps and 12 fps for the video frame rate and 0.5 and 0.95 for the duty cycle parameters.

Figure 3.11 presents the case in which all frame rates are 12 fps and the duty cycle is 0.5. As stated previously, the average latency for the bursty video traffic suffers a heavy loss and large latency due to the insufficiency of the bit rate and buffer size of the sensor nodes. Despite this loss, the reception rate of high priority traffic is increased approximately 11% by utilizing non-starving contention priority. The average latency suffered by the video packets is decreased by 33% in this case. The effect of non-starving and starving contention schemes are more apparent here. The non-starving scheme provides improvements on both high and medium priority (26 and 10% respectively), with a relatively small latency increase on low priority traffic (18%). However, if we require a significant improvement in the high priority packets with acceptable performance degradation in the medium priority traffic and if we can tolerate higher latencies for the low priority traffic, then non-starving scheme is shown to be the ideal prioritization scheme.

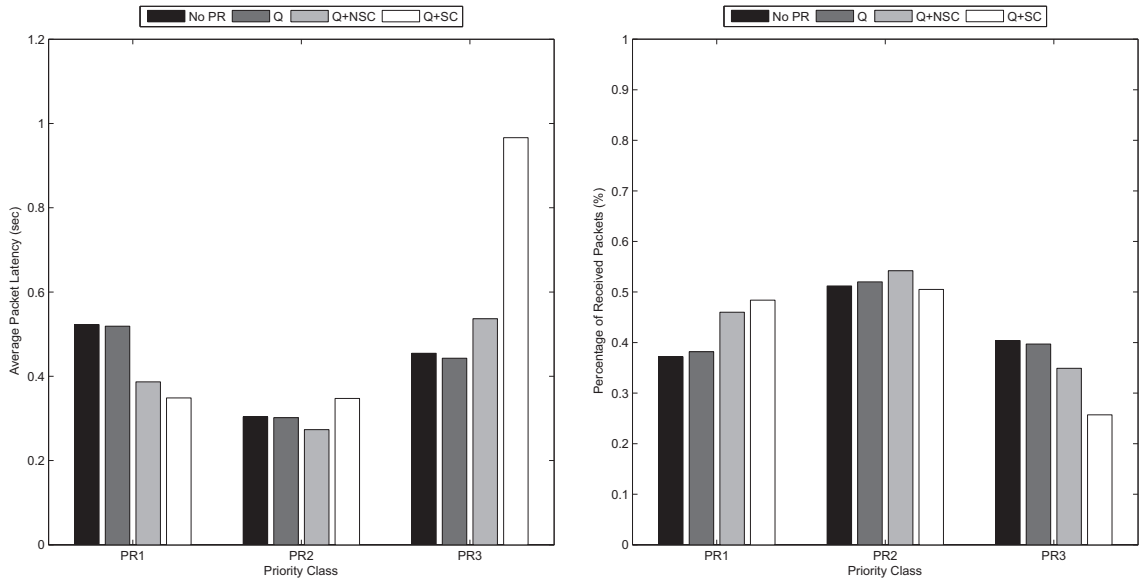

(a) (b)

Figure 3.11. Average latency and percentage of received packets for each priority class using different prioritization schemes in Scenario 3 for video frame rate: 12 fps, duty cycle: 0.5.

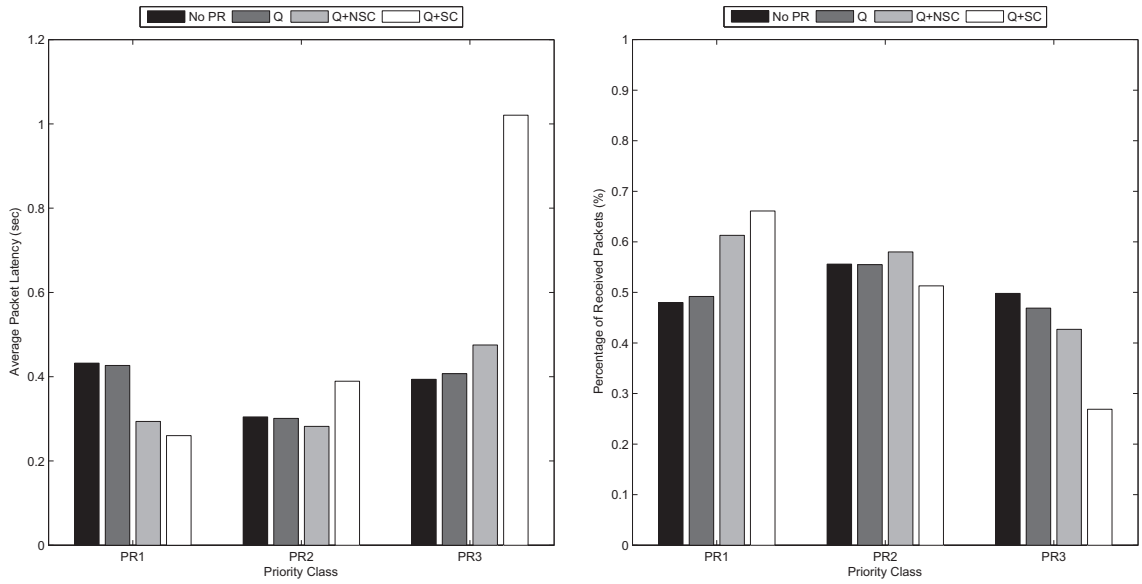

(a) (b)

Figure 3.12. Average latency and percentage of received packets for each priority class using different prioritization schemes in Scenario 3 for video frame rate: 12 fps, duty cycle: 0.95.

When the duty cycle is increased to 0.95 as shown in Figure 3.12, the average reception rate is shown to improve because the sensors have more time to transmit the accumulated packets prior to the arrival of new frames, resulting in buffer overflows and drops. The average latencies for the no-priority cases are also shown to improve because the additional latency of the sleep period is decreased and the effective bit rate (on the average) of the channel approaches the actual bandwidth.

The effect of decreasing the frame rate is more apparent in Figure 3.13 and Figure 3.14. The percentage of reception increases to 70% for the duty cycle of 0.5 and 90% for the duty cycle of 0.95. In both cases, the average latencies are shown to decrease and the packet reception rates are improved by the proposed contention priority schemes for high priority video. The results achieved with a high percentage of received packets justifies our arguments that the proposed schemes provide improvement on the percentage of reception and decrease the average latency for the high priority video packets.

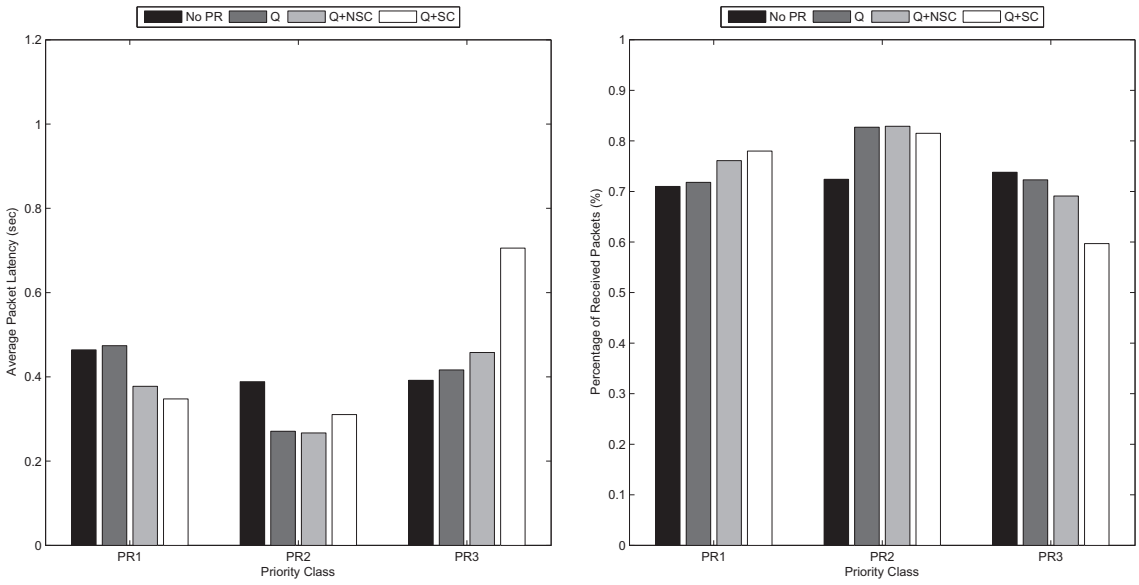

(a) (b)

Figure 3.13. Average latency and percentage of received packets for each priority class using different prioritization schemes in Scenario 3 for video frame rate: 5 fps, duty cycle: 0.5.

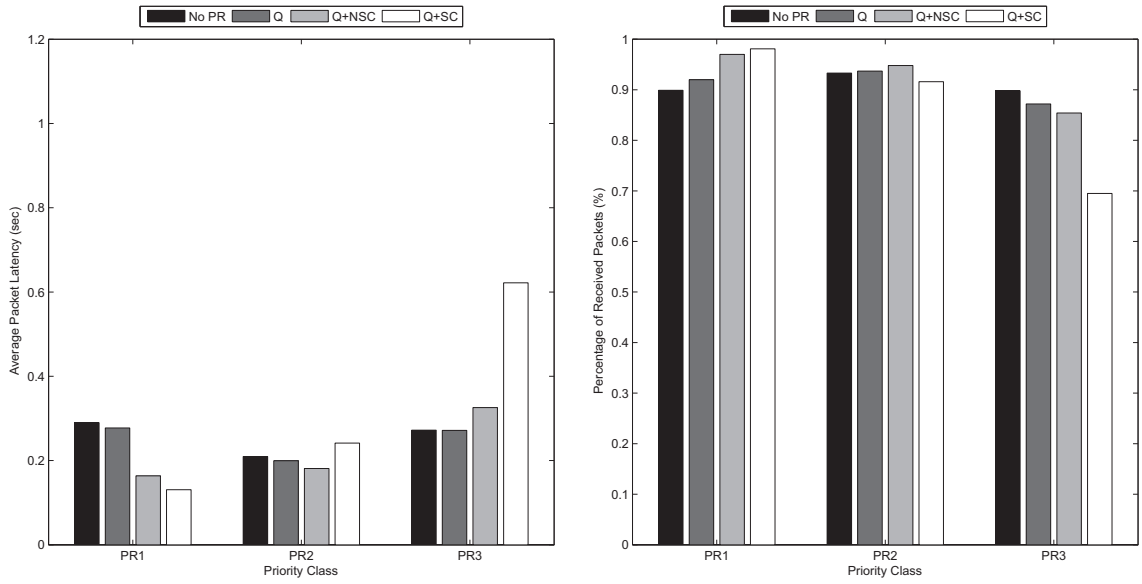

(a) (b)

Figure 3.14. Average latency and percentage of received packets for each priority class using different prioritization schemes in Scenario 3 for video frame rate: 5 fps, duty cycle: 0.95.

3.3.6. Interpretation of Results

The simulation results show that the starving contention scheme causes additional latency for lower priority classes and this causes an excessive increase on the latencies for the low priority class. The reason of this behavior is that these packets should wait for the transmission of the higher priority classes to be able to access the medium. Such an increase in the latency is an indicator of the low priority packets residing in the queues for a long time, which results with packet losses of low priority packets due to buffer overflows. As the number of generated packets per second increases, the packet losses become more apparent for lower priority classes. The percentage of received packets are shown to be significantly low; however, this percentage is not the result of packet losses on the route. These losses are caused by the buffer overflows prior to leaving the source. The prioritization schemes are shown to decrease latencies significantly for the highest priority class in most of the simulation instances. The starving contention approach is shown to decrease the average latency of the highest priority while increasing the latency for both medium and low priority classes. In the

non-starving case, the improvement on high priority packets degrades as the latencies for medium and low priority classes improve.

From the results, we can conclude that each priority class should have its own contention window; however we can let these windows overlap. The demonstrative examples in Figure 3.2b and Figure 3.2c are the special cases of this approach. In the first scheme (Figure 3.2b), the contention windows are disjoint and in the second scheme (Figure 3.2b), they include each other.

In the next chapter, we will introduce an analytical model for a priority-based contention scheme to calculate the expected latency and the energy expenditure for the transmission of packets of each priority class for a given contention window structure. The optimal window sizes and their boundaries derived from the presented model depend on the number of contending nodes in the neighborhood. Using this model, we will be able to explore the effects of various prioritization schemes applied on the contention window.

4. ANALYSIS OF PRIORITIZED CONTENTION IN WIRELESS SENSOR NETWORKS

In this chapter, we present a prioritized contention model to analyze the latency and the energy expenditure of each priority class. In [44], an analytical approach that aims to derive energy and latency optimized contention window sizes for contention based sensor network MAC protocols is proposed as a function of the probability of collision as in [41]. Our analysis incorporates the approach in [44] to analyze the contention window partitioning strategies in a prioritized uniform backoff scheme where two priority classes exist in the network and contend for the medium.

4.1. Prioritized Contention Model

In this section, we will introduce the model of the prioritized contention that will be analyzed for a neighborhood, where each node is assumed to be an immediate neighbor of each other. The neighborhood consists of N_1 nodes with packets of high priority class requiring a low transmission latency and N_2 nodes with the packets of lower class requiring a less strict latency requirement. In addition, we assume that there are M nodes which do not contend but just listen to the medium to receive packets. Our analysis assumes that the neighborhood is heavily loaded and the number of contenders of each priority class is constant. These assumptions are valid especially for multimedia sensor network applications.

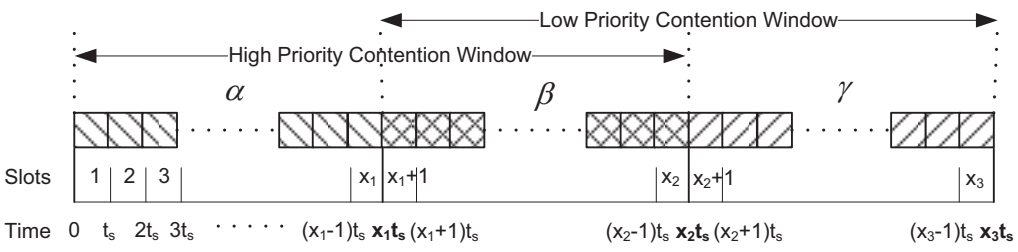

Figure 4.1. The contention window with two priority classes.

The contention period is partitioned into three regions, α, β and γ, as illustrated

in Figure 4.1. The slots $1 \ldots x_2$ are assigned to the high priority class and this interval is called as the High Priority Contention Window, which is the union of α and β regions. Similarly, the slots $x_1 + 1 \ldots x_3$ are assigned to the low priority class and this interval is called as the Low Priority Contention Window, which is the union of β and γ regions. Note that the boundaries of these regions are ordered as $1 \leq x_1 \leq x_2 \leq x_3$, which means that high priority and low priority nodes contend together in the β region consisting of slots $x_1 + 1 \leq i \leq x_2$. The slots in any region are assumed to be selected independently and uniformly randomly. The contention window actually considers the number of slots that will be used for idle waiting to prevent collision selected from a range of $[0, CW_{max}]$ slots. However, for the sake of analytical simplicity, we concentrate on the slot index in which the transmission occurs and which is selected from the range of $[1, CW_{max} + 1]$ slots. Therefore, we assume that the contention window mentioned in this thesis is analogous to the slot selection range.

Based on these constraints, we define the characteristic functions $\chi_i(\psi)$ where ψ is a slot number and $i = 1$ stands for the high priority class and $i = 2$ for the low priority class:

$$\chi_1(\psi) = \begin{cases} 1 & \text{, if } (\psi \in \alpha \vee \psi \in \beta) \wedge N_1 > 0 \\ 0 & \text{, if } otherwise \end{cases} \tag{4.1}$$

$$\chi_2(\psi) = \begin{cases} 1 & \text{, if } (\psi \in \beta \vee \psi \in \gamma) \wedge N2 > 0 \\ 0 & \text{, if } otherwise \end{cases} \tag{4.2}$$

4.2. Analysis of Priority Class Contention Latencies

Latency is an important metric in the evaluation of the performance of a network. Contention latency is one of the main components of the total latency. Nodes of high and low priority classes contend using the partitioned contention window model. We aim to formulate the contention latency experienced by each priority class in terms of the number of nodes in each priority class and the size of the partitions, α, β, γ, which are determined by the boundary slots x_1, x_2 and x_3. Using this formulation, we

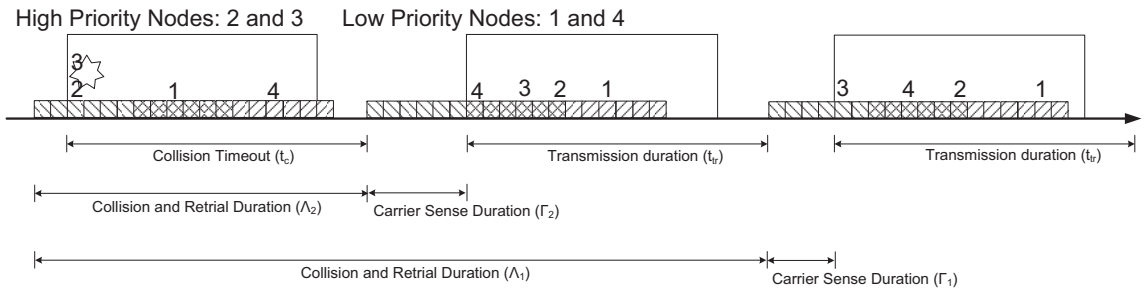

Figure 4.2. A contention-based medium access with two priorities.

are able to analyze how the global contention window should be divided among two priority classes of different latency provisions.

The expected contention latency of a priority class i is denoted by Ω_i, which is defined as the expected duration between the beginning of the contention until a successful medium access. Ω_i can be decomposed into two phases: (i) the expected time spent for collisions, retrials and transmissions of the opponent priority class until the beginning of the collisionless slot selection, Λ_i and (ii) the expected carrier sense duration within this successful contention from the beginning of the contention window until the first occupied slot, where a node of desired priority wins contention, Γ_i. In Figure 4.2, a contention phase with four nodes is illustrated as an example. Nodes 2 and 3 are the high priority nodes and nodes 1 and 4 are the low priority nodes. In the first contention resolution phase, a collision occurs between nodes 2 and 3. After a collision timeout duration, the next contention resolution starts and node 4 wins the contention in the β region. Similarly, in the following phase node 3 wins the contention in the α region.

In the following subsections, the Γ_i and Λ_i components for each priority class will be derived.

4.2.1. Analysis of Average Carrier Sense Durations

In this section, we will analyze the expected carrier sense durations, Γ_i, for a collisionless slot selection for each priority class. For the sake of brevity of the derivations

in the analysis, we will define

$$\xi_{(\psi|i)} = P\left[\Psi = \psi \,|\Upsilon = s_i\right] \tag{4.3}$$

$$\xi_{(\psi,i)} = P\left[\Psi = \psi, \Upsilon = s_i\right] \tag{4.4}$$

$$\xi_i = P\left[\Upsilon = s_i\right] \tag{4.5}$$

where the random variable Ψ represent the first occupied slot number either the slot selection results in collision or not, the random variable Υ represents the slot selection status, s_i indicates that the first occupied slot is collisionless and selected by only one node of class i. $\xi_{(\psi|i)}$ represents the conditional probability that ψ is the first occupied slot if the slot selection is successful for class i. $\xi_{(\psi,i)}$ represents the probability that ψ is the first occupied slot and it is selected by only one node of class i. ξ_i represents the probability that a slot selection results in a collisionless transmission for both priority classes. By the definition of the conditional probability,

$$\xi_{(\psi|i)} = \xi_{(\psi,i)} / \xi_i \tag{4.6}$$

If the first occupied slot is ψ, then the carrier sense duration of that contention will be $(\psi - 1)\, t_s$ where t_s is one slot duration. Then,

$$\Gamma_i = \sum_{\psi=1}^{x_3} \xi_{(\psi|i)}\, (\psi - 1)\, t_s \tag{4.7}$$

Hence, in order to calculate Γ_i, we need to derive $\xi_{(\psi,i)}$ and ξ_i, which also can be formulated in terms of $\xi_{(\psi,i)}$ as:

$$\xi_i = \sum_{\psi=1}^{x_3} \xi_{(\psi,i)} \tag{4.8}$$

Let us define $\tau_{(\psi,m,n)}$ as the probability of m high priority and n low priority nodes

to select the slot ψ and the remaining nodes select slots following ψ. Since there are N_1 high priority nodes and N_2 low priority nodes, there are ${x_2}^{N_1}\left(x_3 - x_1\right)^{N_2}$ possible slot selections.

For m high priority and n low priority nodes to select ψ, ψ should be chosen by any m of N_1 (if $N_1 > 0$) nodes. The remaining $N_1 - m$ nodes randomly choose among $x_2 - \min\left(\psi, x_2\right)$ slots between $\psi + 1$ to x_2. Similarly, n of $N_2 \geq 0$ nodes select ψ and $N_2 - n$ nodes randomly choose among $x_3 - \max\left(x_1, \psi\right)$ slots between $\max\left(\psi + 1, x_1 + 1\right)$ to x_3. However, when there is only one high priority or only one low priority node in the neighborhood, all slots can be chosen equally likely. Hence,

$$\begin{aligned}\tau_{(\psi,m,n)} &= P\left[\Psi = \psi, C_1 = m, C_2 = n\right] \\ &= \begin{cases} \frac{\binom{N_1}{m}\binom{N_2}{n}(x_2 - \min(x_2,\psi))^{N_1-m}(x_3 - \max(x_1,\psi))^{N_2-n}}{x_2^{N_1}(x_3-x_1)^{N_2}} & , \text{if } N_1 > 0, N_1 + N_2 > 1 \\ \frac{\binom{N_2}{n}(x_3 - \max(x_1,\psi))^{N_2-n}}{x_2^{N_1}(x_3-x_1)^{N_2}} & , \text{if } N_1 = 0, N_2 > 1 \\ \frac{1}{x_2} & , \text{if } N_1 = 1, N_2 = 0 \\ \frac{1}{(x_3-x_1)} & , \text{if } N_1 = 0, N_2 = 1 \end{cases}\end{aligned} \tag{4.9}$$

where C_i is the random variable representing the number of colliding class i packets.

For a collisionless transmission of a high priority packet, ψ should be chosen by any of N_1 nodes and the remaining $N_1 - 1$ nodes randomly choose slots following ψ where $\psi < x_2$. N_2 low priority nodes should choose between $\psi + 1$ to x_3. Hence,

$$\begin{aligned}\xi_{(\psi,1)} &= \chi_1(\psi)\tau(\psi, 1, 0) \\ &= \begin{cases} \frac{N_1(x_2-\psi)^{N_1-1}(x_3-x_1)^{N_2}}{x_2^{N_1}(x_3-x_1)^{N_2}} & , \text{if } \psi \in \alpha. \\ \frac{N_1(x_2-\psi)^{N_1-1}(x_3-\psi)^{N_2}}{x_2^{N_1}(x_3-x_1)^{N_2}} & , \text{if } \psi \in \beta. \\ 0 & , \text{if } \psi \in \gamma. \end{cases}\end{aligned} \tag{4.10}$$

On the contrary, for a collisionless transmission of a low priority packet, ψ should

be chosen by any of $N_2 > 0$ nodes and the remaining $N_2 - 1$ nodes randomly choose slots following ψ, where $\psi > x_1$. N_1 high priority nodes choose any of the slots between $\psi + 1$ to x_2. Hence, for low priority nodes,

$$\begin{aligned}\xi_{(\psi,2)} &= \chi_2(\psi)\tau(\psi,0,1) \\ &= \begin{cases} 0 & ,\text{if } \psi \in \alpha. \\ \frac{N_2(x_2-\psi)^{N_1}(x_3-\psi)^{N_2-1}}{x_2^{N_1}(x_3-x_1)^{N_2}} & ,\text{if } \psi \in \beta. \\ 0 & ,\text{if } \psi \in \gamma. \end{cases}\end{aligned} \tag{4.11}$$

When only low priority nodes exist in the neighborhood ($N_2 > 0$), these nodes contend in regions β and γ. Hence,

$$\xi_{(\psi,1)} = \chi_1(\psi)\tau(\psi,1,0) = 0 \tag{4.12}$$

$$\begin{aligned}\xi_{(\psi,2)} &= \chi_2(\psi)\tau(\psi,0,1) \\ &= \begin{cases} 0 & ,\text{if } \psi \in \alpha. \\ \frac{N_2(x_3-\psi)^{N_2-1}}{(x_3-x_1)^{N_2}} & ,\text{if } \psi \in \beta \vee \psi \in \gamma. \end{cases}\end{aligned} \tag{4.13}$$

The probability that a slot selection results in a collisionless transmission for both priority classes can be calculated as:

$$\xi_1 = \sum_{\psi=1}^{x_3} \chi_1(\psi)\tau(\psi,1,0) \tag{4.14}$$

$$\xi_2 = \sum_{\psi=1}^{x_3} \chi_2(\psi)\tau(\psi,0,1) \tag{4.15}$$

4.2.2. Analysis of Average Unsuccessful Medium Access Times

In this section, we will analyze the expected time spent for the collisions, retrials and opponent priority class packet transmissions, Λ_i. Let ζ be the probability that

the contention is unsuccessful due to collision. Note that a contention may be unsuccessful for a priority class due to two reasons. Firstly, there may be a collision during contention, and secondly, a node that belongs to the opponent priority class may win the contention, resulting in a transmission. Hence, a contention has three possible outcomes, success of high priority class, success of low priority class and collision with probabilities ξ_1, ξ_2 and ζ respectively, such that $\xi_1 + \xi_2 + \zeta = 1$.

Clearly, a contention is a generalized form of a Bernoulli trial which is called a "multinomial trial". The contentions will be repeated until a collisionless slot selection occurs. At this point the winner of the contention transmits its data, whereas the contention is considered as an unsuccessful contention for the opponent priority class. Since each contention is an independent and identically distributed random event, the sequence of contentions forms a multinomial trials process.

For the contention scenario, let the random variables X_ℓ indicate the number of times event number ℓ was observed over the n trials. $X = (X_1, X_2, X_3)$ follows a multinomial distribution with parameters n and p, where $p = (\xi_1, \xi_2, \zeta)$, with a probability mass function

$$\begin{aligned} f(n_1, n_2, n_3; n, \xi_1, \xi_2, \zeta) &= P(X_1 = n_1, X_2 = n_2, X_3 = n_3) \\ &= \frac{n!}{n_1! n_2! n_3!} \xi_1^{n_1} \xi_2^{n_2} \zeta^{n_3} \end{aligned} \tag{4.16}$$

given that $n = n_1 + n_2 + n_3$, where n_1, n_2 and n_3 is the number of high priority wins, low priority wins and collisions respectively and X_1, X_2 and X_3 are the corresponding random variables for these occurrence counts.

The inverse sampling, which is the waiting time, of any multinomial process with three outcomes can be explained as the frequency of events $Y = (Y_1, Y_2, Y_3)$ before the k^{th} appearance of Y_1. Then the distribution of (Y_2, Y_3) is a negative multinomial distribution [79] with parameters k and p, where $p = (p_1, p_2, p_3)$, with a probability

mass function

$$\begin{aligned} f(k, y_2, y_3; p_1, p_2, p_3) &= P(Y_2 = y_2, Y_3 = y_3 \,|Y_1 = k\,) \\ &= \frac{(k + y_2 + y_3 - 1)!}{(k-1)! y_2! y_3!} p_1^k p_2^{y_2} p_3^{y_3} \end{aligned} \tag{4.17}$$

which we denote by $\phi_{(Y_1,Y_2,Y_3)}(k, y_2, y_3)$. The expected value of Y_i is given as

$$E\left[Y_i\right] = k\frac{p_i}{p_1} \tag{4.18}$$

The expected time spent for collisions, retrials and opponent priority class packet transmissions for each priority class equals the sum of the expected number of collisions times the expected time elapsed in one collision, λ, and the expected number of transmissions of the opponent class times the expected time elapsed in one transmission of the opponent of class i, μ_i.

Firstly, we will calculate this expected time for high priority class. The distribution of the occurrence of the three events until the first successful slot selection of high priority class is given as $\phi_{(X_1,X_2,X_3)}(1, n_2, n_3)$. Hence,

$$\begin{aligned} \Lambda_1 &= \lambda E\left[X_3\right] + \mu_1 E\left[X_2\right] \\ &= \lambda\frac{\zeta}{\xi_1} + \mu_1\frac{\xi_2}{\xi_1} \end{aligned} \tag{4.19}$$

Next, we will calculate this expected time for low priority class. The distribution of the occurrence of the three events until the first successful slot selection of low priority class is given as $\phi_{(X_2,X_1,X_3)}(1, n_1, n_3)$. Hence,

$$\begin{aligned} \Lambda_2 &= \lambda E\left[X_3\right] + \mu_2 E\left[X_1\right] \\ &= \lambda\frac{\zeta}{\xi_2} + \mu_2\frac{\xi_1}{\xi_2} \end{aligned} \tag{4.20}$$

As in Section 4.2.1, we will define the representations:

$$\zeta_{(\psi,m,n,c)} = P\left[\Psi = \psi, C_1 = m, C_2 = n, \Upsilon = c\right] \tag{4.21}$$

$$\zeta_{(\psi|c)} = P\left[\Psi = \psi \,|\, \Upsilon = c\right] \tag{4.22}$$

$$\zeta_{(\psi,c)} = P\left[\Psi = \psi, \Upsilon = c\right] = \sum_{n}\sum_{m} \zeta_{(\psi,m,n,c)} \tag{4.23}$$

$$\zeta = P\left[\Upsilon = c\right] \tag{4.24}$$

where C_i is the random variable representing the number of colliding packets of class i, c indicates that a collision occurs in the first occupied slot. $\zeta_{(\psi,m,n,c)}$ is the probability that m high and n low priority nodes select the first occupied slot ψ and a collision occurs. $\zeta_{(\psi|c)}$ is the probability that ψ is the first occupied slot in a collision and $\zeta_{(\psi,c)}$ is the probability that ψ is the first occupied slot and a collision occurs.

The probability of collision, ζ, in a slot selection can be found as:

$$\zeta = 1 - \xi_1 - \xi_2 \tag{4.25}$$

Assume that t_c is the time required for the collision to be understood until the beginning of the new contention, which is referred as the collision timeout. By the definition of conditional probability, the expected time elapsed in one collision, λ, is

$$\begin{aligned} \lambda &= \sum_{\psi=1}^{x_3} \zeta_{(\psi|c)} \left(\psi - 1\right) t_s + t_c \\ &= \sum_{\psi=1}^{x_3} \frac{\zeta_{(\psi,c)}}{\zeta} \left(\psi - 1\right) t_s + t_c \end{aligned} \tag{4.26}$$

Finally, we should derive the expected time, μ_i, elapsed in one transmission of the opponent of class i. This is the sum of the expected time elapsed within a successful contention from the beginning of the contention window until the first occupied slot

and the time required for a successful transmission of a packet, t_{tr}. Hence,

$$\mu_1 = \Gamma_2 + t_{tr} \tag{4.27}$$

$$\mu_2 = \Gamma_1 + t_{tr} \tag{4.28}$$

where $t_{tr} = t_{rts} + t_{cts} + t_{data} + t_{ack}$. t_{rts}, t_{cts}, t_{data} and t_{ack} are the transmission duration of the RTS packet, the CTS packet, the data packet and the ACK packet respectively. The size and count of these packets depend on the MAC protocol design to be analyzed.

In order to derive Λ_i, we need to derive the probability $\zeta_{(\psi,c)}$, which can be found by deriving $\zeta_{(\psi,m,n,c)}$ as indicated in Equation 4.23. Initially, we shall distinguish three mutually disjoint reasons of collisions. These are the collisions caused by only high priority nodes, c_1, only low priority nodes, c_2 or mixture of both priorities, c_3. Note that the collision event $c = \bigcup_{i=1}^{3} c_i$ where $\forall i, j \in \{1,2,3\} \wedge i \neq j, c_i \cap c_j = \emptyset$.

When there are N_1 high priority nodes and N_2 low priority nodes, if only high priority nodes or low priority nodes are involved in collision, ψ should be chosen by any m high or n low priority nodes where $m, n \geq 2$ (collision events c_1 and c_2). If both high priority nodes and low priority nodes are involved in collision, ψ should be chosen by any m high and any n low priority nodes where $m, n \geq 1$. The remaining $N_1 - m$ high priority nodes and $N_2 - n$ low priority nodes select slots after ψ. Hence $\zeta_{(\psi,m,n,c)}$ and consequently $\zeta_{(\psi,c)}$ can be found as:

$$\zeta_{(\psi,m,n,c)} = \begin{cases} \chi_1(\psi)\tau\left(\psi,m,0\right) & ,\text{if } m \geq 2, n = 0 \ (c_1) \\ \chi_2(\psi)\tau\left(\psi,0,n\right) & ,\text{if } m = 0, n \geq 2 \ (c_2) \\ \chi_1(\psi)\chi_2(\psi)\tau\left(\psi,m,n\right) & ,\text{if } m > 0, n > 0 \ (c_3) \\ 0 & ,\text{if } otherwise \end{cases} \tag{4.29}$$

$$\zeta_{(\psi,c)} = \sum_{m=0}^{N_1}\sum_{n=0}^{N_2} \zeta_{(\psi,m,n,c)} \tag{4.30}$$

Note that when only one high priority or only one low priority node exists in the

neighborhood, no collision occurs in the neighborhood.

Finally, after substituting λ and μ_i in Λ_i, and substituting Λ_i and Γ_i in Ω_i, since $P[\Psi = \psi] = \xi_{(\psi,1)} + \xi_{(\psi,2)} + \zeta_{(\psi,c)}$, we get:

$$\Omega_1 = \left(t_c\zeta + t_{tr}\xi_2 + \sum_{\psi=1}^{x_3} P[\Psi = \psi]\,(\psi - 1)\,t_s\right)/\xi_1 \tag{4.31}$$

$$\Omega_2 = \left(t_c\zeta + t_{tr}\xi_1 + \sum_{\psi=1}^{x_3} P[\Psi = \psi]\,(\psi - 1)\,t_s\right)/\xi_2 \tag{4.32}$$

Note that $\tau(\psi - 1, 0, 0)$ is the probability of all nodes to select slots following $\psi - 1$ and $\tau(\psi, 0, 0)$ is the probability of all nodes to select slots following ψ. Hence

$$P[\Psi = \psi] = \tau(\psi - 1, 0, 0) - \tau(\psi, 0, 0) \tag{4.33}$$

4.3. Analysis of the Expected Energy Expenditures for Priority Classes

Network lifetime maximization is another crucial objective for wireless sensor networks. One of the main power consumption components is the energy consumed by the neighborhood of a node until it wins the contention, determined by the probabilities derived in Section 4.2. This energy consumed for the resolution of a contention has to be minimized in a good communication protocol. In this section, we derive the expected energy consumption of the neighborhood of the sensor that wins a contention depending on the priority class that it belongs to.

The energy consumed by the neighborhood of a single sensor consists of two energy consumption components: (i) the expected energy consumed for collisions, retrials and transmissions of the opponent priority class until the beginning of the collisionless slot selection, Θ_i, and (ii) the expected energy consumed for the carrier sensing within this successful contention from the beginning of the contention window until the first

occupied slot, where a node of desired priority wins contention, Φ_i.

Let E_{rx}, E_{idle} and E_{tx} be the energy consumed per second in the receive state of the antenna, in the idle state of the antenna, and in the transmit state of the antenna respectively. For each contention, each contending node chooses a contention slot and the entire nodes listen to the medium until the first occupied contention slot. Clearly, Φ_i equals the number of neighbor nodes listening to the medium times the expected duration of the carrier sense for the node of desired priority class, Γ_i, times the energy consumed per second for the listening process.

$$\begin{aligned}\Phi_i &= (N_1 + N_2 + M)\,\Gamma_i E_{idle} \\ &= \sum_{\psi=1}^{x_3} \frac{\xi_{(\psi,i)}}{\xi_i}\,(\psi - 1)\,t_s\,(N_1 + N_2 + M)\,E_{idle}\end{aligned} \tag{4.34}$$

The second energy consumption component is the expected total energy spent for the collisions, retrials and opponent priority class packet transmissions, Θ_i. The derivation of Θ_i is similar to the derivation of the corresponding latency component, Λ_i, since the energy components also relies on the expected number of the three outcomes of a contention solved by the negative multinomial distribution given by Equation 4.18.

The expected total energy spent for collisions, retrials and opponent priority class packet transmissions equals the sum of the expected number of collisions times the expected total energy elapsed in one collision, θ, and the expected number of transmissions of the opponent class times the expected total energy elapsed in one transmission of the opponent of class i, δ_i. Hence,

$$\begin{aligned}\Theta_1 &= \theta E\left[X_3\right] + \delta_1 E\left[X_2\right] \\ &= \theta\frac{\zeta}{\xi_1} + \delta_1\frac{\xi_2}{\xi_1}\end{aligned} \tag{4.35}$$

$$\begin{aligned}\Theta_2 &= \theta E\left[X_3\right] + \delta_2 E\left[X_1\right] \\ &= \theta\frac{\zeta}{\xi_2} + \delta_2\frac{\xi_1}{\xi_2}\end{aligned} \tag{4.36}$$

The number of contending nodes has to be incorporated by distinguishing the transmitting and the receiving nodes in the energy calculations. The expected total energy spent in one collision until its retrial, θ, is:

$$\theta = \sum_{\psi=1}^{x_3} \sum_{m=m_0}^{N_1} \sum_{n=n_0}^{N_2} \frac{\zeta_{(\psi,m,n,c)}}{\zeta} \dot{\theta}\left(\psi, m+n\right) \tag{4.37}$$

where $m_0 = 2 - \min(2, N_2)$, $n_0 = 2 - \min(2, m)$, $N_1 + N_2 \geq 2$ and $\dot{\theta}\left(\psi, m+n\right)$ is the total energy consumed for one retrial if the first selected slot is ψ and $m+n$ nodes out of $N_1 + N_2 + M$ select that slot, which is formulated as

$$\begin{aligned} \dot{\theta}\left(\psi, k\right) &= \left(N_1 + N_2 + M\right)\left(\psi - 1\right) t_s E_{idle} \\ &+ k\left(t_{rts} E_{tx} + t_{tout} E_{idle}\right) \\ &+ \left(N_1 + N_2 + M - k\right)\left(t_{rts} E_{rx} + t_{tout} E_{idle}\right) \end{aligned} \tag{4.38}$$

where t_{tout} is the timeout duration required after the collision for the collision to be understood where $t_c = t_{rts} + t_{tout}$.

Finally, we should derive δ_i, the expected energy elapsed in one transmission of the opponent of class i. This is equal to the expected energy consumed within a successful contention from the beginning of the contention window until the first occupied slot which is the Φ energy component of the opponent class. Since recent MAC layer protocols involve virtual carrier sensing mechanisms, contending nodes only receive RTS packets. Hence,

$$\begin{aligned} \delta_1 &= \Phi_2 + t_{rts} E_{tx} + \left(N_1 + N_2 + M - 1\right) t_{rts} E_{rx} \\ &+ t_{cts} E_{rx} + t_{data} E_{tx} + t_{ack} E_{tx} \end{aligned} \tag{4.39}$$

$$\begin{aligned} \delta_2 &= \Phi_1 + t_{rts} E_{tx} + \left(N_1 + N_2 + M - 1\right) t_{rts} E_{rx} \\ &+ t_{cts} E_{rx} + t_{data} E_{tx} + t_{ack} E_{tx} \end{aligned} \tag{4.40}$$

4.4. Effect of the Contention Window Partitioning Strategy

In this section, we explore the effect of the contention window size and the partitioning strategies on the latency and the energy expenditure for a successful transmission of each priority class for various number of contending nodes. In addition, we verify the analytical results derived in Section 4.2 and 4.3 using simulations implemented in MATLAB [80]. Each simulation instance consists of 10000 iterations. Along each run, we collected the number of successful contentions of each priority class and the number of collisions for a fixed contention window size (x_3), the partitioning strategy (determined by x_1 and x_2) and number of contending nodes in each priority class (N_1 and N_2). Moreover, the energy expenditures and the time required to initiate a successful data transmission is gathered counting in the statistics collected for collisions prior to a successful contention. We do not present the simulations for the cases where the number of collected samples in 10000 iterations is insufficient to form a statistic value. In addition, the simulation results of some selected statistics are presented for the validation of the analytical results to improve the presentation quality in the figures. The simulation parameters are listed in Table 4.1.

4.4.1. Effect of the Partitioning Strategy on the Probability of Success and Collision

As we recall from Section 4.2, the probability of success is one of the main factors affecting the contention latency. Figure 4.3 presents the probability of success for both priority classes, ξ_1 and ξ_2, for varying x_1 values. The probabilities for high priority nodes are shown to converge, overlap on distinct lines forming a group for each N_1 value regardless of the number of low priority nodes in Figure 4.3a. The grouping behavior demonstrates the dominance of the chosen α region in slot selection, and hence, the number of high priority nodes. It should be noted that the convergence of lines are ordered in decreasing order of high priority node count, since a higher number of nodes results in more collisions. For a constant x_2 value of 64 slots, increasing x_1 extends the α region and curtails the β region where the low priority nodes are

Table 4.1. Simulation parameters for the proposed contention model.

Parameter	**Value**
#Sensors in Neighborhood	30 sensors
#Contending High Priority Nodes	5*/10/15 sensors
#Contending Low Priority Nodes	5*/10/15 sensors
Data Packet Size	200 bits
RTS/CTS/ACK/SYNC Size	20 bits
Slot Size	20 bits
Timeout duration (in bits)	30 bits
Contention Window Size (slots)	96
x_1 (slots)	0-x_2 (32*)
x_2 (slots)	x_1-96 (64*)
Channel Bitrate	20 Kbps
TX Power	200mW
RX Power	80mW
IDLE Power	80mW

* These are the default values used in the simulations.

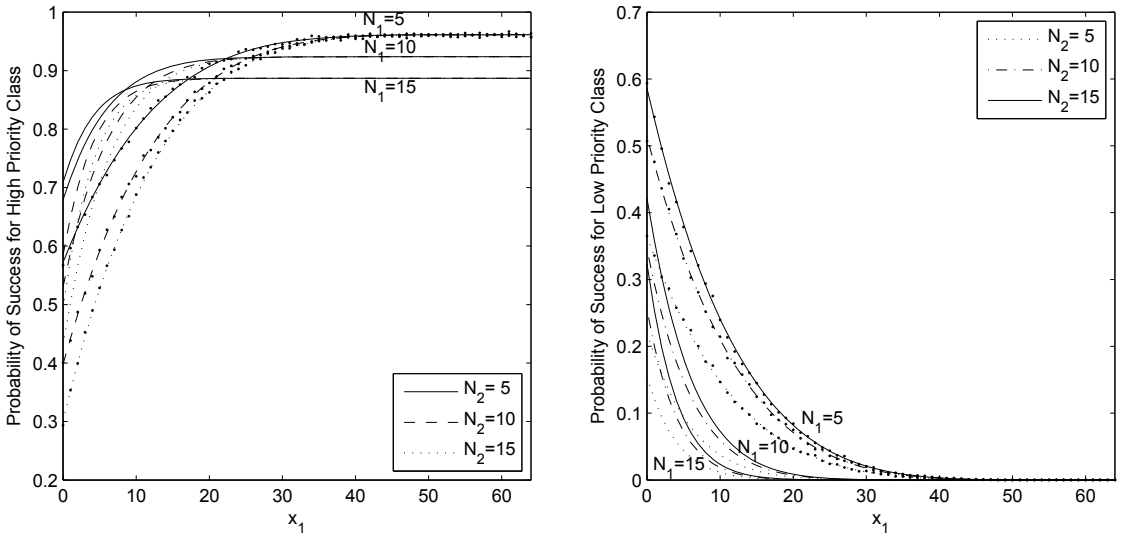

(a) (b)

Figure 4.3. Probability of success for varying x_1: (a) for high priority class. (b) for low priority class.

allowed to win the contention in the presence of the high priority nodes. Hence, the increase in x_1 brings about the resource starvation problem for the low priority class

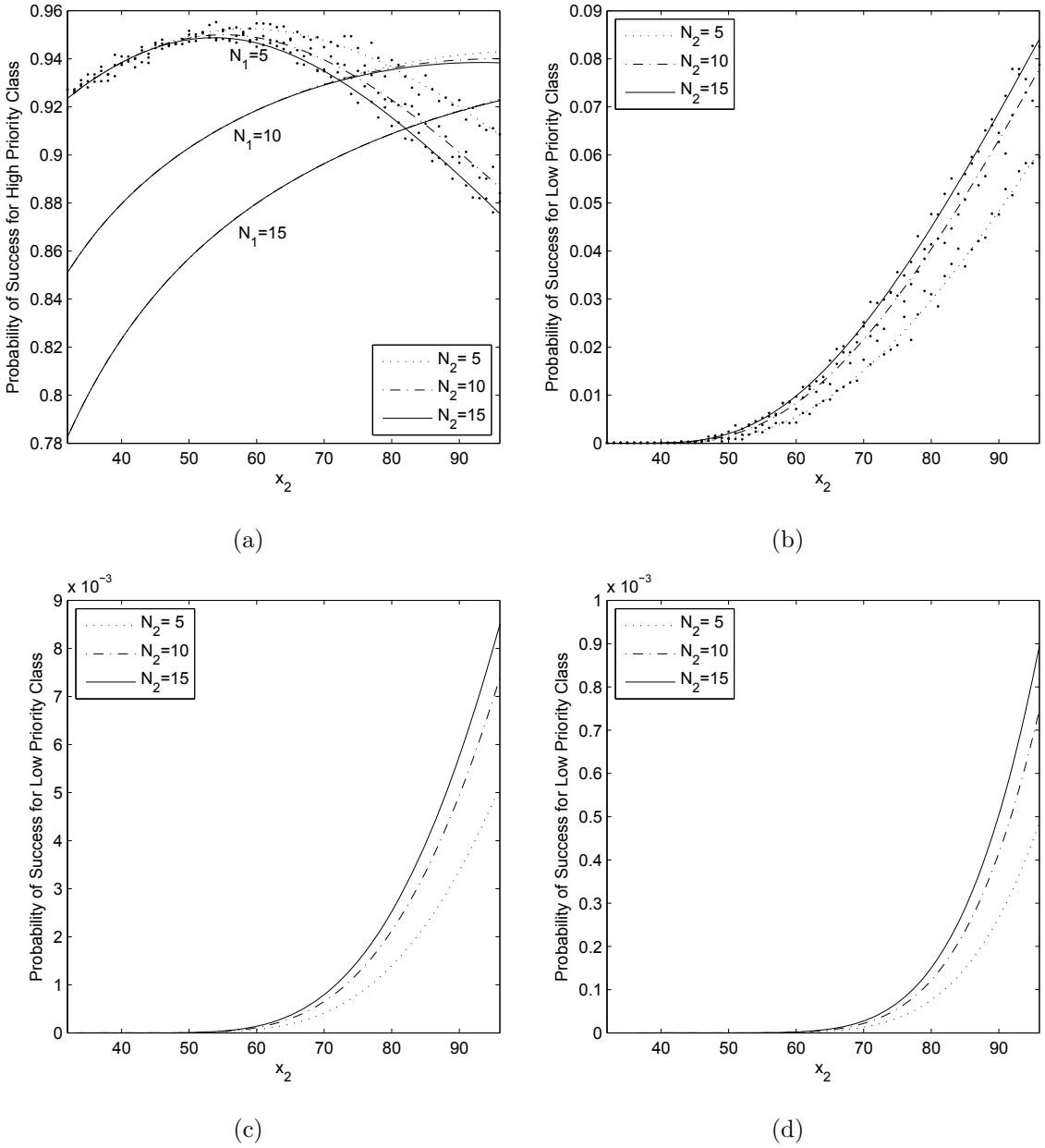

Figure 4.4. Probability of success for varying x_2: (a) for high priority class. (b) for low priority class when $N_1 = 5$. (c) for low priority class when $N_1 = 10$. (d) for low priority class when $N_1 = 15$.

in the contention. The negative effects of the starvation can be summarized as the increased idle listening induced by the α region, the increased success probability of high priority class in the α region and the reduced success probability of low priority class in the β region, delaying the transmission of low priority packets. These effects bring about the problem of exponential decrease in the number of low priority wins (Figure 4.3b). In spite of the exacerbation of the negative effects of the starvation on the

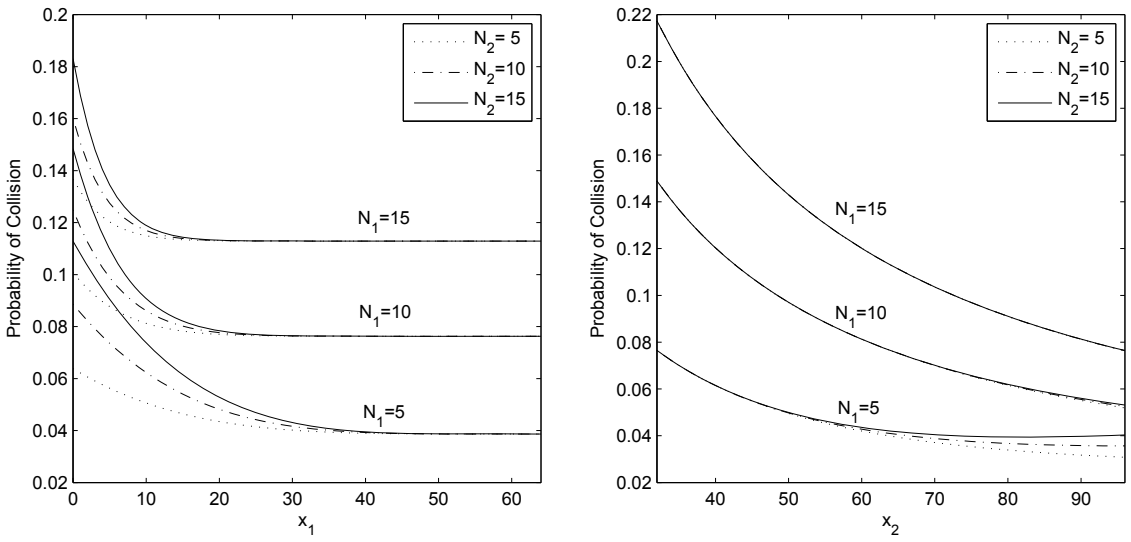

(a) (b)

Figure 4.5. Probability of collision: (a) with respect to x_1. (b) with respect to x_2.

low priority class, the success rate of the high priority class is increasing logarithmically and negligibly affected by the size of the α region after a certain x_1 value for a given high priority node count. After this value, since the success rate is not affected significantly, the increase in the size of α region causes a tradeoff between the increase and the decrease in the success probabilities of the high and low priority classes respectively. In addition, the probability of collision decreases as the size of the β region decreases since the probability of the first occupied slot to be in β and a low priority node to choose that slot decreases. Consequently, the effect of low priority nodes on the probability of collision decreases (Figure 4.5a). Hence being the determining factor in this tradeoff, x_1 value should be chosen properly to optimize the medium access latency. The simulation results for the $N_1 = 5$ group are presented in both figures to show that they match with the analytical results.

The success probabilities when x_2 is increased for a constant x_1 value of 32 slots are presented in Figure 4.4. In Figure 4.4a, the probabilities with same N_1 count form groups. These groups overlap and separate after the peak point for a given number of high priority nodes. The increase in x_2 extends the β region, which increases the number of slots to contend for both priority classes. The size of the β region brings about another tradeoff between the success probabilities of both priority classes. For

smaller values of x_2, the likelihood of low priority nodes to select the first occupied slot in β region is smaller, and the success probability of the high priority class increases. The ratio of β region size in both the low priority and the high priority contention windows increases with x_2 which exponentially increases the success probability of low priority class and exponentially decreases the collision probability in the β region (Figure 4.5b). Hence the success probability of the high priority class deteriorates and it starts to decrease after reaching its peak point. The success probability of the low priority class for different number of high priority nodes are presented in Figure 4.4b-d separately since there is a 10-fold increase in the success probability for given N_1 values. Also note that, the collision probability tends to increase after a certain x_2 value since the β region will grow sufficiently, so that all nodes select a slot in β with high probability, which increases the collision probability. The simulation results for the $N_1 = 5$ group are presented in both figures to show that they match with the analytical results.

4.4.2. Effect of the Non-Existence of the Opponent Class on the Contention Latency

In Figure 4.3b, we stated the increased idle listening time as one of the negative effects of the starvation induced by growing x_1. In order to analyze the effect of x_1 and x_2 on the contention latency for both priority classes, we demonstrate the average latency and corresponding simulation results in the presence of only one priority class in Figure 4.6a and Figure 4.6b. In the high priority case, the probability of success is affected only by the increase in x_2, which can be considered as a contention window analyzed in [44] in the non-existence of low priority class. The optimal number of contention window size to achieve a minimum latency is found to be below 20 slots. A higher value for the x_2 value will improve the success probability but will result in an excessive idle listening time.

The effect of starvation caused by α region is apparent in Figure 4.6b. In this case, the probability of success is affected only by the x_1 value, separating the α region from the β and γ regions. The probability of success for a given low priority node

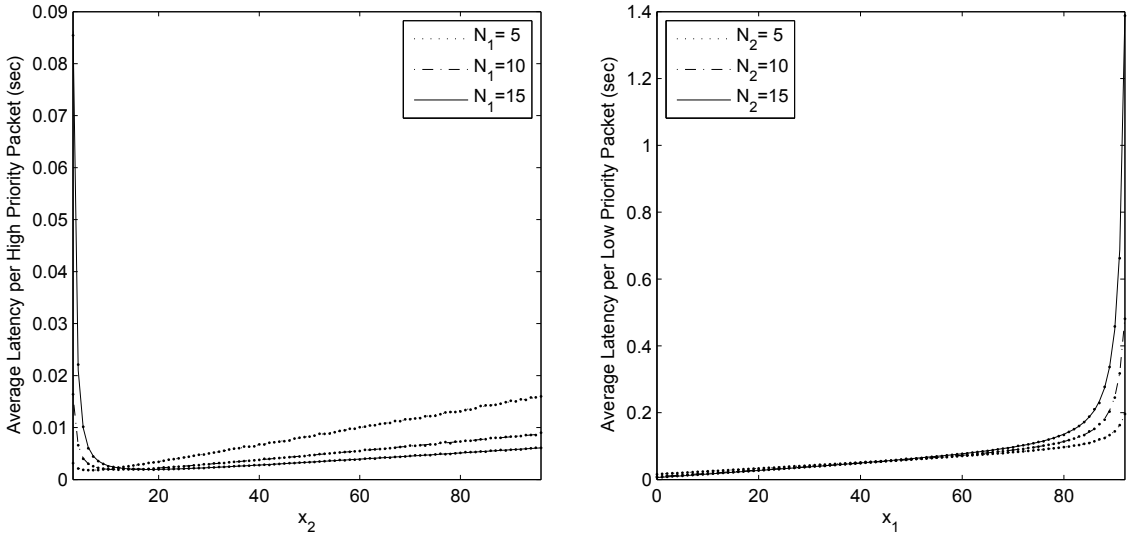

(a) (b)

Figure 4.6. Average latency in the non-existence of the opponent priority class: (a) for high priority class. (b) for low priority class.

count and x_1 value is the same as the probability of success for the same number of high priority nodes where $x_2 = x_3 - x_1$. However, for each x_1 value, an additional idle waiting time is added to the latency results as the starvation component which clearly grows with the x_1 value.

4.4.3. Effect of the Partitioning Strategy on the Contention Latency

The average contention latency for both priority classes and the corresponding simulation results for varying x_1 value are presented in Figure 4.7 where x_2 value is set to 64 slots. The convergence phenomenon in Figure 4.3a is also observed apparently in the latency performances. The results again form three groups with respect to their N_1 values. Since, the probability of success for the high priority class logarithmically increases with the x_1 value, the average latency per transmitted packet exponentially decreases in Figure 4.7a. Moreover, lower number of high priority nodes suffer more latency due to increased idle listening. This phenomenon is caused by the increase in the expected ψ value as number of contenders decrease. The latency results for the low priority contention for different number of high priority nodes are presented in Figure 4.7b-d. We observe a 33-fold increase in the latency of the low priority class for

given N_1 values. Although the presented results are infeasible for the network operation, we present them to show the extent of performance degradation with increasing x_1 value. The selection of an improper x_1 value exacerbates the starvation effect which exponentially increases the expected contention latency for low priority nodes and is even more crucial for the cases where higher number of high priority nodes contend. The simulation results for the $N_1 = 5$ group are presented in both figures to show that

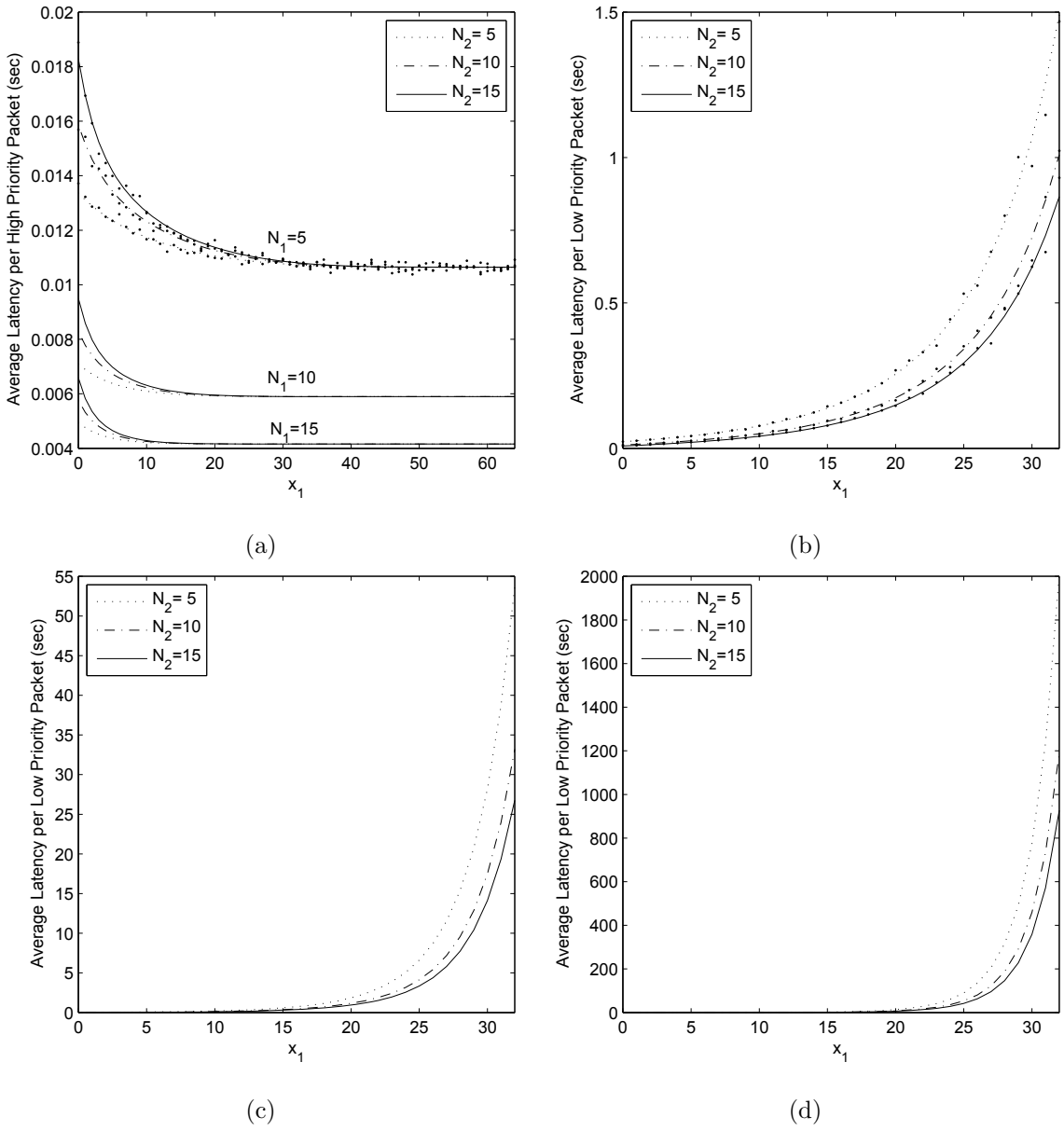

Figure 4.7. Average latency for varying x_1: (a) for high priority class. (b) for low priority class when $N_1 = 5$. (c) for low priority class when $N_1 = 10$. (d) for low priority class when $N_1 = 15$.

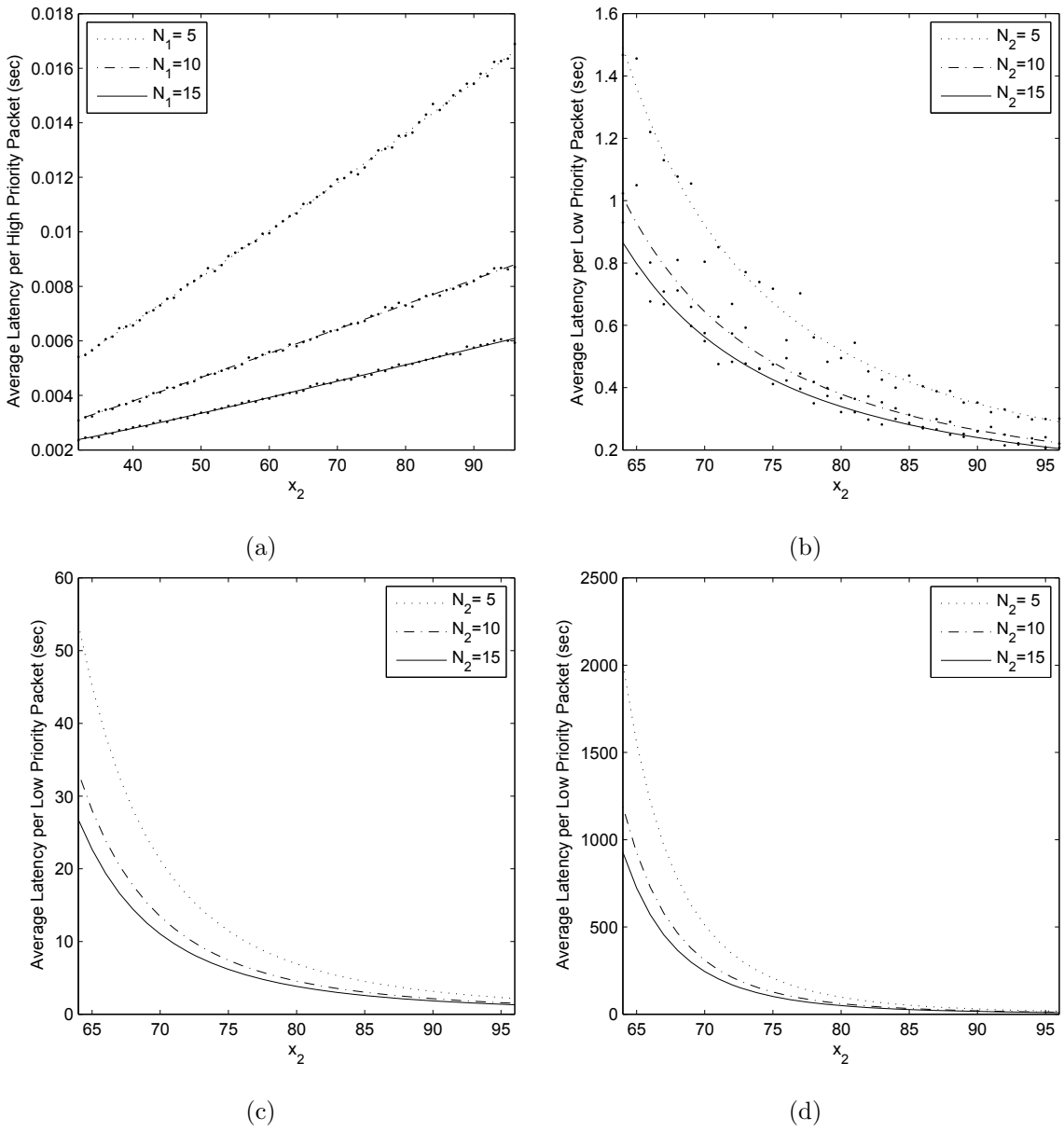

Figure 4.8. Average latency for varying x_2: (a) for high priority class. (b) for low priority class when $N_1 = 5$. (c) for low priority class when $N_1 = 10$. (d) for low priority class when $N_1 = 15$.

they match with the analytical results.

When the x_2 value is varied for a fixed x_1 value of 32 slots, the expected contention latency results for a given number of high priority nodes are very close to each other. Hence, we only illustrate the cases where $N_2 = 5$ in Figure 4.8a. The latencies are almost linearly increasing and diverging from each other. This behavior is a consequence of the significant increase in the idle listening time which is mainly caused

by the increase in the high priority contention window size and is reduced for higher number of contenders. These results match with the ones observed for the high priority class in the non-presence of the low priority nodes in Figure 4.6a. The low priority latencies are exponentially decreasing in Figure 4.8b-d, since the success probability increases exponentially with x_2 (Figure 4.4). The increase in N_1 causes a 33-fold increase in the low priority class latency. We again present these results to show the extent of performance degradation with increasing x_2 value. The simulation results for all cases in Figure 4.8a and the $N_1 = 5$ group in Figure 4.8b are presented in both figures to show that they match with the analytical results.

The effect of the β region of size 32 slots on the contention latency performance of both priority classes is presented in Figure 4.9. In these figures, the β region slides from the beginning to the end of the contention window. The latency performance of the high probability class shows similar behavior with Figure 4.6a. The phenomenon of grouping with respect to N_1 is also observed in this figure. As the contention window size of the high priority class grows with x_2, the probability of success increases, the collision probability decreases and the duration of idle listening increases. In addition, when the β region is near the beginning of the contention window, the expected number of contenders to select the first occupied slot will increase. In other words, the high priority class will benefit from the short idle listening time, but will suffer from the low priority wins, increased number of contenders and high number of collisions. As the β region slides towards the end of the contention window, the low priority class starts to starve with the increase in the size of the α region. The success probability of the low priority class decreases due to this starvation and the probability of collision decreases since the expected number of nodes in a collision decreases. Hence, the high priority class latency decreases. However, nodes suffer from the increased idle listening time, caused by too much increase in the α region size, which brings about an increase in the contention latency. The low priority class always suffers from exacerbated starvation induced by the α region size and the length of its contention window size (Figure 4.9b-d). Hence, the low priority class latency is exponentially increasing. The increase in N_1 causes a 33-fold increase in the latency of the low priority class. These results are again presented to show the extent of performance degradation with increasing x_1 value.

Figure 4.10 presents the joint effect of x_1 and x_2 on the contention latency of both priority classes. As a demonstrative example, we present the results for the case where $N_1 = 5$ and $N_2 = 5$. The average latency is at most 21 ms for the high priority packet (Figure 4.10a). We can see that for smaller values of x_1 and x_2, the probability of collision is very high, and hence, the latency is high due to high probability of collision. The β region negatively affects the latency for the high priority class, since the number

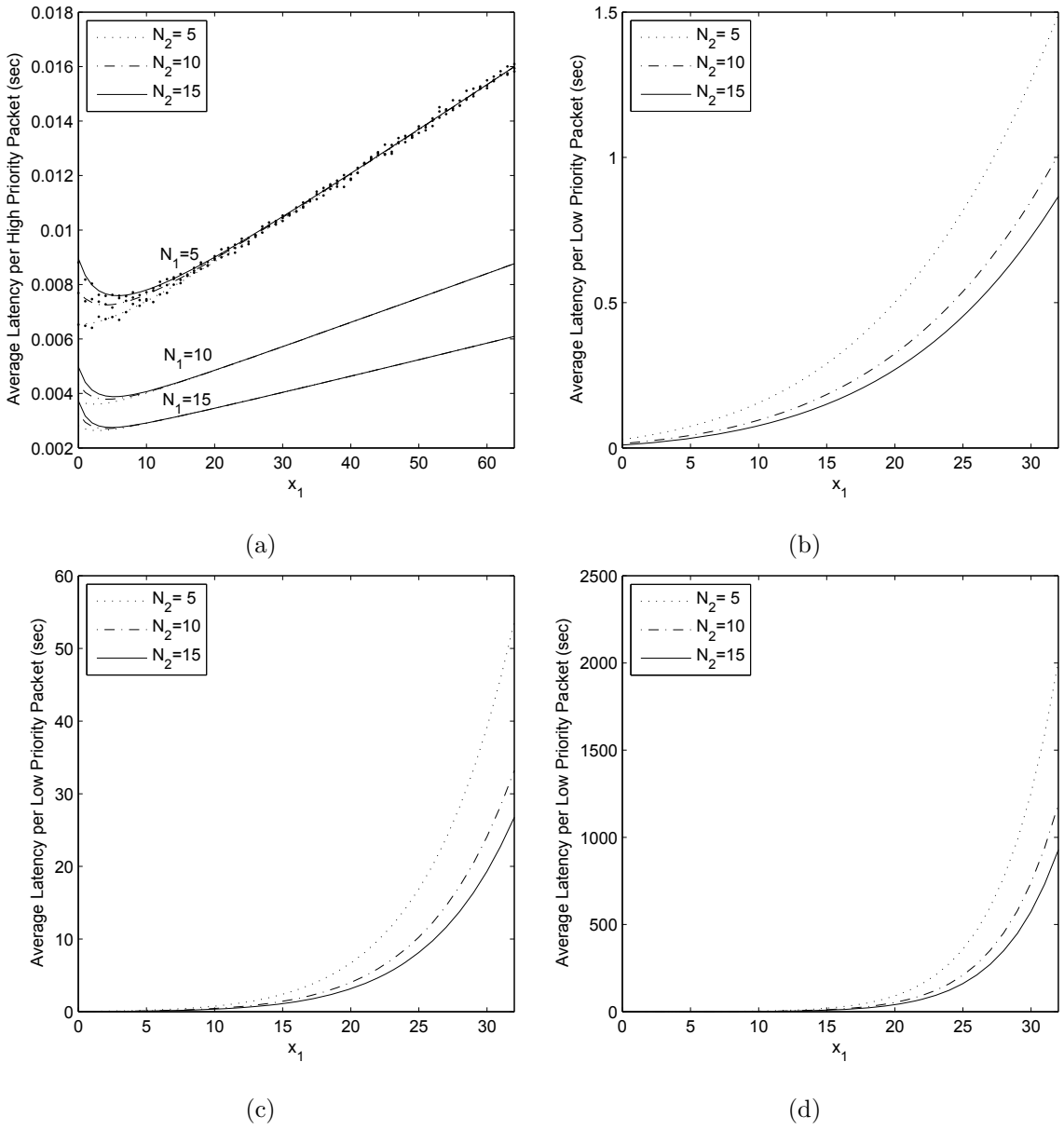

Figure 4.9. Average latency where $x_2 - x_1 = 32$: (a) for high priority class. (b) for low priority class when $N_1 = 5$. (c) for low priority class when $N_1 = 10$. (d) for low priority class when $N_1 = 15$.

of nodes in the contention increases, causing an increase in the probability of collision and a decrease in the probability of success. Hence, for any x_2 value, the highest and the lowest latency results are attained when $x_1 = 0$ (the size of the α region is 0 and the size of the β region is x_2) and $x_1 = x_2$ (the size of the α region is x_2 and the size of the β region is 0) respectively. The minimum value is achieved to be 1.78 ms when $x_1 = 6$ and $x_2 = 6$. For greater x_2 values, the latency performance degrades due to the increased idle listening time.

However, for the low priority class, the starvation deteriorates the latency performance. In Figure 4.10b, we present the latency results smaller than one second, since a higher latency is infeasible and assigning a β region to the low priority class in these conditions unnecessarily degrades the performance of the high priority class. In this case, many (x_1,x_2) tuples are eliminated since the resulting average latency exceeds one second. The latency is shown to increase exponentially as the size of the β region decreases, and hence, the size of the α region increases, which is the main factor in the starvation of the low priority class. Hence for any x_2 value, the highest and the lowest latency results are attained when $x_1 = x_2$ (the size of the α region is x_2 and the size of the β region is 0) and $x_1 = 0$ (the size of the α region is 0 and the size of

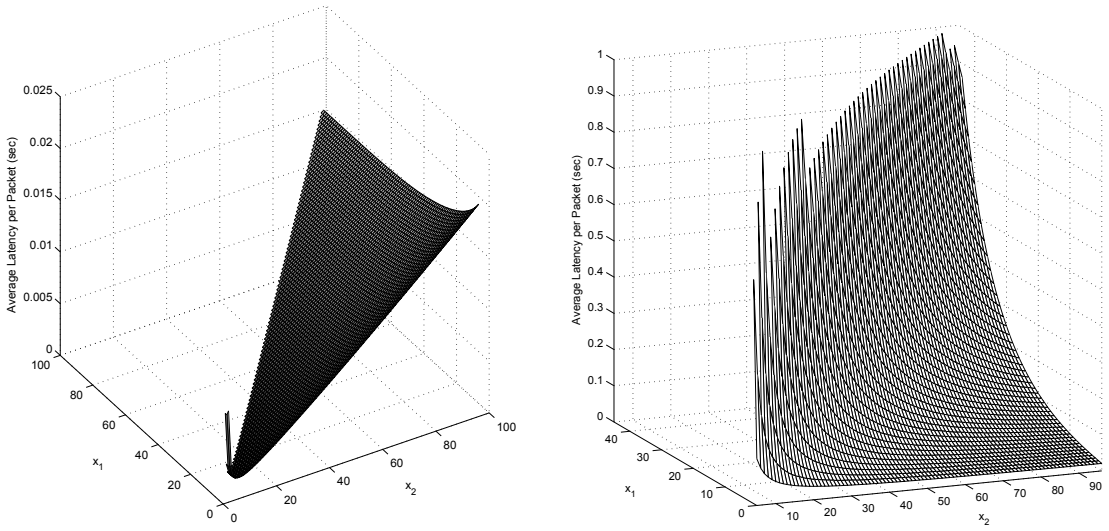

(a) (b)

Figure 4.10. Average latency for varying x_1 and x_2 where $x_2 \geq x_1$: (a) for high priority class. (b) for low priority class.

the β region is x_2) respectively. The minimum value is achieved to be 20.52 ms when $x_1 = 0$ and $x_2 = 96$. For smaller x_2 values, the latency performance degrades since the expected number of low priority nodes selecting a slot in β decreases. For greater x_1 values, the size of the α region increases, which causes an exponential increase in the latency of the low priority class. Hence, there is a tradeoff between the latency of the high priority packets, which improves for the x_1 values where $x_1 = x_2$, and the latency of the low priority packets, which improves for the x_1 values where $x_1 = 0$.

4.4.4. Effect of the Partitioning Strategy on the Energy Expenditure

Figure 4.11 presents the joint effect of x_1 and x_2 on the average energy expenditure in the neighborhood for both priority classes where $N_1 = 5$ and $N_2 = 5$. The presented energy expenditures exhibits a similar behavior with the latency results in Figure 4.10, since both results depend on the same success and collision probabilities. The minimum energy expenditure is at most 44 mJ for the high priority packet (Figure 4.11a). As in the latency case, we can see that for smaller values of x_1 and x_2, the probability of collision is very high, which significantly increases the energy expenditure in the neighborhood. For any x_2 value, the highest and the lowest latency results are attained

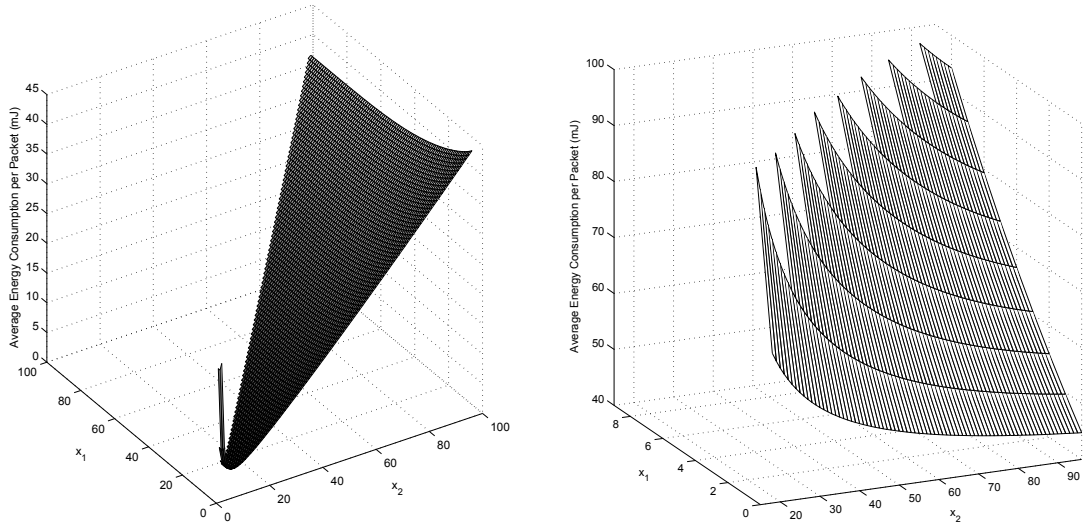

(a) (b)

Figure 4.11. Average energy consumption for varying x_1 and x_2 where $x_2 \geq x_1$: (a) for high priority class. (b) for low priority class.

when $x_1 = 0$ (the size of the α region is 0 and the size of the β region is x_2) and $x_1 = x_2$ (the size of the α region is x_2 and the size of the β region is 0) respectively. The minimum value is achieved to be 4.42 mJ when $x_1 = 7$ and $x_2 = 7$. For greater x_2 values, the latency performance degrades due to the increased idle listening.

Similarly, for the low priority class, the starvation deteriorates the latency performance. In Figure 4.11b, we present the neighborhood energy expenditure results smaller than 100 mJ. In this case, most of the (x_1,x_2) tuples are eliminated since their resulting energy expenditures exceed 100 mJ. The results exhibit an exponential increase with the α region size due to starvation. Hence for any x_2 value, the highest and the lowest energy expenditure results are attained when $x_1 = x_2$ (the size of the α region is x_2 and the size of the β region is 0) and $x_1 = 0$ (the size of the α region is 0 and the size of the β region is x_2) respectively. The minimum value is achieved to be 44.76 mJ when $x_1 = 0$ and $x_2 = 96$. As in the low priority latency case, for smaller x_2 values, the energy expenditure decreases with the expected number of low priority nodes selecting a slot in β. For greater x_1 values, the energy expenditure for the transmission of the low priority class increases exponentially with the size of the α region. Hence, the same tradeoff in the latency case is also observed here. Note that the minimum value of the low priority energy expenditure is greater than the maximum value of the high priority energy expenditure.

5. ADAPTATION OF PRIORITIZED CONTENTION ANALYSIS FOR DUTY CYCLED SENSOR NETWORKS

One of the main objectives in a wireless sensor network design is to minimize the energy expenditure because of the limited energy budget of the sensors. SMAC introduces the low-duty-cycle operation on nodes in a multi-hop network which reduces idle listening by periodically putting nodes into sleep state. The analysis in the previous chapter provides a generic model for the prioritized uniform contention schemes. This chapter incorporates the contention analysis approach of [44] into the analysis of the duty cycled operation of SMAC by taking the data size into account which has a joint impact with the duty cycle and the contention window size on the throughput and the energy expenditure of an SMAC cluster.

Prior to the derivation of the analysis for the duty-cycle based prioritized contention case, we need to provide a model for the duty-cycled structure of SMAC. We will explore the effect of operational parameters of SMAC such as the duty cycle, the contention window size and the data size on the performance in terms of throughput and energy expenditure.

5.1. SMAC Model

For the sake of completeness, we will briefly describe the SMAC operation and introduce the system parameters that will be used in the analysis. The basic scheme of SMAC [18] is shown in Figure 5.1. Each node sleeps for a duration of T_{sleep} and then wakes up to see if any other node wants to talk to it. During the sleep period, the node turns off its radio, and sets a timer to awake itself later. The complete cycle of awake and sleep is called a frame. The awake interval is composed of synchronization and listen periods. In the synchronization period, nodes exchange their schedules by periodically broadcasting a SYNC packet to their immediate neighbors. In the listen period, if a node has data to deliver, it contends for the medium, otherwise it listens to

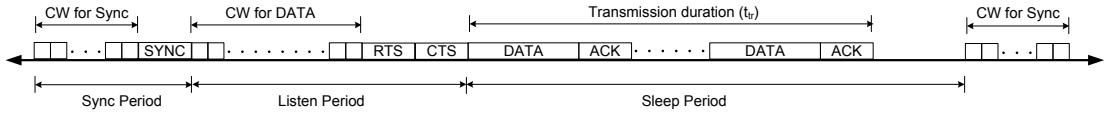

Figure 5.1. Frame structure of SMAC.

see if a neighbor wants to deliver a packet to it. Each period has a contention window with many time slots for senders to perform carrier sense. For example, if a sender wants to send a SYNC packet, it starts carrier sense when the receiver begins listening. It randomly selects a time slot to finish its carrier sense. If it has not detected any transmission by the end of that time slot, it wins the contention and starts sending its SYNC packet. A similar procedure is followed while sending data packets. If two or more awake nodes have data packets to send, and select the same slot in the contention period, these nodes experience a collision in that frame. Hence, the data transmission in that SMAC frame fails due to collision and all nodes in the neighborhood of collision sleeps until the next SMAC frame. The medium access attempts by the nodes to transmit packets are postponed to the contention period of the subsequent SMAC frame. If no collision occurs in the contention, the winner node transmits its data packet, while the other nodes not involved in the communication sleep until the end of the transmission according to the overhearing avoidance mechanism of SMAC. At the end of the data transmission, the communicating nodes sleep until the beginning of the subsequent SMAC frame.

SMAC applies message passing to reduce application-perceived latency and control overhead. A message is the collection of meaningful, interrelated units of data. SMAC fragments the long message into many small fragments, and transmit them in a burst to decrease the penalty of accumulated contention latency for individual fragments. Only one RTS packet and one CTS packet are used. They reserve the medium for transmitting all the fragments. Every time a data fragment is transmitted, the sender waits for an ACK from the receiver. If it fails to receive the ACK, it will extend the reserved transmission time for one more fragment, and re-transmit the current fragment immediately.

Typically, the duration of synchronization (T_{sleep}) and listen periods (T_{listen}) are determined as the time required for the contention window in that period plus the time required to send a SYNC packet or the time required to send RTS and CTS packets, respectively. The duty cycle (r_{dc}) is defined as the ratio of the awake interval (T_{active}) to the frame length (T_{frame}). The size of each period is normally fixed according to physical-layer and MAC parameters such as the radio channel bitrate (c) and the contention window sizes for the data period (W) and the SYNC period (W_s). The contention window actually considers the number of slots that will be used for idle waiting to prevent collision selected from a range of $[0, CW_{max}]$ slots. However, for the sake of analytical simplicity, we concentrate on the slot index in which the transmission occurs and which is selected from the range of $[1, CW_{max} + 1]$ slots. Therefore, we assume that the contention window mentioned in this thesis is analogous to the slot selection range. The frame length, the duration of the sleep period and the transmission duration (T_{tr}) can be calculated as:

$$\begin{aligned} T_{frame} &= T_{active}/r_{dc} \\ &= (T_{sync} + T_{listen})/r_{dc} \\ &= ((W_s - 1)t_{slot} + t_{SYNC} \\ &\quad + (W - 1)t_{slot} + t_{RTS} + t_{CTS})/r_{dc} \\ T_{sleep} &= T_{active}(1 - r_{dc})/r_{dc} \\ T_{tr} &= n(t_{DATA} + t_{ACK}) \end{aligned} \tag{5.1}$$

where t_{slot}, t_{SYNC}, t_{RTS}, t_{CTS}, t_{DATA}, t_{ACK} are the durations for a single contention slot and n is the packets of SMAC in a channel of bitrate c bits per second.

5.2. Throughput and Energy Expenditure Analysis of SMAC

In this section, we will derive the expected time and the expected energy expenditures of a heavily loaded virtual cluster of SMAC with constant number of contenders to finalize a transmission successfully. The nodes in a cluster are assumed to be the immediate neighbors of each other. The analysis aims to inspect the interdependency

between the number of contenders, contention window size, duty cycle and data size. The throughput of the virtual cluster is obtained using the expected time analysis.

5.2.1. Expected Time to Finalize a Transmission

The expected time in terms of SMAC frames required for a successful data transmission, Ω', is defined as the duration between the start of the frame where the contention for the data begins to the end of the frame, in which the data transmission is finalized. Hence Ω' can be decomposed into two phases: Λ, the expected duration consumed for the frames in which collision occurs and Γ', the expected duration of the frames in which the contention is successful and transmission is finalized. If the transmission duration is longer than the sleep interval which is determined by the duration of active interval and the duty cycle, data transmission may last more than one frame, which should be considered in the derivation of Γ'. The equations for these components are derived in terms of the contention window size, W, number of contending nodes, N, and SMAC duration parameters. We assume that each contending node selects a slot independently and uniformly from the slots $1 \dots W$.

Initially, we define the following single-priority probabilities:

$$\tau(\psi, m) = P[\Psi = \psi, C = m] \tag{5.2}$$

$$\xi_{(\psi)} = P[\Psi = \psi, \Upsilon = success] = \tau(\psi, 1) \tag{5.3}$$

$$\xi = P[\Upsilon = success] \tag{5.4}$$

where Ψ, C and Υ are random variables for the first occupied slot number in a slot selection, the number of colliding nodes and the status of the slot selection respectively.

Clearly, as we recall the definition of $\tau(\psi, m, n)$ from Section 4.2.1, we can derive

$\tau(\psi, m)$ under the assumption of single priority case by:

$$\tau(\psi, m) = \begin{cases} \frac{\binom{N}{m}(W-\psi)^{N-m}}{W^N} & , \text{if } N > 1 \\ \frac{1}{W} & , \text{if } N = 1 \end{cases} \tag{5.5}$$

The derivations of Λ and Γ' are based on the probability of a contention to be successful, ξ. Since the successful contention means that the first occupied slot ψ is selected by only one node, we need the probability of successful slot selection for each ψ. The success probability, ξ, and therefore the collision probability, ζ are found as:

$$\begin{aligned} \xi &= (1 - \zeta) \\ &= \sum_{\psi=1}^{W} \tau(\psi, 1) \\ &= N \frac{\sum_{\psi=1}^{W} (W - \psi)^{N-1}}{W^N} \end{aligned} \tag{5.6}$$

In order to derive Γ', initially we need to calculate α_ψ, the number of SMAC frames required to finalize a data transmission, when slot ψ is selected. Since the winner node transmits its RTS packet in the slot ψ, the time required for the medium access is $(\psi - 1)t_{slot}$. The durations of synchronization period (T_{sync}), and transmission durations of RTS (t_{RTS}), CTS (t_{CTS}) and data packets (T_{tr}) can be calculated as presented in Equation 5.1. Hence,

$$\alpha_\psi = \left\lceil \frac{T_{sync} + (\psi - 1)t_{slot} + t_{RTS} + t_{CTS} + T_{tr}}{T_{frame}} \right\rceil \tag{5.7}$$

Since we know that the contention is successful in the current SMAC frame, now we need to calculate the probability of the first selected slot to be ψ given that it is

selected by only one node. By the definition of the conditional probability,

$$\begin{aligned} \Pr[\Psi = \psi | \Upsilon = success] &= \frac{\tau(\psi, 1)}{\xi} \\ &= \frac{(W-\psi)^{N-1}}{\sum_{f=1}^{W} (W-f)^{N-1}} \end{aligned} \tag{5.8}$$

Therefore,

$$\Gamma' = \sum_{\psi=1}^{W} \frac{\tau(\psi, 1)}{\xi} \alpha_{\psi} T_{frame} \tag{5.9}$$

In SMAC, if a collision occurs in a slot selection in a frame, the retrial will be postponed to the next frame. Therefore, the derivation of Λ is based on the expected number of SMAC frames, β, in which the contention resolution results with collision before a successful data transmission. Since contentions in each SMAC frame are independent and random events, contentions can be modeled as a Bernoulli trial with success and fail probabilities of ξ and ζ as in [44], and therefore

$$\beta = \frac{1}{\xi} - 1 \tag{5.10}$$

Hence, the expected time spent for collisions and retrials, Λ, equals the expected number of SMAC frames elapsed before the frame in which the successful data transmission starts, β, times the time elapsed in each retrial, T_{frame}.

$$\begin{aligned} \Lambda &= \beta T_{frame} \\ &= \left(\frac{1}{\xi} - 1 \right) T_{frame} \end{aligned} \tag{5.11}$$

Since we derived the durations of the phases Λ and Γ', we combine Equation 5.11,

Equation 5.8 and Equation 5.9 to find the expected time in terms of SMAC frames required for a successful data transmission, Ω':

$$\begin{aligned}\Omega' &= \Lambda + \Gamma' \\ &= \left(\left(\frac{1}{\xi} - 1 \right) + \sum_{\psi=1}^{W} \frac{(W-\psi)^{N-1}}{\sum_{f=1}^{W} (W-f)^{N-1}} \alpha_\psi \right) T_{frame} \end{aligned} \tag{5.12}$$

T_{frame} and therefore α_ψ in Equation 5.7 depends on r_{dc} in Equation 5.1. The transmission duration, T_{tr} is independent from T_{sync} and T_{listen} which are constant for given W and W_s values. However, the duration of SMAC frame, T_{frame}, is determined by T_{sync} and T_{listen} together with the duty cycle, r_{dc}. W and N parameters jointly determine the number of collisions before successful contention and the expected slot number, ψ^*, where the first successful slot selection occurs. ψ^* and r_{dc} jointly determine the number of SMAC frames required for the transmission to finalize.

Note that, $1 \,/\, \Omega'$ gives the system throughput of the contending neighborhood in terms of message per second where a message is the data unit composed of many packets via the message passing function of SMAC.

5.2.2. Expected Energy Expenditure to Finalize a Transmission

As in Section 5.2.1, the energy consumption of a virtual cluster until the end of successful data transmission, E_{tot}, can be decomposed into two components: Θ, as the total energy consumption in the neighborhood during collisions and, Φ as the total energy consumption in the neighborhood within the SMAC frames containing the successful contention and the data transmission. The equations for these components are derived in terms of the contention window size, W, number of contending nodes, N, number of idle nodes that do not have data to send, M and SMAC duration parameters. We assume that each contending node selects a slot independently and uniformly from the slots $1 \ldots W$.

In order to derive the energy consumption in the Θ component, we need to calculate the probability of collision in a contention period of an SMAC frame. Assuming that m of N contenders collide in the first occupied slot ψ,

$$\begin{aligned} \Pr\left[\Psi = \psi, C = m, \Upsilon = fail\right] &= \tau\left(\psi, m\right) \\ &= \frac{\binom{N}{m}\left(W - \psi\right)^{N-m}}{W^N} \end{aligned} \tag{5.13}$$

The probability of collision in a contention period of an SMAC frame (ζ) can be obtained from Equation 5.6 as

$$\begin{aligned} \zeta = 1 - \xi &= \Pr\left[\Upsilon = fail\right] \\ &= \frac{W^N - N\sum_{\psi=1}^{W}\left(W - \psi\right)^{N-1}}{W^N} \end{aligned} \tag{5.14}$$

Since Θ component is composed of the energy consumption in the presence of collision, now we need to calculate the probability of the first selected slot to be ψ given that it is selected by m nodes. By the definition of the conditional probability,

$$\begin{aligned} P\left[\Psi = \psi, C = m \,|\, \Upsilon = fail\right] &= \frac{\tau\left(\psi, m\right)}{\zeta} \\ &= \frac{\binom{N}{m}\left(W - \psi\right)^{N-m}}{W^N - N\sum_{\psi=1}^{W}\left(W - \psi\right)^{N-1}} \end{aligned} \tag{5.15}$$

In each collision, the energy consumption $\dot{\theta}\left(\psi, m\right)$ for the single priority case is determined by the number of nodes (m) colliding in the first occupied slot ψ and is

calculated as:

$$\begin{aligned}\dot{\theta}(\psi, m) = (N+M) E_{sync} + (N+M)(\psi-1) t_{slot} E_{idle} \\ + m t_{RTS} E_{tx} + (N+M-m) t_{RTS} E_{rx}\end{aligned} \tag{5.16}$$

where E_{rx}, E_{tx} and E_{idle} are the energy consumed in reception, transmission and idle states of SMAC frame per unit time respectively. E_{sync} is the average energy consumption per node in the synchronization period of an SMAC frame. The derivation of E_{sync} can be found in Section 5.2.3. Hence the expected energy consumption in any collision, θ, is:

$$\begin{aligned}\theta &= \sum_{\psi=1}^{W} \sum_{m=2}^{N} P[\Psi = \psi, C = m \,|\, \Upsilon = fail] \, \dot{\theta}(\psi, m) \\ &= \sum_{\psi=1}^{W} \sum_{m=2}^{N} \frac{\tau(\psi, m)}{\zeta} \dot{\theta}(\psi, m) \\ &= \sum_{\psi=1}^{W} \sum_{m=2}^{N} \frac{\binom{N}{m} (W-\psi)^{N-m}}{W^N - N \sum_{f=1}^{W} (W-f)^{N-1}} \bar{\theta}(\psi, m)\end{aligned} \tag{5.17}$$

As in Section 5.2.1, the retrials will continue until a slot selection without collision. In SMAC, if collision occurs in a slot selection in a frame, the retrial will be postponed to the next frame. Therefore, the expected energy consumption for collisions and retrials equals to the expected number of SMAC frames elapsed before the frame where successful data transmission starts, β, times the expected energy consumption in each retrial, θ. Substituting β from Equation 5.10,

$$\Theta = \theta\beta = \theta \left(\frac{1}{\xi} - 1 \right) \tag{5.18}$$

The energy consumption in the Φ component can also be decomposed into three parts: the energy consumptions during the synchronization period, during the carrier sensing in the successful contention period and during data transmission. $N + M$

nodes are involved in the first two parts, whereas only the communicating parties are involved in the transmission phase, since all other nodes sleep according to the overhearing avoidance mechanism of SMAC after the reception of RTS message.

Firstly, we need to calculate the expected carrier sense time, Γ, elapsed until the first occupied slot, ψ selected by only one node in the SMAC frame where the data transmission starts. The carrier sense duration of a successful contention is $(\psi - 1)\, t_{slot}$. Then by using Equation 5.8,

$$\begin{aligned}\Gamma &= \sum_{\psi=1}^{W} \Pr[\Psi = \psi | \Upsilon = success](\psi - 1)t_{slot} \\ &= \sum_{\psi=1}^{W} \frac{\tau\,(\psi, 1)}{\xi}(\psi - 1)t_{slot} \\ &= \sum_{\psi=1}^{W} \frac{(W - \psi)^{N-1}}{\sum_{f=1}^{W} (W - f)^{N-1}}(\psi - 1)t_{slot}\end{aligned} \tag{5.19}$$

Hence,

$$\Phi = (N + M)\, E_{sync} + (N + M)\, \Gamma E_{idle} + E_{tr} \tag{5.20}$$

where,

$$\begin{aligned}E_{tr} = {} & (N + M - 1)E_{rx}t_{RTS} + E_{tx}t_{RTS} + E_{rx}t_{CTS} \\ & + n(E_{tx}t_{DATA} + E_{rx}t_{ACK})\end{aligned} \tag{5.21}$$

5.2.3. Derivation of Energy Expenditure in the Synchronization Period

Finally, we will derive the expected energy consumed per node in the synchronization period, E_{sync}. Each node is assumed to transmit a SYNC message in every τ_{sync} seconds. We assume that all nodes create their SYNC packets in the same SMAC

frame. Hence N_{sync} nodes (which is equal to $N + M$ for our case) in the neighborhood start contending in the subsequent synchronization period and the winner nodes transmit their SYNC messages. Colliding nodes are assumed to transmit their packets regardless of the occurrence of a collision and do not contend in the following synchronization periods until a new SYNC packet is created. The remaining nodes contend in the subsequent synchronization periods in the same way until all nodes transmit their SYNC packets.

We can model this process as a discrete time Markov chain (DTMC) where the time unit is an SMAC frame duration. There are $N_{sync} + 1$ states, each representing the number of remaining nodes to contend in that synchronization period. A state s_i $(i = 0 \dots N_{sync})$ represents the case where $N_{sync} - i$ nodes remains in the contention of that synchronization period. The state N_{sync}, representing 0 nodes is the absorbing state of the DTMC. The state transition probabilities of the transition matrix $\mathbf{P}$ for the absorbing DTMC are given as:

$$p_{ij} = \begin{cases} \sum_{\psi=1}^{W_s} \frac{\binom{N_{sync}-i}{j-i}(W_s-\psi)^{N_{sync}-j}}{W_s^{N_{sync}-i}} & j > i \\ 0, & i \geq j, j \neq N_{sync} \\ 1, & i, j = N_{sync} \end{cases} \tag{5.22}$$

The matrix $\mathbf{P}$ has the canonical form [81]

$$\mathbf{P} = \begin{pmatrix} \mathbf{Q}_{\mathrm{N_{sync}} \times \mathrm{N_{sync}}} & \mathbf{R}_{\mathrm{N_{sync}} \times 1} \\ \mathbf{0}_{1 \times \mathrm{N_{sync}}} & \mathbf{I}_{1 \times 1} \end{pmatrix} \tag{5.23}$$

where there are N_{sync} transient states and only one absorbing state. The fundamental matrix $\mathbf{M}$ of $\mathbf{P}$ can be found as:

$$\mathbf{M} = (\mathbf{I} - \mathbf{Q})^{-1}, \tag{5.24}$$

where the entry m_{ij} of $\mathbf{M}$ gives the expected number of times that the process is in

the transient state s_j if it is started in the transients state s_i. Then the ith entry t_i of the column vector $\mathbf{t} = \mathbf{M} \times \mathbf{c}$, where $\mathbf{c}$ is a column vector all of whose entries are 1, gives the expected number of steps before the chain is absorbed given that the chain starts in state s_i. Hence, t_1 gives us the expected number of SMAC frames required for N_{sync} nodes to finish the transmissions of their SYNC messages.

Since the number of SYNC messages is N_{sync}, the total energy consumed for the transmissions of these messages is

$$E_t = N_{sync} t_{SYNC} E_{tx}. \tag{5.25}$$

The expected number of nodes that transmit SYNC messages in one frame is found to be $\frac{N_{sync}}{t_1}$. Consequently, the total number of SYNC message receptions is found as $(N_{sync} - \frac{N_{sync}}{t_1})t_1$. Hence, the total energy consumed for the receptions is

$$E_r = N_{sync}(t_1 - 1) t_{SYNC} E_{rx}. \tag{5.26}$$

In case of a transmission or reception, the idle waiting time reduces to $t_{slot} W_s$ per node per SMAC frame. Since the number of communicating nodes is N_{sync} and the expected number of SMAC frames required to exhaust all messages is t_1, the total idle time energy expenditure of the synchronization periods with communication is:

$$E_{ci} = N_{sync} t_1 t_{slot} W_s E_{idle} \tag{5.27}$$

On the other hand, in each synchronization period without a transmission or reception, the total idle waiting time is $t_{slot} W_s + t_{SYNC}$ where W_s is the contention window size for synchronization period. Hence, in case of an idle synchronization

period, the total energy expenditure is:

$$E_i = (t_{slot} W_s + t_{SYNC})\, E_{idle}. \tag{5.28}$$

Combining Equation 5.25, Equation 5.26 and Equation 5.27, the total energy consumed for communication in the synchronization period is calculated as:

$$\begin{aligned} E_c &= E_t + E_r + E_{ci} \\ &= N_{sync} t_{SYNC} E_{tx} \\ &+ N_{sync}(t_1 - 1) t_{SYNC} E_{rx} \\ &+ N_{sync} t_1 t_{slot} W_s E_{idle} \end{aligned} \tag{5.29}$$

Each node generates its SYNC message in every $\left\lceil \frac{\tau_{sync}}{T_{frame}} \right\rceil$ SMAC frames and the expected number of frames to finalize N_{sync} transmissions is t_1. Hence, each node consumes energy for communication in t_1 SMAC frames and stays idle in the synchronization periods of the remaining $\left\lceil \frac{\tau_{sync}}{T_{frame}} \right\rceil - t_1$ frames. The expected energy expenditure per SMAC frame per node in the synchronization period is:

$$E_{sync} = \frac{\left(\left\lceil \frac{\tau_{sync}}{T_{frame}} \right\rceil - t_1 \right) E_i + E_c}{\left\lceil \frac{\tau_{sync}}{T_{frame}} \right\rceil (N + M)} \tag{5.30}$$

5.3. Effect of Contention Window Size and Duty Cycle on SMAC Operation

In this section, we explore the effect of contention window size and duty cycle on time, throughput and energy expenditure for a successful transmission for various number of contending nodes and message sizes. In addition, we verify the analytical results derived in Section 5.2 using the simulations implemented in MATLAB [80]. The duration of the simulation is configured to be 30 minutes. Along each run, we

collected the number of successful contentions and number of collisions per success for a fixed contention window size (W), number of contending nodes (N), duty cycle (r_{dc}) and message size (n). In addition, the energy expenditures and the time required for a successful data transmission is gathered counting in the statistics collected for collisions prior to a successful contention. Each simulation instance is repeated 10 times and their averages are presented. The simulation parameters are listed in Table 5.1.

Table 5.1. Simulation parameters for the presented SMAC model.

Parameter	**Value**
#Sensors in Neighborhood	30 sensors
#Contending Nodes	5/10/15 sensors
Duty Cycle	1-100% (Default:15%)
#Data Packets per Message	1/5/10 packets
Data Packet Size	1000 bits
RTS/CTS/ACK/SYNC Size	200 bits
Slot Size	20 bits
DATA Contention Window Size	2-150 slots
SYNC Contention Window Size	32 slots
Channel Bitrate	250 Kbps
TX Power	200mW
RX Power	80mW
IDLE Power	80mW

The figures in this section presents the analysis and simulation results for the statistics related with energy expenditure and throughput. We observe that the simulation results matches with the analytical results supporting the validity of the analysis for the assumptions given in Section 5.2.1.

Figure 5.2 presents the effect of contention window size for different number of contenders on Ω', which is the expected time per successful data transmission. In the test case for this figure, the data message is composed of 10 data packets which corresponds to 10 Kbits. We observe that there is a common behavior of a sharp decrease for Ω' at the contention window size of 40. In order to inspect this behavior,

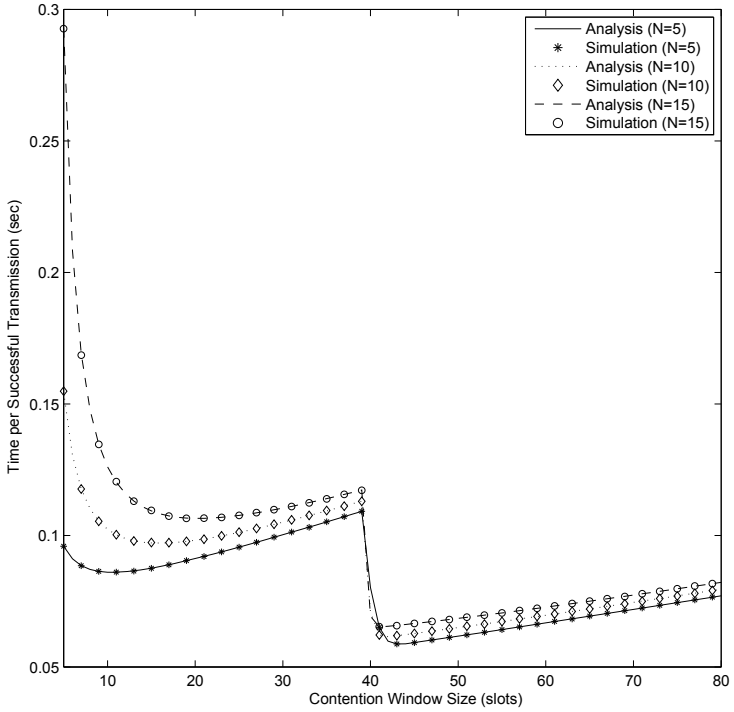

Figure 5.2. The effect of contention window size on Ω' for N=5,10,15.

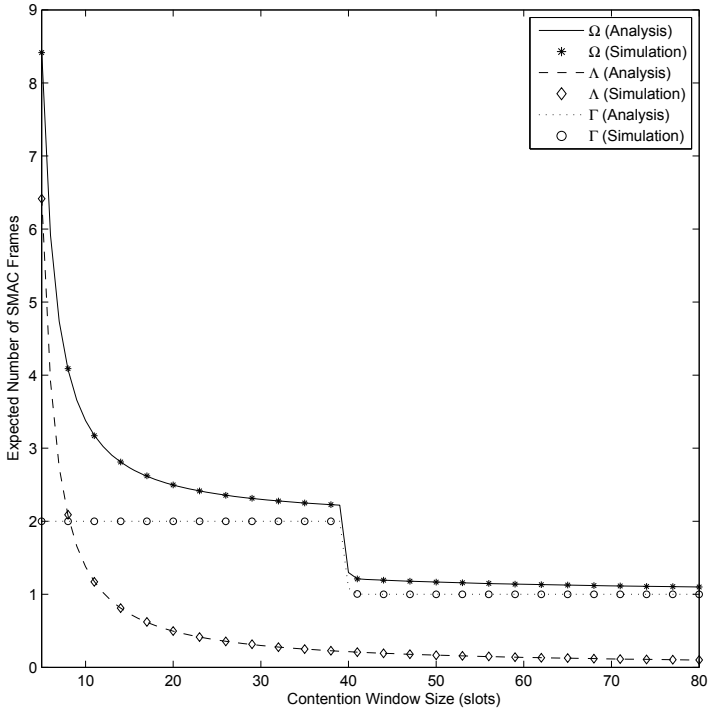

Figure 5.3. The expected number of SMAC frames for Λ, Γ' and Ω' for N=15.

for the instance of 15 contending nodes, we decomposed Ω' to its components, Λ and Γ' in terms of the expected number of SMAC frames, size of which is determined by

the corresponding contention window size. Figure 5.3 presents the expected number of SMAC frames for Λ, Γ' and Ω'.

The sharp decrease in Figure 5.2 is also observed in Figure 5.3 as a decrease from two to one SMAC frame for Γ'. From Equation 5.7 and Equation 5.9, Γ' is the expected duration in terms of the SMAC frames which contains the duration of the synchronization period, the carrier sense duration of a successful slot selection in the contention period and the transmission duration. As shown in Equation 5.1, the durations of the active and sleep periods, and consequently, the duration of an SMAC frame is extended by the increase in the contention window size for a given duty cycle. Since the transmission duration is constant, the transmission is expected to be finalized in less than two SMAC frames if the contention window size is extended to 40 slots and beyond. From our analysis, we find out that the expected transmission duration decreases to one frame at the size of 42 slots. The reason of the difference in the number of SMAC frames between the sizes of 40 to 42 slots is the result of likelihood of the selection of higher indexed slots (which depends on W and N) causing the transmission to extend to more than one frames, which affects the value of α_{ψ}.

The increase in the SMAC frame duration caused by an increase in W is reflected on Ω' as a multiple of the number of expected SMAC frames required per successful transmission (Figure 5.3). On the contrary, the expected number of collisions decreases as W increases since the collision probability for the first occupied slot for fixed number of contenders decreases. Hence, the contention window size causes a tradeoff on Ω' between the expected number of collisions and the duration of an SMAC frame.

When the contention window size is less than 40 in a neighborhood of 30 nodes containing 5,10 and 15 contenders, the optimal contention window sizes minimizing Ω' values presented in Figure 5.2 are 11, 16 and 20 slots, and otherwise, the optimal contention window sizes are 43, 42 and 41 slots respectively. Note that the order of optimal contention window size are reversed. As the number of contenders increases the index of the first occupied slot in a successful slot selection decreases and hence Γ' decreases, which is the dominant component of Ω' for W values greater than 40.

For the contention window size less than 40, as the window size is increased to the optimal values, the effect of the decrease in the collision probability, and consequently the effect of the decrease in the number of collisions dominates the effect of the increase in the frame size. The dominance is reversed after the optimal window sizes. For contention window sizes greater than 40, the transmission is finalized in one SMAC frame, which decreases the effect of increase in SMAC frame duration on Ω'. As W increases beyond 40, the collision probabilities for 5,10 and 15 contenders approach to each other. Hence, the gap between the expected time per successful transmission curves decreases.

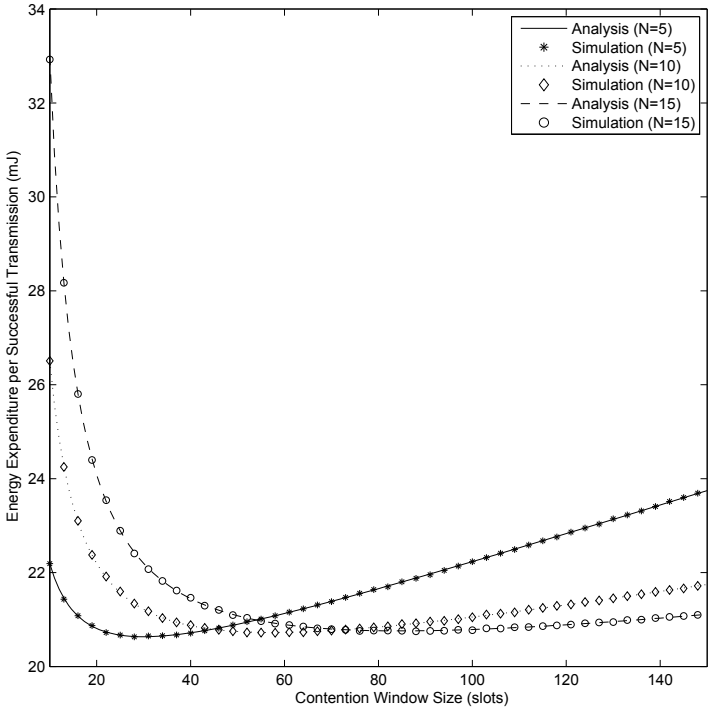

Figure 5.4. The effect of contention window size on E_{tot} for N=5,10,15.

Figure 5.4 presents the effect of the contention window size for different number of contenders on E_{tot}, which is the expected energy consumption in the neighborhood per successful data transmission. A tradeoff similar to the one observed on Ω' is also observed on E_{tot} between the expected number of collisions (increasing the energy for retransmissions) and the duration of an SMAC frame (increasing the energy for carrier sensing). We observe that the optimal contention window sizes which minimize E_{tot} in a neighborhood of 30 nodes containing 5,10 and 15 contenders are 30, 57 and 85 slots

respectively. Up to the optimal W values for each curve, the energy consumption due to the retrials is dominant and as the number of contenders decreases, the number of collisions decreases. On the contrary, beyond the optimal W values, the energy consumption due to carrier sensing is dominant and as the number of contenders decreases, the expected carrier sense duration increases by Equation 5.19. As a consequence, we observe that for the contention window sizes smaller than 45, the order of the energy expenditures is ascending in the number of contenders, whereas the order is totally reversed beyond the contention window of size 73.

Note that the optimal contention window sizes differ for time and energy expenditure cases (Figure 5.2 and Figure 5.4). Depending on the application requirements, the preference between the two metrics varies. Hence, a joint metric should be introduced to optimize the contention window size including both metrics whose weights are determined regarding the application requirements. $\Omega' E_{tot}$ is a simple example for the joint metric [25, 82] where time and energy expenditures have equal weights in the optimization.

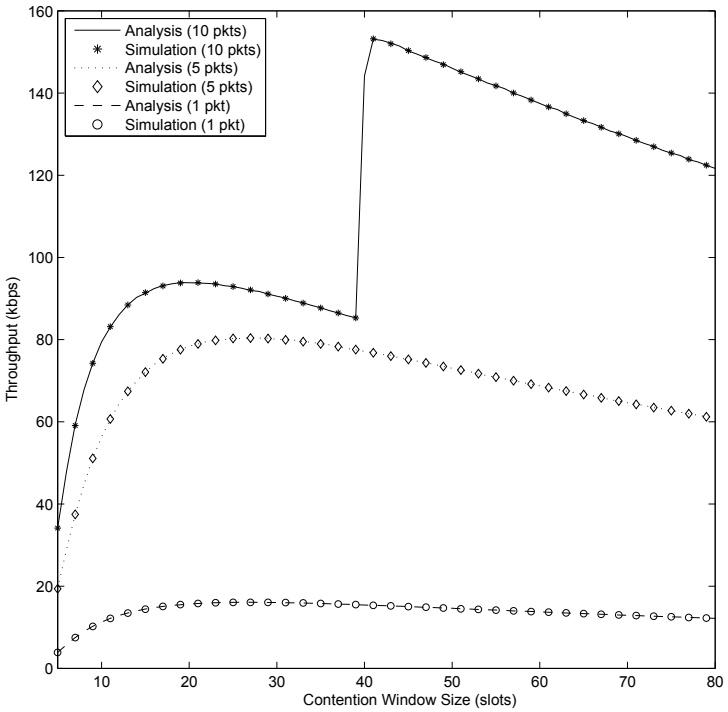

Figure 5.5. The effect of contention window size on message throughput ($1/\Omega'$) for message sizes of 1, 5 and 10 packets for N=15.

In Figure 5.5, the number of data packets per message is varied to present the effect of the contention window size on $\frac{1}{\Omega'}$, which is the system message throughput of the contending neighborhood in terms of Kbps. We observe that when the duty cycle is 15%, transmission of messages of 1 and 5 packets are finalized in one SMAC frame regardless of the contention window size. However, in the 10 packets case, the transmission finalizes in two SMAC frames for the contention window sizes less than 40, which is the reason for the sharp increase in the throughput. We observe that the optimal contention window sizes which maximize the throughput in a neighborhood of 30 nodes containing 15 contenders for the message sizes of 1, 5 and 10 packets are 27, 27 and 41 slots respectively. However, when the contention window size is less than 40, the optimal throughput for the message size of 10 packets is obtained for the window size of 19 slots. Since for this message size, the transmission finalizes in two SMAC frames when the window size is less than 40, the increase in W increases the frame duration and Ω' increases at least by a factor of two frame durations. Hence, the optimal window size that maximizes $\frac{1}{\Omega'}$ is obtained at a smaller value as compared to smaller message sizes.

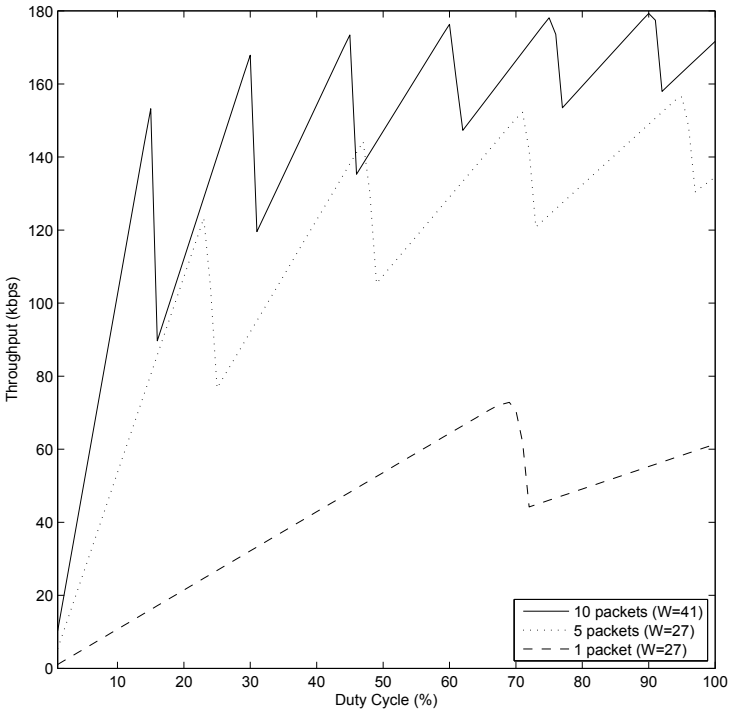

Figure 5.6. The effect of duty cycle on message throughput ($1/\Omega'$) for message sizes of 1, 5 and 10 packets for N=15.

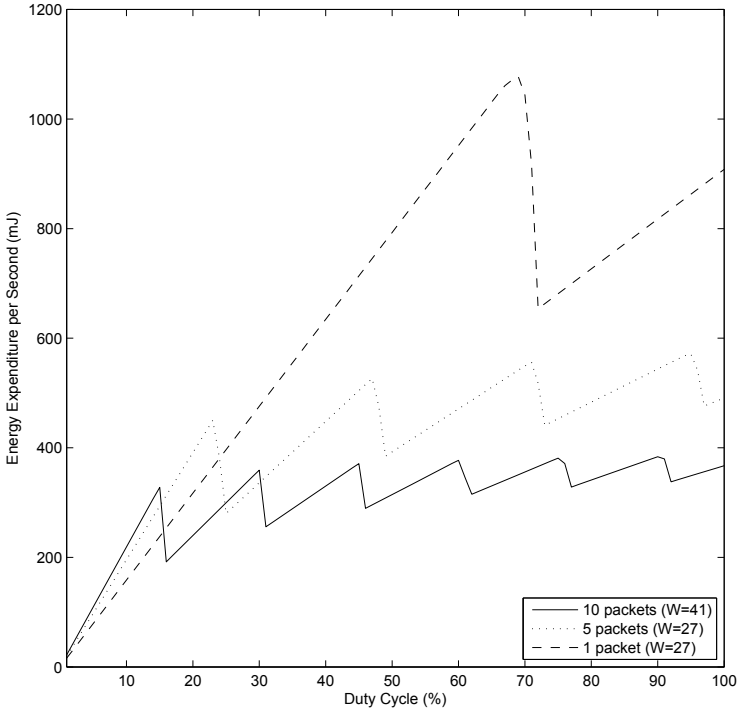

Figure 5.7. The effect of duty cycle on energy expenditure for message sizes of 1, 5 and 10 packets for N=15.

Figure 5.6 and Figure 5.7 present the analysis results obtained for the effect of duty cycle on the expected throughput and on the expected energy expenditure of an SMAC virtual cluster for messages of size 1, 5 and 10 packets. In these figures, the contention window size for each curve is set as the optimal value determined for the corresponding message size in Figure 5.5. A common intuition on the effect of duty cycle is that the throughput and the energy expenditure of the cluster monotonically increase with the increase in the duty cycle. However, we observe that the curves in both figures exhibits a sawtooth behavior.

As the duty cycle is increased, the duration of the sleep period decreases and therefore the expected throughput and the expected energy expenditure increase since more messages are transmitted per second. However, when the sleep period duration is smaller than the message size, we observe a sudden decrease followed by a gradual increase until the next duty cycle value where the expected carrier sense duration together with the data transmission are finalized in exactly two frames. The same

pattern is observed for higher duty cycle values where a transmission is finalized in multiple frames.

As stated in Section 5.1, the nodes not involved in the communication sleep during transmission according to the overhearing avoidance mechanism of SMAC. Moreover, at the end of the data transmission, all nodes sleep until the beginning of the subsequent SMAC frame. Hence, due to the under-utilization of the channel, the curves in each figure exhibits rapid degradation in the throughput and the energy expenditure. The number and location of the of peaks varies with respect to the message size which determines the transmission duration.

It should be noted that as the duty cycle increases, the decrease in the duration of SMAC frame leads to an increase in the number of frames per second. Such an increase in the number of frames lead to an increase in the idle state energy consumption since the energy consumption per frame remains constant for fixed contention window sizes for data and synchronization periods. Considering both figures together with the idle energy consumption, we can conclude that the initial duty cycle value for which the desired level of throughput and energy consumption is observed should be selected as the system duty cycle in order to optimize the SMAC operation for the given application constraints.

5.4. SMAC Protocol with Multiple Priority Classes

In this section, we will extend the prioritized contention analysis provided in the previous chapter for the SMAC protocol by integrating the effect of the duty cycle in the analysis. We will derive the expected time and the expected energy expenditures of a heavily loaded virtual cluster of SMAC with constant number of contenders from each priority class to finalize a transmission successfully. The nodes in a cluster are assumed to be the immediate neighbors of each other. The model assumptions in Section 4.1 also hold for this section.

To adapt the SMAC analysis to the prioritized contention analysis in Chapter 4,

we need to integrate the duration of a frame, T_{frame} and the number of SMAC frames required to finalize a data transmission for a chosen ψ, α_ψ into the prioritized contention model. We borrow all probability definitions and their formulations introduced in Section 4.2.1 and Section 4.2.2 since our assumption of uniform contention window is also valid for the prioritized SMAC scheme. These probabilities depend only on the number of contending nodes and the size of the contention window partitions.

The expected time in terms of SMAC frames required for a successful data transmission of class i, Ω'_i can be decomposed into two phases: Λ_i, the expected duration consumed for the frames in which collision occurs or the opponent class transmits, and Γ'_i, the expected duration of the frames in which the contention is successful and transmission is finalized.

The Γ'_i component differs from the Γ component in Equation (4.7) in the sense that instead of calculating only the carrier sensing phase before transmitting the data, Γ_i, calculates the duration of whole frames used for transmission. Given a slot ψ, the number of frames used in transmission is given by α_ψ and hence,

$$\begin{aligned}\Gamma'_i &= \sum_{\psi=1}^{x_3} \xi_{(\psi|i)} \alpha_\psi T_{frame} \\ &= \sum_{\psi=1}^{x_3} \frac{\xi_{(\psi,i)}}{\xi_i} \alpha_\psi T_{frame} \end{aligned} \tag{5.31}$$

The derivation of the Λ_i component is similar in both derivations. We need to derive λ and μ_i for both priority classes.

$$\begin{aligned}\Lambda_1 &= \lambda E[X_3] + \mu_1 E[X_2] \\ &= \lambda \frac{\zeta}{\xi_1} + \mu_1 \frac{\xi_2}{\xi_1} \end{aligned} \tag{5.32}$$

$$\begin{aligned}\Lambda_2 &= \lambda E[X_3] + \mu_2 E[X_1] \\ &= \lambda \frac{\zeta}{\xi_2} + \mu_2 \frac{\xi_1}{\xi_2} \end{aligned} \tag{5.33}$$

The expected duration elapsed for collisions is represented by λ. Since in the case of a collision, the nodes wait until the end of that SMAC frame to select a new slot, the expected duration of a collision is found as:

$$\begin{aligned}\lambda &= \sum_{\psi=1}^{x_3} \zeta_{(\psi|c)} T_{frame} \\ &= \sum_{\psi=1}^{x_3} \frac{\zeta_{(\psi,c)}}{\zeta} T_{frame} \\ &= \sum_{\psi=1}^{x_3} \frac{P\left[\Psi=\psi\right] - \xi_{(\psi,1)} - \xi_{(\psi,2)}}{\zeta} T_{frame}\end{aligned} \tag{5.34}$$

where $\zeta_{(\psi,c)} = P\left[\Psi=\psi\right] - \xi_{(\psi,1)} - \xi_{(\psi,2)}$. Clearly, the duration for the SMAC frames required to finalize the transmission of the opponent priority class is equivalent to the Γ' of the opponent class.

$$\mu_1 = \Gamma'_2 \tag{5.35}$$

$$\mu_2 = \Gamma'_1 \tag{5.36}$$

Combining Γ'_i and Λ_i, we find the expected duration of the SMAC frames from the end of a transmission to the end of the subsequent transmission of priority class i:

$$\begin{aligned}\Omega'_1 &= \Gamma'_1 + \Lambda_1 \\ &= \sum_{\psi=1}^{x_3} \frac{\xi_{(\psi,1)}}{\xi_1} \alpha_\psi T_{frame} + \sum_{\psi=1}^{x_3} \frac{\zeta_{(\psi,c)}}{\zeta} T_{frame} \frac{\zeta}{\xi_1} \\ &+ \sum_{\psi=1}^{x_3} \frac{\xi_{(\psi,2)}}{\xi_2} \alpha_\psi T_{frame} \frac{\xi_2}{\xi_1} \\ &= \sum_{\psi=1}^{x_3} \frac{\left(\xi_{(\psi,1)} + \xi_{(\psi,2)}\right)\alpha_\psi + P\left[\Psi=\psi\right] - \xi_{(\psi,1)} - \xi_{(\psi,2)}}{\xi_1} T_{frame}\end{aligned} \tag{5.37}$$

$$\begin{aligned}\Omega'_2 &= \Gamma'_2 + \Lambda_2 \\ &= \sum_{\psi=1}^{x_3} \frac{\left(\xi_{(\psi,1)} + \xi_{(\psi,2)}\right)\alpha_\psi + P\left[\Psi=\psi\right] - \xi_{(\psi,1)} - \xi_{(\psi,2)}}{\xi_2} T_{frame}\end{aligned} \tag{5.38}$$

The energy consumption of a virtual cluster until the end of successful data transmission for each priority class i can be decomposed into two components: Θ_i, the total energy consumption in the neighborhood during collisions or the transmission of the opponent class, and Φ_i as the total energy consumption in the neighborhood within the SMAC frames containing the successful contention and the data transmission. Clearly, the energy consumption model considers only the communication phase, and hence the duty cycle and the SMAC frame duration are not involved in the derivations.

The Φ_i component is calculated using the expected carrier sense duration, Γ_i, derived in Section 4.3. The expected energy consumption in the synchronization period is not affected by the prioritization scheme and is given in Section 5.2.3.

$$\begin{aligned}\Phi_i &= (N_1 + N_2 + M)\, E_{sync} + (N_1 + N_2 + M)\, \Gamma_i E_{idle} + E_{tr} \\ &= \sum_{\psi=1}^{x_3} \frac{\xi_{(\psi,i)}}{\xi_i} (\psi - 1) t_s (N_1 + N_2 + M)\, E_{idle} \\ &+ (N_1 + N_2 + M)\, E_{sync} + E_{tr} \end{aligned} \tag{5.39}$$

where,

$$\begin{aligned}E_{tr} &= (N_1 + N_2 + M - 1) E_{rx} t_{RTS} + E_{tx} t_{RTS} + E_{rx} t_{CTS} \\ &+ n\,(E_{tx} t_{DATA} + E_{rx} t_{ACK}) \end{aligned} \tag{5.40}$$

In order to derive Θ_i, the expected duration elapsed until the SMAC frame that the transmission is initiated, we need to derive θ and δ_i for both priority classes.

$$\begin{aligned}\Theta_1 &= \theta E[X_3] + \delta_1 E[X_2] \\ &= \theta \frac{\zeta}{\xi_1} + \delta_1 \frac{\xi_2}{\xi_1} \end{aligned} \tag{5.41}$$

$$\begin{aligned}\Theta_2 &= \theta E[X_3] + \delta_2 E[X_1] \\ &= \theta \frac{\zeta}{\xi_2} + \delta_2 \frac{\xi_1}{\xi_2} \end{aligned} \tag{5.42}$$

The expected energy consumption in the neighborhood during collisions is represented by θ. A collision consists of three phases, the energy consumptions for synchronization period, the idle listening until collision and the collision itself. Hence,

$$\theta = \sum_{\psi=1}^{x_3} \sum_{m=m_0}^{N_1} \sum_{n=n_0}^{N_2} \frac{\zeta_{(\psi,m,n,c)}}{\zeta} \dot{\theta}\left(\psi, m+n\right) \tag{5.43}$$

where $m_0 = 2 - \min(2, N_2)$, $n_0 = 2 - \min(2, m)$, $N_1 + N_2 \geq 2$ and

$$\begin{aligned} \dot{\theta}\left(\psi, k\right) = {} & \left(N_1 + N_2 + M\right) E_{sync} + \left(N_1 + N_2 + M\right)\left(\psi - 1\right) t_s E_{idle} \\ & + k\left(t_{RTS} E_{tx}\right) + \left(N_1 + N_2 + M - k\right)\left(t_{RTS} E_{rx} + t_{tout} E_{idle}\right) \end{aligned} \tag{5.44}$$

Clearly, the δ_i component of Θ_i is equivalent to the energy consumption required for the transmission of the opponent priority class and hence,

$$\delta_1 = \Phi_2 \tag{5.45}$$

$$\delta_2 = \Phi_1 \tag{5.46}$$

Many of the contention based MAC protocols for sensor networks are SMAC variant and these protocols inherit the duty-cycled operation from SMAC. The extension of the mathematical model of SMAC to support multiple priorities will enable the network engineers to explore the effects of the network dynamics such as the number of contenders, network density and traffic density on the network performance.

6. DEPLOYMENT QUALITY ANALYSIS IN WIRELESS SENSOR NETWORKS

The QoS requirements in the communication layers in a WSN are directly related with the sensing coverage of the deployed network. The sensing coverage shall be maintained above a certain threshold in the network for the target detection and the MAC layer forwarding. Hence, apart from the communication based QoS, the sensing quality of the network brings about another perspective to the QoS in WSNs regarding the quality of the deployment.

In this chapter, we will introduce a model for a randomly deployed network possibly containing one or more coverage holes. For this purpose we provide an analytical solution in the geometric domain which is proven to be equivalent to the geographic domain. This solution provides a lower bound for the probability of network detection and is used as a measure for the deployment quality in terms of network parameters.

Our approach presents a deployment quality model for heterogeneous network formations due to sensor losses caused by energy depletion, destruction and jammers. The proposed solution is designed for border surveillance applications, in which a target passes through the network. The sensors are tasked with detecting the intruder over the total area covered by the network. Overcoming sensor losses is not in the scope of our work. We aim to present a fast calculation scheme to understand the overall sensing quality with in the presence of sensor losses at a given snapshot of the border surveillance wireless sensor network.

6.1. Model Assumptions

This section presents the model assumptions used in the analytical derivation of the DQM. In this analysis, we assume a convex 2-D deployment site S of perimeter L sensed by N_s sensors. Each sensor s_i is assumed to have convex sensing coverage of S_i

with perimeter L_i, uniformly and independently distributed within S. In addition, we have N_h jammers, in which each jammer h_j has a jamming coverage area of H_j with a random shape that is uniformly and independently distributed within S.

The coverage holes caused by node losses in the network may occur due to several factors, such as the destruction and energy depletion of sensors and jammer attacks. The area of these coverage holes are determined as follows. Each sensor is assumed to transmit ALIVE messages periodically to the sink, which indicate that the source node is alive upon the reception of the message. The remaining sensors are assumed to be inaccessible and constitute the coverage holes/jammed regions in the network. Since the area of any type of coverage holes is determined similarly, for simplicity, we mention the coverage holes as the jamming areas hereafter.

We assume that the task of delivering ALIVE messages is performed by the underlying protocol stack of the sensors. Given that ALIVE messages have already been received by the sink, the DQM calculations are performed after the reception of these messages. The dead-ends caused by the coverage holes are handled by the dead-end handling mechanism of the underlying protocol stack, such as the right hand rule in GPSR [70] and rainbow scheme in ALBA-R [83]. Such communication tasks are beyond the scope of this chapter.

We assume in our scenarios that the intruder and the attacker have limited or no knowledge about the details of the deployed network, similar to the assumptions on the jamming attacks in [84]. Moreover, the attacker is not able to traverse the field without being detected and perform a strategic jammer placement in the network. A more acceptable deployment strategy is to air-drop the jammers on the network. In the case of coverage holes caused by node failures, they occur independently based on the local traffic load on nodes or unforeseeable node failures. Therefore, we assume a random deployment model for the coverage holes.

In addition to the assumptions that the sensor deployments are random and the intruder has little knowledge about the network details, we also assume that the tra-

jectories of the intruders are straight lines, crossing the deployment area with equal probability along the area border. Although this assumption brings about a restriction on the variety of possible trajectories, the linear trajectory provides the shortest path between arbitrary entry and exit points in the deployment area, thus minimizing the possibility of detection from the intruder's point of view. If the intruder had detailed knowledge of the sensor positions, it would be feasible to follow a longer path to avoid the sensors. However, without such knowledge, increasing the path length in the network would also increase the detection probability of the intruder by any of the sensors. The probability for a linear trajectory provides the worst-case detection probability among all trajectories with the same entry and exit points. Under these circumstances, following a straight line between the entry and exit points of the intrusion is the most plausible choice. In addition, the parameterization of line trajectories can easily be integrated in our analytical calculation and the physical interpretation of the network model.

Finally, the detection model is assumed to be a binary detection model where a target is assumed to be detected if it enters the sensing coverage area of a sensor.

6.2. Problem Definition

In this section, we will provide a formal definition of the SWSN intruder detection problem in the presence of jammers/coverage holes. Moreover, we will provide two additional problems that will be mapped to each other to derive a solution for the geometric domain utilizing metrics and tools from integral geometry and geometric probability [85].

The following definition is the formal statement of our problem:

Problem 6.1. *Border surveillance intruder detection avoiding jammers problem: Let S be a deployment area of perimeter L sensed by N_s sensors, where each sensor s_i has a sensing coverage S_i with perimeter L_i that is uniformly and independently distributed within S. In addition, Let the number of jammers be N_h where each jammer h_j has a jamming coverage area of H_j that is uniformly and independently distributed within*

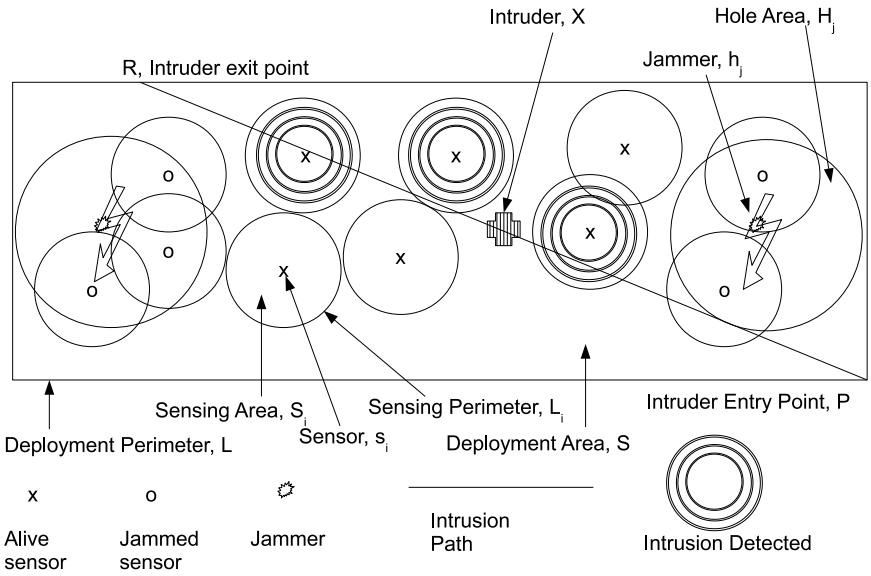

Figure 6.1. Graphical representation of the border surveillance intruder detection avoiding jammers problem.

S. The sensors residing in the jamming area are assumed to be dead. What is the probability $P_D(k)$ that an intruder X randomly crossing S is detected by at least one sensor that does not reside in any of the jamming areas?

A graphical representation of Problem 6.1 is given in Figure 6.1. The probability $P_D(k)$ is defined as the deployment quality metric (DQM) of such a sensor network.

The solution to this problem requires the calculation of the probability of detection for a set of sensors in the network. To provide a solution for this problem, we introduce two additional problems. The first one, Problem 6.2, is the simplified version of Problem 6.1, which does not include jammers. The second one, Problem 6.3, corresponds to the geometric interpretation of such a sensor network. We will provide a mapping between these two problems to show that they are equivalent, i.e. each one can be reduced to the other.

Problem 6.2. *Border surveillance intruder detection problem: Let S be a deployment area of perimeter L sensed by N_s sensors, where each sensor s_i has a sensing coverage S_i with perimeter L_i that is uniformly and independently distributed deployed within S.*

What is the probability $P_D(k)$ that an intruder X randomly crossing S is detected by at least one sensor?

Problem 6.3. *Line-set intersection problem [55]: Let C be a bounded set of perimeter length L and N_s sets C_i with perimeter length L_i that is uniformly and independently distributed inside C. What is the probability $P_D(k)$ that a random line G intersecting C, also intersects at least one of the sets C_i, $i = 1 \ldots N_s$?*

An illustration of the line-set intersection problem is given in Figure 6.2. Our analytical study relies on the fact that these two problems can be reduced to each other with a bijection between two domains. The following lemma presents this bijection.

Lemma 6.1. *The border surveillance intruder detection problem and the line-set intersection problem are equivalent, i.e. one can be reduced to the other with a bijective mapping.*

Proof. We provide the following mapping of the intruder detection problem to the line-set intersection problem proposed in [55] for a more general case of these two problems. We map the deployment area S to a bounded set C, which is a collection of points in the plane with perimeter length L. The sensing area S_i of sensor s_i is mapped to a bounded set C_i with perimeter length L_i that is uniformly and independently distributed in C. We map the trajectory of the intruder X to a straight line $G(p, \phi)$ in the plane defined by p as the shortest distance of G to the origin O of a coordinate system, and ϕ as the angle of the line perpendicular to G with respect to the x axis. This solution provides a mapping between the mobile target detection problem for a stochastic sensor network and the line-set intersection problem. Hence, we conclude that both problems are equivalent. □

The mapping stated in Lemma 6.1 between Problem 6.2 and Problem 6.3 provides a bijection between the physical sensor network domain and the geometric domain. In the next section, we will provide a solution for the probability of detection of a target by a single sensor in the geometric domain because we have shown that Problem 6.2

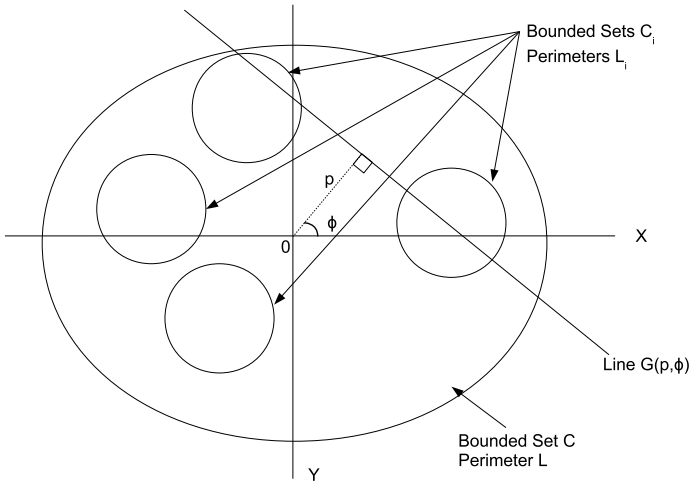

Figure 6.2. Graphical representation of the line-set intersection problem.

and Problem 6.3 can be reduced to each other. The provided solution will be extended to derive the detection for a given set of sensors. Next, we will integrate the probability of being alive, i.e. that the sensors reside outside the jamming coverage area, in this formulation. Finally, we will provide a closed-form solution for the probability of detection in Problem 6.1.

6.3. Deployment Quality of a Border Surveillance WSN

The probability of target detection P_D can be evaluated using the frequency count of lines intersecting geometric shapes. As we consider the set of all possible linear trajectories intersecting the deployment area, P_D is equal to the quotient of the number of lines that intersect any of the sensing areas, over the number of lines that intersect the deployment area. However, the set of lines in the plane intersecting a set is uncountable.

Hence, we will derive an analytical solution to the line-set intersection problem using the line measure. Let $G(p, \phi)$ be a straight line in the plane. Here the density of the line is formulated as

$$dG = dp \wedge d\phi \tag{6.1}$$

The measure $m(G)$ of a set of lines $G(p, \phi)$ is the integral of the density of the line, which is in the differential form, over the set. Hence,

$$m(G) = \int dp \wedge d\phi \tag{6.2}$$

The measure of the set of lines that pass over a bounded convex set, C, defined by the support function $p = p(\phi)$ of the convex set, is given as [85]:

$$m(G : G \cap C \neq 0) = \int_{G \cap C \neq 0} dp \wedge d\phi = \int_0^{2\pi} p d\phi = L \tag{6.3}$$

where L is the perimeter of C. Equation 6.3 can be reinterpreted to mean that the measure of lines intersecting a convex set is equal to the perimeter of that convex set. By Equation 6.3, the perimeters can in turn be used to calculate the intersection of a random line with a convex set C_i within C, which will be used for the proof of the following lemma.

Lemma 6.2. *Let S be the deployment area of a sensor network and let s_i be any of the sensors deployed in the area. The probability that an intruder randomly passing through S is detected by the single sensor s_i is equal to*

$$P_i = \frac{L_i}{L}, \tag{6.4}$$

where L_i is the perimeter of the sensor coverage area and L is the perimeter of the deployment area.

Proof. The probability that an intruder randomly passing through S is detected by a single sensor s_i is derived as follows. By the mapping of the intruder detection problem to a line-set intersection problem provided in Lemma 6.1, this probability is equivalent to the probability that a line G intersecting C also intersects C_i. In terms of the measures, this probability is equal to the ratio of the measure of the set of lines that

intersect both C and C_i to the measure of the set of lines that intersect C.

$$\begin{aligned} P_i &= Pr[G \cap C_i \cap C \neq 0 | G \cap C \neq 0] \\ &= \frac{m(G : G \cap C_i \cap C \neq 0)}{m(G : G \cap C \neq 0)} \end{aligned} \tag{6.5}$$

Since C_i is known to be inside the convex set C, Equation 6.5 can be rewritten as

$$P_i = \frac{m(G : G \cap C_i \neq 0)}{m(G : G \cap C \neq 0)} \tag{6.6}$$

Using Equation 6.3, Equation 6.6 is equal to

$$P_i = \frac{L_i}{L} \tag{6.7}$$

□

Thus, using the mapping provided in Lemma 6.1, the probability that an intruder randomly passing through S is detected by a single sensor s_i is found in terms of L, the perimeter of deployment area, and L_i, the perimeter of the sensing coverage of a sensor. Now, we need to derive the effect of jammers on the probability of detection in the sensor network, i.e. derive a solution for the *border surveillance intruder detection avoiding jammers problem* (Problem 6.1).

Theorem 6.1. *The DQM of any sensor network with N_s sensors deployed in the area and N_h jamming regions is*

$$P_D = \sum_{k=0}^{N_s} \sum_{v=1}^{\left|Z_{N_s,k}\right|} \left(1 - \prod_{i=1}^{k} \left(1 - \frac{L_{\mathbf{z_{k,v}}(i)}}{L}\right)\right) P_a^k \left(1 - P_a\right)^{N_s - k} \tag{6.8}$$

and

$$P_a = \prod_{j=1}^{N_h} \left(1 - \frac{A_j}{A}\right) \tag{6.9}$$

where $Z_{N_s,k}$ *denotes the set of all* $\binom{N_s}{k}$ *vectors* $\mathbf{z_{k,v}}$ *containing ordered and distinct* k *elements of vector* $[1, \ldots, N_s]$. A *denotes the area of the deployment area* S *and* A_j, j = *1,...,*N_h *denotes the area of the jamming region* H_j.

Proof. Our aim is to derive the probability of detection P_D for a given sensor network.

Initially, we will derive the probability that a sensor resides outside all H_j, j=1,...,N_h (i.e. the sensor is alive in the context of communication), P_a.

For this purpose, we need to find the probability that a sensor node s resides in any jamming region H_j. The probability P_{H_j} that a sensor node resides in a given H_j is found to be

$$P_{H_j} = \frac{A_j}{A} \tag{6.10}$$

The probability $P_{\overline{H}_j}$ that the sensor resides outside the given region H_j is found to be

$$\begin{aligned} P_{\overline{H}_j} &= 1 - P_{H_j} \\ &= 1 - \frac{A_j}{A} \end{aligned} \tag{6.11}$$

Using the probability $P_{\overline{H}_j}$, we can now derive the probability P_a that a sensor will reside outside the jamming regions H_j. Since the jamming regions are uniformly

and independently distributed, we have

$$\begin{aligned} P_a &= Pr[s \notin \bigcup_{j=1}^{N_h} H_j] \\ &= Pr[\bigwedge_{j=1}^{N_h} s \notin H_j] \\ &= \prod_{j=1}^{N_h} P_{\overline{H}_j} \\ &= \prod_{j=1}^{N_h} (1 - \frac{A_j}{A}) \end{aligned}$$

which provides Equation 6.9. Note that this probability depends only on the area of each H_j, so the probability remains the same for all sensors. Now, we will derive the probability of detection, when k sensors do not reside in any H_j.

By Lemma 6.2, we know that the probabilities that a sensor s_i detects an intruder (P_{s_i}) and misses an intruder ($P_{\bar{s}_i}$) can be calculated as

$$\begin{aligned} P_{s_i} &= \frac{L_i}{L} \\ P_{\bar{s}_i} &= 1 - P_{s_i} \\ &= 1 - \frac{L_i}{L} \end{aligned} \tag{6.12}$$

Let $\mathbf{z_{k,v}}$ be a k-tuples vector that contains the ordered indices of sensors. Using the mapping provided in Lemma 6.1, this vector also indicates a set of k sets C_i. The sets are uniformly and independently distributed. Hence, the probability that a random line G passes through none of the sets indicated by $\mathbf{z_{k,v}}$, i.e. the sensors miss the target, ($P_{\overline{\mathbf{z}}_{\mathbf{k,v}}}$) and the probability that random line G passes through at least one of these sets, i.e. at least one of these sensors detect the target, ($P_{\mathbf{z_{k,v}}}$) in this instance

is given by

$$\begin{aligned} P_{\overline{\mathbf{z}}_{\mathbf{k},\mathbf{v}}} &= Pr[G \cap \bigcup_{i=1}^{k} C_{\mathbf{z}_{\mathbf{k},\mathbf{v}}(i)} = \emptyset] \\ &= Pr[\bigwedge_{i=1}^{k} G \cap C_{\mathbf{z}_{\mathbf{k},\mathbf{v}}(i)} = \emptyset] \\ &= \prod_{i=1}^{k} P_{\overline{s}_{\mathbf{z}_{\mathbf{k},\mathbf{v}}(i)}} \\ &= \prod_{i=1}^{k} \left(1 - \frac{L_{\mathbf{z}_{\mathbf{k},\mathbf{v}}(i)}}{L}\right) \end{aligned} \tag{6.13}$$

$$\begin{aligned} P_{\mathbf{z}_{\mathbf{k},\mathbf{v}}} &= 1 - P_{\overline{\mathbf{z}}_{\mathbf{k},\mathbf{v}}} \\ &= 1 - \prod_{i=1}^{k} \left(1 - \frac{L_{\mathbf{z}_{\mathbf{k},\mathbf{v}}(i)}}{L}\right) \end{aligned} \tag{6.14}$$

Let $X_{\mathbf{z}_{\mathbf{k},\mathbf{v}}}$ be the event that an intruder passes through the sensing area of any of the k sensors indicated by and $Y_{\mathbf{z}_{\mathbf{k},\mathbf{v}}}$ be the event that only the sensors indicated by $\mathbf{z}_{\mathbf{k},\mathbf{v}}$ are alive in the network. Clearly, $X_{\mathbf{z}_{\mathbf{k},\mathbf{v}}}$ and $Y_{\mathbf{z}_{\mathbf{k},\mathbf{v}}}$ are independent events because the residence of a target in the sensing coverage of a sensor does not affect the residence of that sensor in a jamming region. Since the sensors are uniformly distributed, the probability that the intruder passes through any of these k sensors and that these k sensors are alive is given by

$$\begin{aligned} P_{Z_{k,v}} &= Pr[X_{\mathbf{z}_{\mathbf{k},\mathbf{v}}}, Y_{\mathbf{z}_{\mathbf{k},\mathbf{v}}}] \\ &= Pr[X_{\mathbf{z}_{\mathbf{k},\mathbf{v}}}] Pr[Y_{\mathbf{z}_{\mathbf{k},\mathbf{v}}}] \\ &= P_{\mathbf{z}_{\mathbf{k},\mathbf{v}}} Pr[\bigwedge_{i=1}^{k} (s_{\mathbf{z}_{\mathbf{k},\mathbf{v}}(i)} \notin \bigcup_{i=1}^{j} H_j) \wedge \bigwedge_{i=1}^{N_s-k} (s_{\mathbf{z}'_{\mathbf{k},\mathbf{v}}(i)} \in \bigcup_{i=1}^{j} H_j)] \\ &= P_{\mathbf{z}_{\mathbf{k},\mathbf{v}}} (P_a)^k (1 - P_a)^{N_s - k} \\ &= \left(1 - \prod_{i=1}^{k} \left(1 - \frac{L_{\mathbf{z}_{\mathbf{k},\mathbf{v}}(i)}}{L}\right)\right) (P_a)^k (1 - P_a)^{N_s - k} \end{aligned} \tag{6.15}$$

where $\mathbf{z'_{k,v}}$ denotes the complement of $\mathbf{z_{k,v}}$ with respect to the vector $[1, \ldots, N_s]$. The number of distinct subsets of all sensor nodes containing k nodes is nodes is $\binom{N_s}{k}$, which is the number of $\mathbf{z_{k,v}}$ vectors contained in $Z_{N_s,k}$. In a network with N_s sensors, the probability P_{D_k} of detecting the intruder when k of the nodes are alive is

$$\begin{aligned} P_{D_k} &= \sum_{v=1}^{|Z_{N_s,k}|} P_{Z_{k,v}} \\ &= \sum_{v=1}^{|Z_{N_s,k}|} \left(1 - \prod_{i=1}^{k} \left(1 - \frac{L_{\mathbf{z_{k,v}}(i)}}{L}\right)\right) (P_a)^k (1 - P_a)^{N_s - k} \end{aligned} \tag{6.16}$$

Using Equation 6.16, the probability of detection in our sensor network (i.e. the DQM of our network) is found to be

$$\begin{aligned} P_D &= \sum_{k=0}^{N_s} P_{D_k} \\ &= \sum_{k=0}^{N_s} \sum_{v=1}^{|Z_{N_s,k}|} \left(1 - \prod_{i=1}^{k} \left(1 - \frac{L_{\mathbf{z_{k,v}}(i)}}{L}\right)\right) (P_a)^k (1 - P_a)^{N_s - k} \end{aligned}$$

□

If sensors have sensing areas with perimeters of equal length (not necessarily identical shapes) and the areas of each jamming region are the same, Equation 6.8 can be simplified to the following form.

Corollary 6.1. *When all sensors deployed in the network have sensing areas of equal perimeters L_s, the DQM of the network is equal to:*

$$P_D = 1 - \left(1 - \frac{L_s}{L} P_a\right)^{N_s} \tag{6.17}$$

Moreover, if all jamming regions have the same area A_h, then the probability that a

sensor is alive (P_a) is equal to:

$$P_a = \left(1 - \frac{A_h}{A}\right)^{N_h} \tag{6.18}$$

Proof. By setting $L_i = L_s$ in Equation 6.8 and $A_j = A_h$ in Equation 6.9, we get:

$$\begin{aligned} P_D &= \sum_{k=0}^{N_s} \binom{N_s}{k} \left(1 - \left(1 - \frac{L_s}{L}\right)^k\right) (P_a)^k (1 - P_a)^{N_s - k} \\ &= \sum_{k=0}^{N_s} \binom{N_s}{k} (P_a)^k (1 - P_a)^{N_s - k} \\ &\quad - \sum_{k=0}^{N_s} \binom{N_s}{k} \left(1 - \frac{L_s}{L}\right)^k (P_a)^k (1 - P_a)^{N_s - k} \end{aligned} \tag{6.19}$$

We know that

$$(a + b)^N = \sum_{k=0}^{N} \binom{N}{k} (a)^k (b)^{N-k} \tag{6.20}$$

Hence, with Equation 6.20 in Equation 6.19,

$$\begin{aligned} P_D &= 1 - \sum_{k=0}^{N_s} \binom{N_s}{k} \left(\left(1 - \frac{L_s}{L}\right) P_a\right)^k (1 - P_a)^{N_s - k} \\ &= 1 - \left(\left(1 - \frac{L_s}{L}\right) P_a + (1 - P_a)\right)^{N_s} \\ &= 1 - \left(1 - \frac{L_s}{L} P_a\right)^{N_s} \end{aligned} \tag{6.21}$$

Note that we can also interpret Equation 6.17 as follows: Initially, we derive the probability of detection by an alive sensor, i.e. the probability that a target is sensed by a sensor and the sensor is alive. Since the detection of a target and being alive are

independent events, we get

$$P_{d,a} = \frac{L_s}{L} P_a \tag{6.22}$$

$$P_{\overline{d,a}} = 1 - \frac{L_s}{L} P_a \tag{6.23}$$

Using the probability $P_{\overline{d,a}}$, we can now derive the probability of missing a target in the network, $P_{\overline{D}}$, that a sensor either resides in a jamming region, H_j, or is not sensed by any of the alive sensors. Since the sensors are uniformly and independently distributed, we have:

$$\begin{aligned} P_{\overline{D}} &= \prod_{i=1}^{N_s} P_{\overline{d,a}} \\ &= \prod_{i=1}^{N_a} \left(1 - \frac{L_s}{L} P_a\right) \\ &= \left(1 - \frac{L_s}{L} P_a\right)^{N_s} \end{aligned} \tag{6.24}$$

Hence, we find the probability of detection of a target in the system to be:

$$\begin{aligned} P_D &= 1 - P_{\overline{D}} \\ &= 1 - \left(1 - \frac{L_s}{L} P_a\right)^{N_s} \end{aligned} \tag{6.25}$$

□

In our derivations, we only require the sets representing sensor coverage areas and the deployment area to be convex and all sets to be bounded. However, for simplicity, we assume circular sensing coverage, jamming coverage and deployment areas.

Corollary 6.2. *If the sensors have identical circular sensing coverage areas and jamming regions are circular and identical, then the DQM of a sensor network with a*

circular deployment area is equal to:

$$P_D = 1 - \left(1 - \frac{R_s}{R} P_a\right)^{N_s} \tag{6.26}$$

and

$$P_a = \left(1 - \left(\frac{R_h}{R}\right)^2\right)^{N_h} \tag{6.27}$$

where R_s is the radius of the sensing coverage of a sensor, R_h is the radius of the jamming coverage and R is the radius of the deployment area.

Proof. The perimeters of the sensing coverage and deployment area are given as:

$$L_s = 2\pi R_s$$
$$L = 2\pi R$$

The jamming coverage area and deployment area are given as:

$$A_h = \pi R_h^2$$
$$A = \pi R^2$$

The result directly follows by substituting the perimeter and area formulas in Corollary 6.1. □

6.4. Analytical Results

In this section, we provide a comparison between the analytical and simulation results to present the validity of our analytical estimation. To observe the effects of individual parameters in the model, the following assumptions are made to minimize

the effect of external parameters on our results.

- A binary sensing model is assumed, where for a given sensor s located at z_s, the probability of detection, $P_D(s)$, of a point x is:

$$P_D(s) = \begin{cases} 1, & if\ d(x, z_s) < R_s \\ 0, & otherwise \end{cases} \tag{6.28}$$

- A circular sensing range is assumed on a two-dimensional flat world deployment region.
- Intruders follow a straight line while trespassing the detection area.
- The sink learns the coverage holes and which sensors are alive by the ALIVE messages received from the network via the underlying network protocol stack.
- The sensors are awake and able to detect the intruders at all times.
- Holes are circular inside the deployment region and are due to jamming or destruction of sensors. In either case, the sensors residing in a hole are inoperable.

Our simulations are designed to include different scenarios based on various sets of the parameters involved in the analytical model and are implemented in MATLAB [80]. We evaluated the effects of these parameters for 100 random network deployments and 100 random jamming area placements per simulation test case, where each deployment is tested with each placement. For each (deployment, placement) pair, 1000 random intrusion paths, are generated and the probability of detection is evaluated using the frequency count of lines passing through the sensors that are alive, i.e. outside the jamming areas (Figure 6.1). The results presented in each graph are the mean values of the results obtained for all (deployment, placement) pairs.

Area shape has a very drastic effect on the performance of wireless sensor networks due to the inherent limitations induced by the shape. Hence, we aim to present the effects of the DQM parameters on the probability of detection for two types of deployment sites in our scenarios: circular regions and rectangular regions. In our first

Table 6.1. Tested parameters for circular deployment region scenario.

Parameter	**Tested Values**
Area Radius	2000, 3000, 4000, 5000*, 6000, 7000, 8000 (m)
Jamming Area Radius	50, 100, 150, 200*, 250, 300, 350 (m)
Sensing Radius	15, 20, 25*, 30, 35 (m)
Jamming Area Count	0, 10, 20*, 30, 40, 50, 60, 70, 80
Sensor Count (low)	50, 100, 150, 200, 250, 300, 350, 400, 450
Sensor Count (high)	500*, 600, 700, 800, 900

* These are the default values used in the simulations.

scenario, sensors are deployed over a circular region. Circular regions are introduced to model a circular deployment site, such as a basin or a junction point, on which such surveillance tasks can be performed. The parameter set for the circular deployment scenario is given in Table 6.1.

Table 6.2. Tested parameters for rectangular deployment region scenario.

Parameter	**Tested Values**
Region Height	2000 (m)
Region Width	4000, 6000, 8000, 10000, 12000, 14000*, 16000 (m)
Jamming Area Radius	50, 100, 150, 200*, 250, 300, 350 (m)
Sensing Radius	15, 20, 25*, 30, 35 (m)
Jamming Area Count	0, 10, 20*, 30, 40, 50, 60, 70, 80
Sensor Count (low)	50, 100, 150, 200, 250, 300, 350, 400, 450
Sensor Count (high)	500*, 600, 700, 800, 900

* These are the default values used in the simulations.

Our second scenario is designed with the assumption of rectangular deployment areas to observe their effects on the DQM values. Rectangular regions are introduced to model a border that forms a long strip along a river bank or by a mountain. Security and surveillance tasks are more generally performed on such deployment sites all over the world. Hence, we tested our model on a similar, border-like deployment site to perform more realistic simulations. The parameter set for the rectangular deployment scenario is given in Table 6.2.

In both scenario types, the values indicated with the * sign are used as the default values for fixed parameters in the simulations. Two separate parameter sets are prepared for the sensor count parameter (low and high sensor counts) to simulate low and high density networks. Sensing ranges and jamming ranges are assumed to be circular areas. In addition, the jamming area radii are uniformly distributed in the range $[0.8 \times value, 1.2 \times value]$, where *value* is the jamming area radius parameter value used in the simulation; to be more realistic, the jamming area radii are not exactly equal to but are close to the parameter value used in the simulation.

In the following subsections, the joint effects of the simulation parameters on a deployed sensor network are investigated and presented together with a comparison of the simulation and analytical results. To emphasize the effects of these parameters on the DQM values, some reference DQM values are provided in the feasible operation range of a sample SWSN, which requires the DQM value to be above 90%. More simulation results can be found in [86].

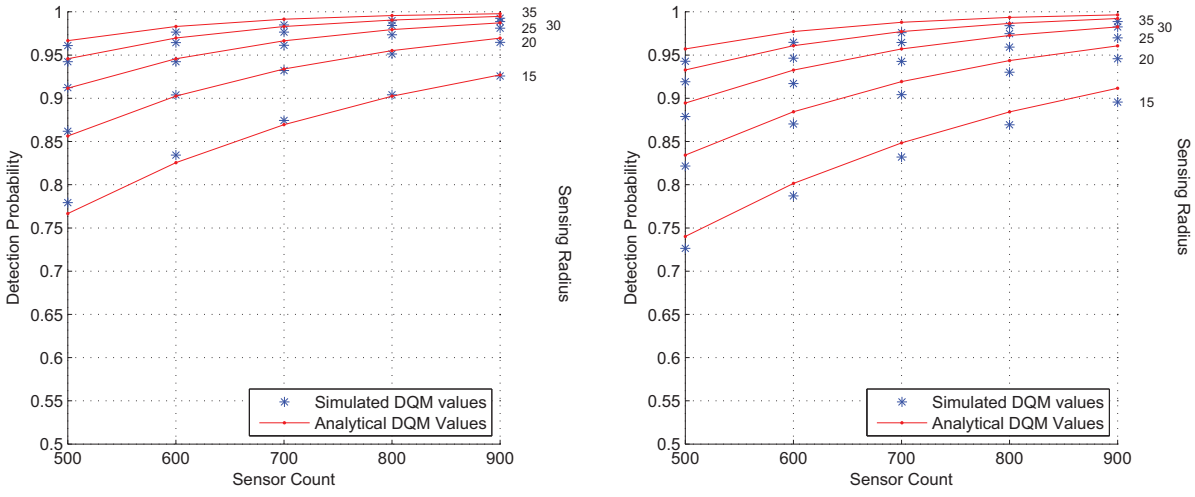

Figure 6.3. Effect of high sensor count and sensing range on the analytical and simulated DQM values. (a) Circular deployment region scenario. (b) Rectangular deployment region scenario.

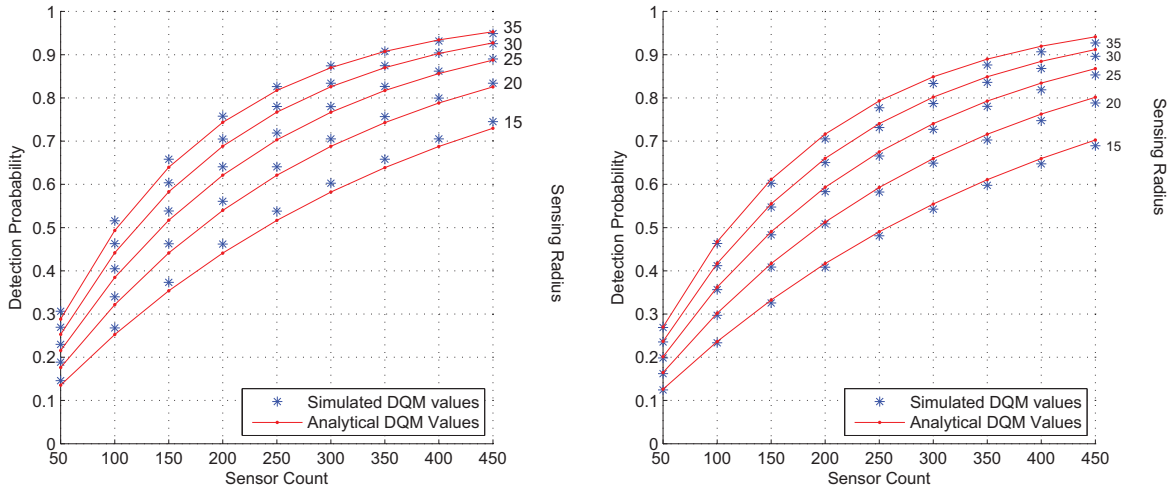

(a) (b)

Figure 6.4. Effect of low sensor count and sensing range on the analytical and simulated DQM values. (a) Circular deployment region scenario. (b) Rectangular deployment region scenario.

6.4.1. The Combined Effect of Sensor Count and Sensing Range on DQM Values

In this test case, the sensor count and the sensing range parameters are changed according to the values given in the parameter sets, while other parameters are fixed to observe the combined effect of these parameters on probability of detection. Separate test cases are designed for high and low sensor counts. Figure 6.3 presents the sensor deployment quality values for the dense networks, where the sensor count is between 500 and 900 nodes. The results for the sparse cases where the sensor count is between 50 and 450 are also available in Figure 6.4. In the circular scenario, the gap between the analytical and simulated DQM values is at most 1.2% for high sensor counts and 2.2% for low sensor counts, whereas the gap is at most 1.6% for both high and low sensor counts in the rectangular scenario. These results show that the DQM values can be utilized as a close estimate of the detection probability of the simulated networks for the given test cases.

The sensor count and sensor range parameters are observed to be proportional to the probability of detection, as indicated in the DQM formulation. For a border

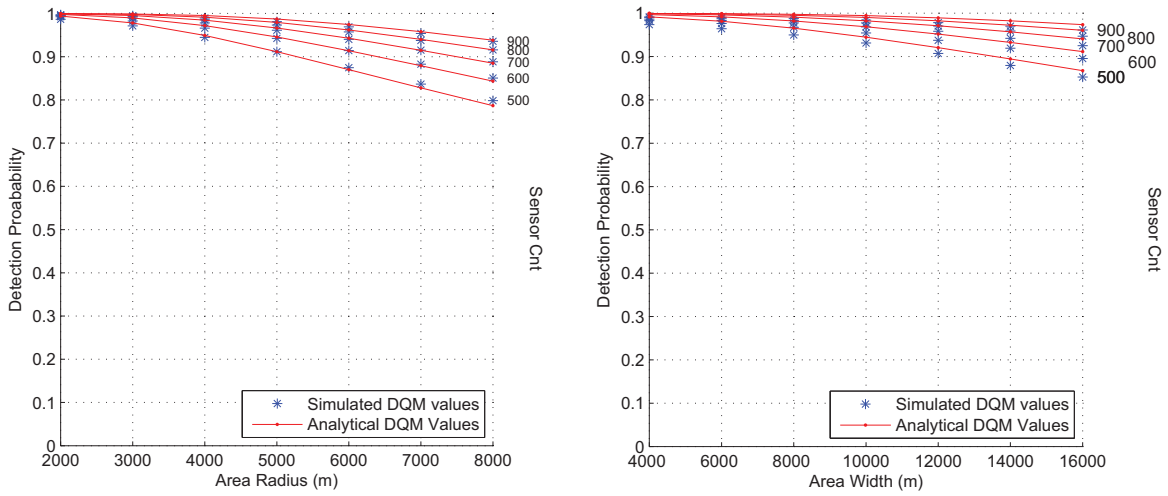

(a) (b)

Figure 6.5. Effect of area size and high sensor count on the analytical and simulated DQM values. (a) Circular deployment region scenario. (b) Rectangular deployment region scenario.

surveillance scenario, DQM values above 90% are generally required. Hence, we can state that under the given assumptions and default parameter values, the feasible range of operation requires the sensor count to be above 800 for the circular scenario and above 900 for the rectangular scenario, if the sensing range is set to be 15 m. Similarly, for a sensor count of 500, the sensing range is required to be above 35 m for the circular scenario and above 40 m for the rectangular scenario.

6.4.2. The Combined Effect of Area Size and Sensor Count on DQM Values

In this test case, the area size and the sensor count parameters are changed according to the values given in the parameter sets, while other parameters are fixed to observe the combined effect of these parameters on probability of detection. Separate test cases are designed for high and low sensor counts. Sensor deployment quality values for these test cases are presented in Figure 6.5 and Figure 6.6 for high and low sensor counts, respectively. In the circular scenario, the gap between the analytical and simulated DQM values is at most 1.1% for high sensor counts and 2.2% for low sensor counts, whereas the gap is at most 1.8% for high sensor counts and 2.4% for low sensor counts in the rectangular scenario. Hence, the narrow gap between analytical

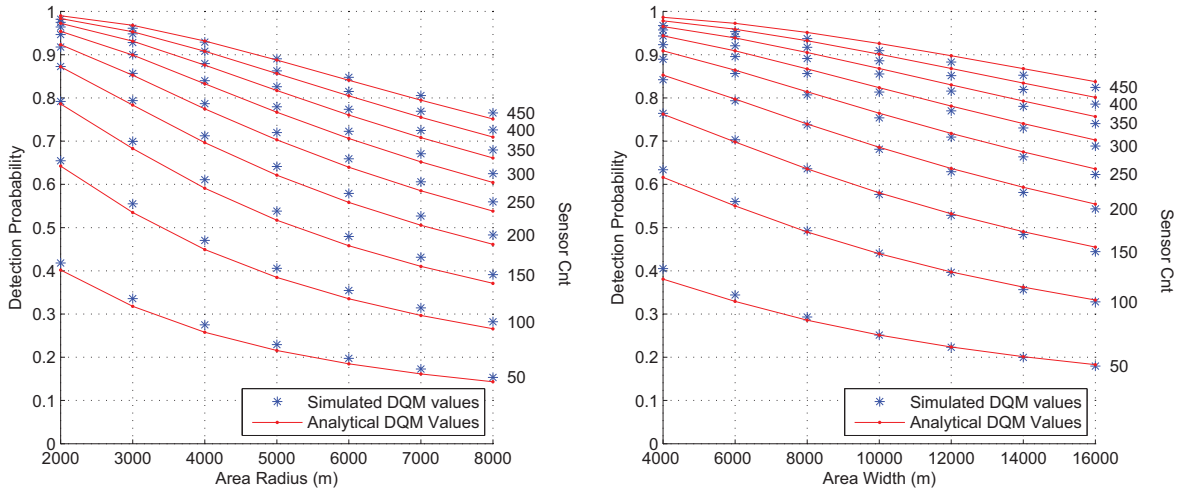

(a) (b)

Figure 6.6. Effect of area size and low sensor count on the analytical and simulated DQM values. a) Circular deployment region scenario. (b) Rectangular deployment region scenario.

and simulation results indicate that the provided DQM metric is a close estimate of the simulated detection probability in the given cases.

The area size is observed to be inversely proportional to the probability of detection, as indicated in the DQM formulation. Under the given assumptions and default parameter values, the feasible range of operation, where the DQM value is above 90%, requires the sensor count to be above 800 in a circular region with a 8000 m radius and above 600 in a 2000 m $\times$ 14000 m rectangular region. Similarly, for a sensor count of 400, a circular area with up to a 4000 m radius and a rectangular area with up to a 1000 m width can be monitored for a feasible DQM.

6.4.3. The Combined Effect of Jamming Area Radius and Jamming Area Count on DQM Values

In this section, a test case involving only the properties of the jamming areas is designed. In this test case, the jamming area radius and the jamming area count parameters are changed according to the values given in the parameter sets, while other parameters are fixed. The DQM values for these test cases are presented in Figure 6.7.

In the circular scenario, the gap between the analytical and simulated DQM values is at most 0.3%, whereas the gap is at most 2.9% in the rectangular scenario. These results show that the DQM values can be utilized as a close estimate of the detection probability of the simulated networks for the given test cases.

In this section, we justify our observations about the effect of the jamming area on the DQM value. The jamming area radius and count parameters are observed to be inversely proportional to the probability of detection. For low jamming area values, deployment quality loss is not very high; however, the effect is clear when jamming areas occupy more than 20% of the network. Under the given assumptions and default parameter values, the feasible range of operation, where the DQM value is above 90%, requires the jamming area count to be below 50 in the circular scenario and below 10 in the rectangular scenario, where the jamming are radius is set to be 200 m. Similarly, if the number of jamming areas is given as 30, the jamming area radius is required to be below 250 m for the circular scenario and below 100 m for the rectangular scenario for a feasible DQM (i.e. $P_D > 0.9$).

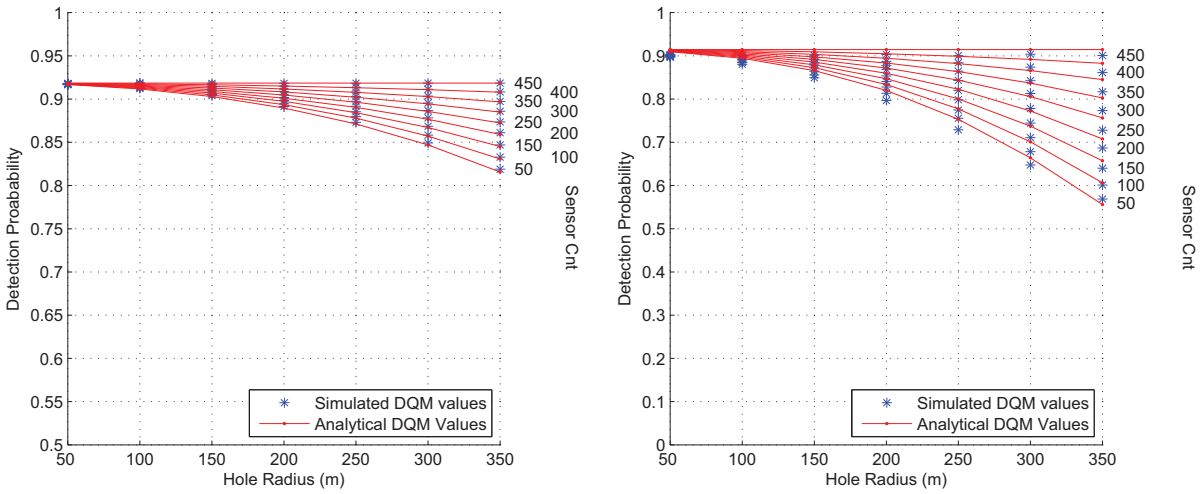

(a) (b)

Figure 6.7. Effect of jamming area radius and jamming area count on the analytical and simulated DQM values. (a) Circular deployment region scenario (b) Rectangular deployment region scenario.

6.4.4. Comparison of the Intruder Detection Probabilities for the Linear and Meandering Paths

The results presented in the previous sections were obtained by setting a linear trajectory for the intruder. To observe the detection results when the intruder does not follow a straight line, we use a random walk mobility model where the intruder step size is varied according to the uniform distribution and its distance to the exit point. Figure 6.8 presents a comparison between the meandering and linear paths together with the DQM values for the scenario where the sensor count, sensing radius, hole radius and hole count values are set to 500, 25 m, 250 m and 20, respectively.

The results indicate that if the intruder chooses to follow a meandering path, the probability of the network to detect the intruder increases. As we discussed in Section 6.1, this increase is caused by the increase in the length of the trajectory inside the network. Since we assume that the intruder has no knowledge about the position of the sensors and the sensors are randomly deployed, a meandering mobility approach increases the possibility of the intruder to be detected by any of the sensors. Hence, a linear trajectory presents the worst-case detection of the intruder. For border

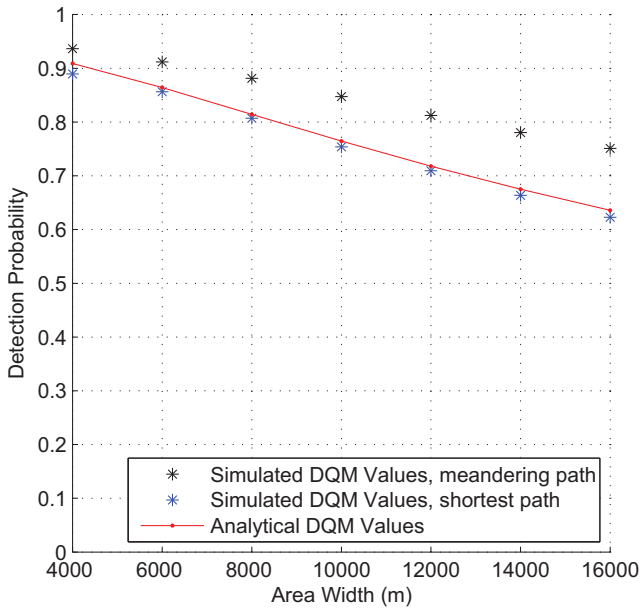

Figure 6.8. Comparison of DQM values for the shortest vs. meandering paths.

surveillance operations, the worst-case capability of the network is very important; therefore, we used linear trajectories in our simulations and analysis. The DQM values presented in Figure 6.8 are shown to provide a good estimation of the worst-case sensing capability of the network.

7. CONCLUSIONS

In an environment with heterogenous traffic, prioritization based service differentiation mechanisms are applied in all layers of communication to satisfy the QoS requirements of each traffic class. The contention prioritization is one of these differentiation techniques applied in the MAC layer. The contention latency in a prioritized contention based MAC protocol is one of the main components of the latency in WSN. In this thesis, we proposed an analytical model for the contention latencies and energy expenditures of low and high priority classes. The contention window is divided into three partitions which are allocated for the use of only high priority, both priorities and only low priority classes. In the analysis, we explored the optimum sizes of these partitions in terms of the contention latency and the total energy expenditure in the neighborhood for each priority class. This analytical model is also useful for the evaluation of various contention prioritization schemes in WSNs.

The analysis is verified by simulations for various node counts in each priority class. The results show that the disjoint partitioning is the most beneficial strategy for the high priority class in terms of latency and energy expenditure, whereas the low priority class gains the highest benefit when the size of the overlapping partitioning is maximized. Considering the QoS requirements of the priority classes, the optimal contention partition sizes can be obtained to balance the tradeoff between the latency of the high priority and the low priority classes. An objective function that contains the latency and energy consumption terms for each priority class can be used in such an optimization problem.

We adapt the proposed analysis for the uniform contention model to a real life MAC protocol SMAC, which introduces the low-duty-cycle operation for energy efficiency. The message passing function is enabled and the contention resolution and synchronization mechanisms are involved in the analysis of the SMAC model. Initially, we explore the effect of the duty cycle on the network performance, so we assume that there is one priority class in the network. The analysis is based on the number

of contending nodes (N) in a virtual cluster, the contention window size (W), duty cycle (r_{dc}) and the number of data packets per message (n). The analysis assumes a heavily loaded system such that the system is in the steady state and the number of contenders is constant at any time. We derive the metrics Ω' and E_{tot}, which are the expected time and expected energy expenditure for a successful transmission to finalize including retrials caused by collisions. We introduced the message throughput of the cluster ($\frac{1}{\Omega'}$), which is an important metric for the assessment of the performance of SMAC. We also derive the expected per node energy expenditure in a synchronization period, which is a component of E_{tot}, using a discrete time Markov chain analysis. The simulation results corroborate the analytical derivations for the provided metrics.

Furthermore, we extend the prioritized contention analysis for the SMAC protocol by integrating the duty cycle parameter in the analysis. The expected time and the expected energy expenditures of a heavily loaded virtual cluster of SMAC to finalize a transmission successfully is derived for constant number of contenders from each priority class by combining the SMAC contention model with prioritized contention model.

Considering the analysis results, we conclude that in order to provide an efficient operation of SMAC in terms of energy expenditure and throughput, for a given N and n, W and r_{dc} should be optimized together. In other words, for any W, we should find the duty cycle value for which the transmission is expected to be finalized in one SMAC frame. Hence, the results shows that in order to improve the efficiency of the operation of SMAC, a proper adjustment of (W, r_{dc}) pair is required.

Apart from the communication-based QoS, the feasible operation of the network requires the quality of the deployment to be above a certain threshold in critical sensor network applications, such as border surveillance and target detection applications. However, various factors, such as the existence of jammers and sensor deaths combined with the physical properties of the deployed sensor network, affect this quality.

In this thesis, we introduced a method to calculate the metric for this deployment quality, which is analogous to the probability of detection in the network, and presented a formulation for this quality metric that integrates the stated factors. The proposed formulation can be used for different types of border surveillance scenarios, where one or more physical properties may differ from one to another. Being in closed form, it is scalable and suitable for different types of sensor network operations.

The effects of these properties were extensively analyzed running various parameter test cases to conclude that the proposed DQM provides realistic results, with a deviation of $\pm 3.2\%$ with the simulation results. We observe that the results reflect the effects of the sensing coverage losses due to jamming, sensor node death and node destruction on the deployment quality, which are all, for simplicity, considered jamming areas. In addition, some reference parameter values of the proposed DQM are provided regarding the maintenance of the feasible operation range of a surveillance sensor network, which generally requires DQM values above 90%.

As a future work, we aim to develop a mechanism which enables the efficient use of the prioritized contention results dynamically in a distributed manner, where the number of high and low priority nodes varies locally throughout the network. In addition, we need to propose a method to obtain a feasible value range for contention partition sizes that balances the tradeoff between the latency and the energy consumption of both priority classes. The analysis should be improved under the assumptions of more than two priority classes, a non-uniform contention window and a non-saturated network environment.

The adaptation of the analytical model for SMAC shall be evolved to model other contention based MAC protocols. A contention prioritization scheme shall be devised that is based on the results of the proposed analysis, buffer level, number of contenders and distance to the sink.

We aim to provide further improvements on our DQM formulation. In this thesis, we assumed a binary sensing model. We aim to integrate a probabilistic detection

model in our formulations. The deployment sites are assumed to be a flat world. A three-dimensional deployment model is much more realistic. However, for relatively flat borders, a two-dimensional formulation is sufficient and very useful for the network engineers to determine the physical properties of the border surveillance sensor network.

REFERENCES

1. Yick, J., B. Mukherjee and D. Ghosal, "Wireless Sensor Network Survey", *Computer Networks*, Vol. 52, No. 12, pp. 2292–2330, 2008.

2. Akyildiz, I., T. Melodia and K. R. Chowdhury, "A Survey on Wireless Multimedia Sensor Networks", *Computer Networks*, Vol. 51, No. 4, pp. 921–960, 2007.

3. Zeng, Y., N. Xiong, J. H. Park and G. Zheng, "An Emergency-Adaptive Routing Scheme for Wireless Sensor Networks for Building Fire Hazard Monitoring", *IEEE Sensors*, Vol. 10, No. 6, pp. 6128–6148, 2010.

4. Sitanayah, L., C. Sreenan and K. Brown, "ER-MAC: A Hybrid MAC Protocol for Emergency Response Wireless Sensor Networks", *Proceedings of the 4th International Conference on Sensor Technologies and Applications*, pp. 244–249, 2010.

5. Chen, D. and P. K. Varshney, "QoS Support in Wireless Sensor Networks: A Survey", *Proceedings of International Conference on Wireless Networks*, pp. 227–233, 2004.

6. Li, Y., C. S. Chen, Y.-Q. Song and Z. Wang, "Real-time QoS Support in Wireless Sensor Networks: A Survey", *Proceedings of the 7th IFAC International Conference on Fieldbuses & Networks in Industrial & Embedded Systems*, Vol. 7, pp. 373–380, Toulouse France, 2007.

7. Slama, I., B. Jouaber and D. Zeghlache, "A Free Collision and Distributed Slot Assignment Algorithm for Wireless Sensor Networks", *Proceedings of Global Telecommunications Conference*, pp. 367–372, 2008.

8. Sahoo, A. and P. Baronia, "An Energy Efficient MAC in Wireless Sensor Networks to Provide Delay Guarantee", *Proceedings of IEEE Workshop on Local Metropolitan Area Networks*, pp. 25–30, 2007.

9. Busch, C., M. Magdon-Ismail, F. Sivrikaya and B. Yener, "Contention-Free MAC Protocols for Asynchronous Wireless Sensor Networks", *Distributed Computing*, Vol. 21, No. 1, pp. 23–42, 2008.

10. Namboodiri, V. and A. Keshavarzian, "Alert: An Adaptive Low-Latency Event-Driven MAC Protocol for Wireless Sensor Networks", *Proceedings of International Conference on Information Processing in Sensor Networks*, pp. 159–170, 2008.

11. Kim, J., K. Sohn, C. Koh and Y. Kim, "A Probabilistic Transmission Slot Selection Scheme for MC-CDMA Systems Using QoS History and Delay Bound", T. Braun, G. Carle, Y. Koucheryavy and V. Tsaoussidis (Editors), *Wired/Wireless Internet Communications*, Vol. 3510 of *Lecture Notes in Computer Science*, pp. 128–137, Springer Berlin / Heidelberg, 2005.

12. Saxena, N., A. Roy and J. Shin, "Dynamic Duty Cycle and Adaptive Contention Window Based QoS-MAC Protocol for Wireless Multimedia Sensor Networks", *Computer Networks*, Vol. 52, No. 13, pp. 2532–2542, 2008.

13. Yigitel, M. A., O. Durmaz Incel and C. Ersoy, "Diff-MAC: A QoS-Aware MAC Protocol with Differentiated Services and Hybrid Prioritization for Wireless Multimedia Sensor Networks", *Proceedings of ACM Workshop on QoS and Security for Wireless and Mobile Networks*, pp. 62–69, 2010.

14. Rhee, I., A. Warrier, M. Aia, J. Min and M. L. Sichitiu, "Z-MAC: A Hybrid MAC for Wireless Sensor Networks", *IEEE/ACM Transactions on Networking*, Vol. 16, No. 3, pp. 511–524, 2008.

15. Kim, H. and S.-G. Min, "Priority-Based QoS MAC Protocol for Wireless Sensor Networks", *Proceedings of IEEE International Symposium on Parallel Distributed Processing*, pp. 1–8, 2009.

16. Liu, Y., I. Elhanany and H. Qi, "An Energy-efficient QoS-Aware Media Access Control Protocol for Wireless Sensor Networks", *Proceedings of IEEE International*

Conference on Mobile Adhoc and Sensor Systems Conference, pp. 191–193, 2005.

17. Nguyen, K., T. Nguyen, C. K. Chaing and M. Motani, "A Prioritized MAC Protocol for Multihop, Event-Driven Wireless Sensor Networks", *Proceedings of International Conference on Communications and Electronics*, pp. 47–52, 2006.

18. Ye, W., J. Heidemann and D. Estrin, "Medium Access Control with Coordinated Adaptive Sleeping for Wireless Sensor Networks", *IEEE/ACM Transactions on Networking*, Vol. 12, No. 3, pp. 493–506, 2004.

19. van Dam, T. and K. Langendoen, "An Adaptive Energy-Efficient MAC Protocol for Wireless Sensor Networks", *International Conference on Embedded Networked Sensor Systems*, pp. 171–180, 2003.

20. Ye, W., F. Silva and J. Heidemann, "Ultra-Low Duty Cycle MAC with Scheduled Channel Polling", *Proceedings of International Conference on Embedded Networked Sensor Systems*, pp. 321–334, ACM, New York, USA, 2006.

21. Du, S., A. Saha and D. Johnson, "RMAC: A Routing-Enhanced Duty-Cycle MAC Protocol for Wireless Sensor Networks", *Proceedings of IEEE International Conference on Computer Communications*, pp. 1478–1486, 2007.

22. Sun, Y., S. Du, O. Gurewitz and D. B. Johnson, "DW-MAC: A Low Latency, Energy Efficient Demand-Wakeup MAC Protocol for Wireless Sensor Networks", *Proceedings of ACM International Symposium on Mobile Ad Hoc Networking and Computing*, pp. 53–62, ACM, New York, USA, 2008.

23. Onur, E., C. Ersoy, H. Delic and L. Akarun, "Surveillance Wireless Sensor Networks: Deployment Quality Analysis", *IEEE Network*, Vol. 21, No. 6, pp. 48–53, 2007.

24. Guo, S., T. He, M. Mokbel, J. A. Stankovic and T. Abdelzaher, "On Accurate and Efficient Statistical Counting in Sensor-Based Surveillance Systems", *Proceedings*

of the 5th IEEE International Conference on Mobile Ad-hoc and Sensor Systems, pp. 24–35, Atlanta, Georgia, 2008.

25. Lu, G., B. Krishnamachari and C. S. Raghavendra, "An Adaptive Energy-Efficient and Low-Latency MAC for Tree-Based Data Gathering in Sensor Networks", *Wireless Communications and Mobile Computing*, Vol. 7, No. 7, pp. 863–875, 2007.

26. Oh, S., P. Chen, M. Manzo and S. Sastry, "Instrumenting Wireless Sensor Networks for Real-Time Surveillance", *Proceedings of the 2006 IEEE International Conference on Robotics and Automation*, pp. 3128–3133, 2006.

27. Bokareva, T., W. Hu, S. Kanhere, B. Ristic, N. Gordon, T. Bessell, M. Rutten and S. Jha, "Wireless Sensor Networks for Battlefield Surveillance", *Proceedings of the Land Warfare Conference*, Brisbane, Queensland, Australia, 2006.

28. Jamieson, K., H. Balakrishnan and Y. Tay, "Sift: A MAC Protocol for Event-Driven Wireless Sensor Networks", K. Römer, H. Karl and F. Mattern (Editors), *Wireless Sensor Networks*, Vol. 3868 of *Lecture Notes in Computer Science*, pp. 260–275, 2006.

29. Liu, Z. and I. Elhanany, "RL-MAC: A QoS-Aware Reinforcement Learning Based MAC Protocol for Wireless Sensor Networks", *Proceedings of IEEE International Conference on Networking, Sensing and Control*, pp. 768–773, 2006.

30. Becker, P., R. Gotzhein and T. Kuhn, "MacZ - A Quality-of-Service MAC Layer for Ad-Hoc Networks", *Proceedings of International Conference on Hybrid Intelligent Systems*, pp. 277–282, 2007.

31. Firoze, A., L. Ju and L. Kwong, "PR-MAC - A Priority Reservation MAC Protocol for Wireless Sensor Networks", *Proceedings of International Conference on Electrical Engineering*, pp. 1–6, 2007.

32. Aad, I. and C. Castelluccia, "Differentiation Mechanisms for IEEE 802.11", *Pro-*

ceedings of Annual Joint Conference of the IEEE Computer and Communications Societies, Vol. 1, pp. 209–218, 2001.

33. Anjum, B. and Z. Uzmi, "Multi-Class QoS in 802.11 Networks Using Gentle Decrease of Multiple Contention Windows", *Proceedings of IEEE Global Telecommunications Conference*, pp. 5242–5247, 2007.

34. Lu, C., B. Blum, T. Abdelzaher, J. Stankovic and T. He, "RAP: A Real-Time Communication Architecture for Large-Scale Wireless Sensor Networks", *Proceedings of Real-Time and Embedded Technology and Applications Symposium*, pp. 55–66, 2002.

35. Mishra, M. and A. Sahoo, "A Contention Window Based Differentiation Mechanism for Providing QoS in Wireless LANs", *Proceedings of International Conference on Information Technology*, pp. 72–76, 2006.

36. Nafaa, A., A. Ksentini, A. Mehaoua, B. lshibashi, Y. Iraqi and R. Boutaba, "Sliding Contention Window (SCW): Towards Backoff Range-Based Service Differentiation over IEEE 802.11 Wireless LAN Networks", *IEEE Network*, Vol. 19, No. 4, pp. 45–51, 2005.

37. Artail, H., H. Safa, J. Naoum-Sawaya, B. Ghaddar and S. Khawam, "A Simple Recursive Scheme for Adjusting the Contention Window Size in IEEE 802.11e Wireless Ad-Hoc Networks", *Computer Communications*, Vol. 29, No. 18, pp. 3789–3803, 2006.

38. Pang, A.-C. and H.-W. Tseng, "Dynamic Backoff for Wireless Personal Networks", *Proceedings of IEEE Global Telecommunications Conference*, Vol. 3, pp. 1580–1584, 2004.

39. Kim, E.-J., M. Kim, S.-K. Youm, S. Choi and C.-H. Kang, "Priority-Based Service Differentiation Scheme for IEEE 802.15.4 Sensor Networks", *International Journal of Electronics and Communications*, Vol. 61, No. 2, pp. 69–81, 2007.

40. Kim, M. and C.-H. Kang, "Priority-Based Service-Differentiation Scheme for IEEE 802.15.4 Sensor Networks in Nonsaturation Environments", *IEEE Transactions on Vehicular Technology*, Vol. 59, No. 7, pp. 3524–3535, 2010.

41. Tian, Q. and E. Coyle, "A MAC-Layer Retransmission Algorithm Designed for the Physical-Layer Characteristics of Clustered Sensor Networks", *IEEE Transactions on Wireless Communications*, Vol. 5, No. 11, pp. 3153–3164, 2006.

42. Ramachandran, I., A. K. Das and S. Roy, "Analysis of the Contention Access Period of IEEE 802.15.4 MAC", *ACM Transactions on Sensor Networks*, Vol. 3, No. 1, 2007.

43. Haque, A., M. Murshed and M. Ali, "Adaptive Contention Window Based Wireless Medium Access Mechanism for Periodic Sensor Data Collection Applications", *Proceedings of IEEE International Conference on Communications*, pp. 917–921, 2009.

44. Demirkol, I. and C. Ersoy, "Energy and Delay Optimized Contention for Wireless Sensor Networks", *Computer Networks*, Vol. 53, No. 12, pp. 2106–2119, 2009.

45. Chiasserini, C.-F. and M. Garetto, "An Analytical Model for Wireless Sensor Networks with Sleeping Nodes", *IEEE Transactions on Mobile Computing*, Vol. 5, No. 12, pp. 1706–1718, 2006.

46. Tseng, H.-W., S.-H. Yang, P.-Y. Chuang, H.-K. Wu and G.-H. Chen, "An Energy Consumption Analytic Model for a Wireless Sensor MAC Protocol", *Proceedings of IEEE Vehicular Technology Conference*, Vol. 6, pp. 4533–4537, 2004.

47. Zhang, Y., C. He and L. Jiang, "Performance Analysis of S-MAC Protocol under Unsaturated Conditions", *IEEE Communications Letters*, Vol. 12, No. 3, pp. 210–212, 2008.

48. Bianchi, G., "Performance Analysis of the IEEE 802.11 Distributed Coordination

Function", *IEEE Journal on Selected Areas in Communications*, Vol. 18, No. 3, pp. 535–547, 2000.

49. Sung, S., S. Woo and K. Kim, "Packet Delay and Energy Consumption Based on Markov Chain Model of the Frame-Based S-MAC Protocol under Unsaturated Conditions", *International Conference on Information Networking*, pp. 604–613, Berlin, Heidelberg, 2008.

50. Luo, J., L. Jiang and C. He, "An Analytical Model for SMAC Protocol in Multi-Hop Wireless Sensor Networks", *Science China Information Sciences*, Vol. 53, No. 11, pp. 2323–2331, 2010.

51. Yang, O. and W. Heinzelman, "Modeling and Throughput Analysis for SMAC with a Finite Queue Capacity", *Proceedings of International Conference on Intelligent Sensors, Sensor Networks and Information Processing*, pp. 409–414, 2009.

52. Li, C., K.-R. Wang, J.-L. Zhang, D.-X. Zhao and W. Li, "Optimization of Listening Time of S-MAC for Wireless Sensor Networks", *The Journal of China University of Posts and Telecommunications*, Vol. 16, No. 5, pp. 41–45, 2009.

53. Cho, K.-T. and S. Bahk, "Duty Cycle Optimization for a Multi Hop Transmission Method in Wireless Sensor Networks", *IEEE Communications Letters*, Vol. 14, No. 3, pp. 269–271, 2010.

54. Ergen, S., C. Fischione, D. Marandin and A. Sangiovanni-Vincentelli, "Duty-Cycle Optimization in Unslotted 802.15.4 Wireless Sensor Networks", *Proceedings of IEEE Global Telecommununications Conference*, pp. 388–393, 2008.

55. Lazos, L., R. Poovendran and J. A. Ritcey, "Analytic Evaluation of Target Detection in Heterogeneous Wireless Sensor Networks", *ACM Transactions on Sensor Networks*, Vol. 5, No. 2, pp. 18–55, 2009.

56. Wang, Y., X. Wang, D. P. Agrawal and A. A. Minai, "Impact of Heterogeneity on

Coverage and Broadcast Reachability in Wireless Sensor Networks", *Proceedings of the 2006 International Conference on Computer Communications and Networks*, pp. 63–67, Arlington, USA, 2006.

57. Dousse, O., C. Tavoularis and P. Thiran, "Delay of Intrusion Detection in Wireless Sensor Networks", *Proceedings of the 7th ACM International Symposium on Mobile Ad Hoc Networking and Computing*, pp. 155–165, Florence, Italy, 2006.

58. Cao, Q., T. Yan, J. A. Stankovic and T. F. Abdelzaher, "Analysis of Target Detection Performance for Wireless Sensor Networks", *Proceedings of the Distributed Computing in Sensor Systems*, Vol. 3560 of *Lecture Notes in Computer Science*, pp. 276–292, Springer, Marina del Rey, USA, 2005.

59. Wang, Y.-C., K.-Y. Cheng and Y.-C. Tseng, "Using Event Detection Latency to Evaluate the Coverage of a Wireless Sensor Network", *Computer Communications*, Vol. 30, No. 14-15, pp. 2699–2707, 2007.

60. Ren, S., Q. Li, H. Wang, X. Chen and X. Zhang, "Analyzing Object Detection Quality Under Probabilistic Coverage in Sensor Networks", *Proceedings of the International Workshop on Quality of Service*, Vol. 3552 of *Lecture Notes in Computer Science*, pp. 107–122, 2005.

61. Clouqueur, T., K. K. Saluja and P. Ramanathan, "Fault Tolerance in Collaborative Sensor Networks for Target Detection", *IEEE Transactions on Computers*, Vol. 53, No. 3, pp. 320–333, 2004.

62. Niu, R., P. K. Varshney and Q. Cheng, "Distributed Detection in a Large Wireless Sensor Network", *Information Fusion*, Vol. 7, No. 4, pp. 380–394, 2006.

63. Saipulla, A., C. Westphal, B. Liu and J. Wang, "Barrier coverage of line-based deployed wireless sensor networks", *Proceedings of the 28th IEEE Conference on Computer Communications*, pp. 127–135, Rio de Janeiro, Brazil, 2009.

64. Xu, W., W. Trappe, Y. Zhang and T. Wood, "The Feasability of Launching and Detecting Jamming Attacks in Wireless Networks", *Proceedings of the 6th ACM International Symposium on Mobile Ad Hoc Networking and Computing*, pp. 46–57, Urbana-Champaign, USA, 2005.

65. Ngai, E. C. H., J. Liu and M. R. Lyu, "An Efficient Intruder Detection Algorithm Against Sinkhole Attacks in Wireless Sensor Networks", *Computer Communications*, Vol. 30, No. 11-12, pp. 2353–2364, 2007.

66. Li, M., I. Koutsopoulos and R. Poovendran, "Optimal Jamming Attacks and Network Defense Policies in Wireless Sensor Networks", *Proceedings of the 26th IEEE International Conference on Computer Communications*, pp. 1307–1315, 2007.

67. Cagalj, M., S. Capkun and J.-P. Hubaux, "Wormhole-Based Antijamming Techniques in Sensor Networks", *IEEE Transactions On Mobile Computing*, Vol. 6, No. 1, pp. 100–114, 2007.

68. Chen, X., K. Makki, K. Yen and N. Pissinou, "Attack Distribution Modeling and Its Applications in Sensor Network Security", *EURASIP Journal on Wireless Communications and Networking*, Vol. 2008, pp. 1–11, 2008.

69. Li, X. and D. K. Hunter, "Distributed Coordinate-Free Hole Recovery", *Proceedings of 13th IEEE International Conference on Communications Workshops*, pp. 189–194, 2008.

70. Karp, B. and H. T. Kung, "GPSR: Greedy Perimeter Stateless Routing for Wireless Networks", *Proceedings of the 6th annual international conference on Mobile computing and networking*, pp. 243–254, ACM Press, 2000.

71. Huang, X. and Y. Fang, "End-to-End Delay Differentiation by Prioritized Multipath Routing in Wireless Sensor Networks", *Proceedings of IEEE Military Communications Conference*, Vol. 2, pp. 1277–1283, 2005.

72. Younis, M., K. Akkaya, M. Eltoweissy and A. Wadaa, "On Handling QoS Traffic in Wireless Sensor Networks", *Proceedings of the 37th Annual Hawaii International Conference on System Sciences*, pp. 1–10, 2004.

73. Wagner, D. and U. R. Krieger, "Analysis of a Finite Buffer with Non-Preemptive Priority Scheduling", *Stochastic Models*, Vol. 15, No. 2, pp. 345–365, 1999.

74. Sun, Y., H. Ma and L. Liu, "Traffic Scheduling Based on Queue Model with Priority for Audio/Video Sensor Networks", *Proceedings of International Conference on Pervasive Computing and Applications*, pp. 709–714, 2007.

75. OPNET Technologies Inc., "OPNET Modeler", `http://www.opnet.com`, accessed at September 2011.

76. Kulkarni, P., D. Ganesan, P. Shenoy and Q. Lu, "SensEye: a Multi-Tier Camera Sensor Network", *Proceedings of the 13th ACM international conference on Multimedia*, pp. 229–238, Singapore, 2005.

77. Downes, I., L. B. Rad and H. Aghajan, "Development of a Mote for Wireless Image Sensor Networks", *Proceedings of Cognitive Systems with Interactive Sensors*, Paris, France, 2006.

78. Zixiang, X., A. D. Liveris and S. Cheng, "Distributed Source Coding for Sensor Networks", *IEEE Signal Processing Magazine*, Vol. 21, No. 5, pp. 80–94, 2004.

79. Sibuya, M., I. Yoshimura and R. Shimizu, "Negative Multinomial Distribution", *Annals of the Institute of Statistical Mathematics*, Vol. 16, No. 1, pp. 409–426, 1964.

80. The MathWorks Inc., "MATLAB", `http://www.mathworks.com`, accessed at September 2011.

81. Grinstead, C. M. and J. L. Snell, *Introduction to Probability*, American Mathematical Society, Providence, 1997.

82. Wen, Y.-F., Y.-Q. Chen and M. Pan, "Adaptive Ant-Based Routing in Wireless Sensor Networks Using Energy*Delay Metrics", *Journal of Zhejiang University - Science A*, Vol. 9, No. 4, pp. 531–538, 2008.

83. Casari, P., M. Nati, C. Petrioli and M. Zorzi, "Efficient Non-Planar Routing around Dead Ends in Sparse Topologies using Random Forwarding", *Proceedings of IEEE International Conference on Communications*, pp. 3122–3129, 2007.

84. Law, Y. W., M. Palaniswami, L. V. Hoesel, J. Doumen, P. Hartel and P. Havinga, "Energy-Efficient Link-Layer Jamming Attacks Against Wireless Sensor Network MAC Protocols", *ACM Transantions on Sensor Networks*, Vol. 5, No. 1, pp. 1–38, 2009.

85. Santalo, L. A., *Integral Geometry and Geometric Probability*, Addison-Wesley Publishing, Reading, 1976.

86. Donmez, M. Y., R. Kosar and C. Ersoy, "An Analytical Approach to the Deployment Quality of Surveillance Wireless Sensor Networks Considering the Effect of Jammers and Coverage Holes", *Computer Networks*, Vol. 54, No. 18, pp. 3449–3466, 2010.